Task 12: Beta-Beam Aspects

Conceptual Design Report
(Published on CD only)

November 2009

PROJECT RIDS 51576

Conceptual Design Report for a Beta-Beam Facility

A. Bechtold[1], M. Benedikt[2], F. Borgnolutti[2], E. Bouquerel[2], L. Bozyk[3], J. Bruer[2], A. Chancé[4], P. Delahaye[2,5], A. Fabich[2], S. Hancock[2], C. Hansen[2], E. Jensen[2], A. Källberg[6], M. Kirk[3], A. Lachaize[7], M. Lindroos[2,8], M. Magistris[2], A. Mueller[7], J. Payet[4], H. Podlech[1], P. Puppel[3], M. Silari[2], A. Simonsson[6], P. Spiller[3], S. Stadlmann[3], A. Tkatchenko[7], S. Trovati[2], V. Vlachoudis[2], and E. Wildner[2]

1   IAP, University of Frankfurt
2   CERN, Geneva
3   GSI, Darmstadt
4   CEA Saclay
5   GANIL, Caen
6   MSL, Stockholm
7   IPN Orsay
8   ESS-S, Lund

Beta-Beam task leader: M. Benedikt, CERN

Contents

I.   Introduction

The Beta-Beam [1] is a concept of large scale facility that aims at providing pure electronic neutrino and antrineutrino beams for the measurement of $v_e \rightarrow v_\mu$ oscillations, with unprecedented sensitivity for detection of the θ_{13} mixing angle and CP violating phase. In the scenario presented in different publications[2][3][4], a Beta-Beam facility could be advantageously placed at CERN making use of the PS and SPS for accelerating the beta-decaying, neutrino-emitting beams to a Lorentz gamma of 100. Intense beams of ^{6}He and ^{18}Ne would be produced using the so-called "isotope-separation on line" ISOL method in a facility of the scale of EURISOL. The synergy between the two projects was pointed out in [5]. The task 12 of the EURISOL design study aimed at producing a conceptual design report for the accelerator chain of a EURISOL/CERN-baseline Beta-Beam facility (Figure 1). CERN was leading the task. This document summarizes the achievements made during the time of the study and constitutes the final conceptual report of the beta-beam facility.
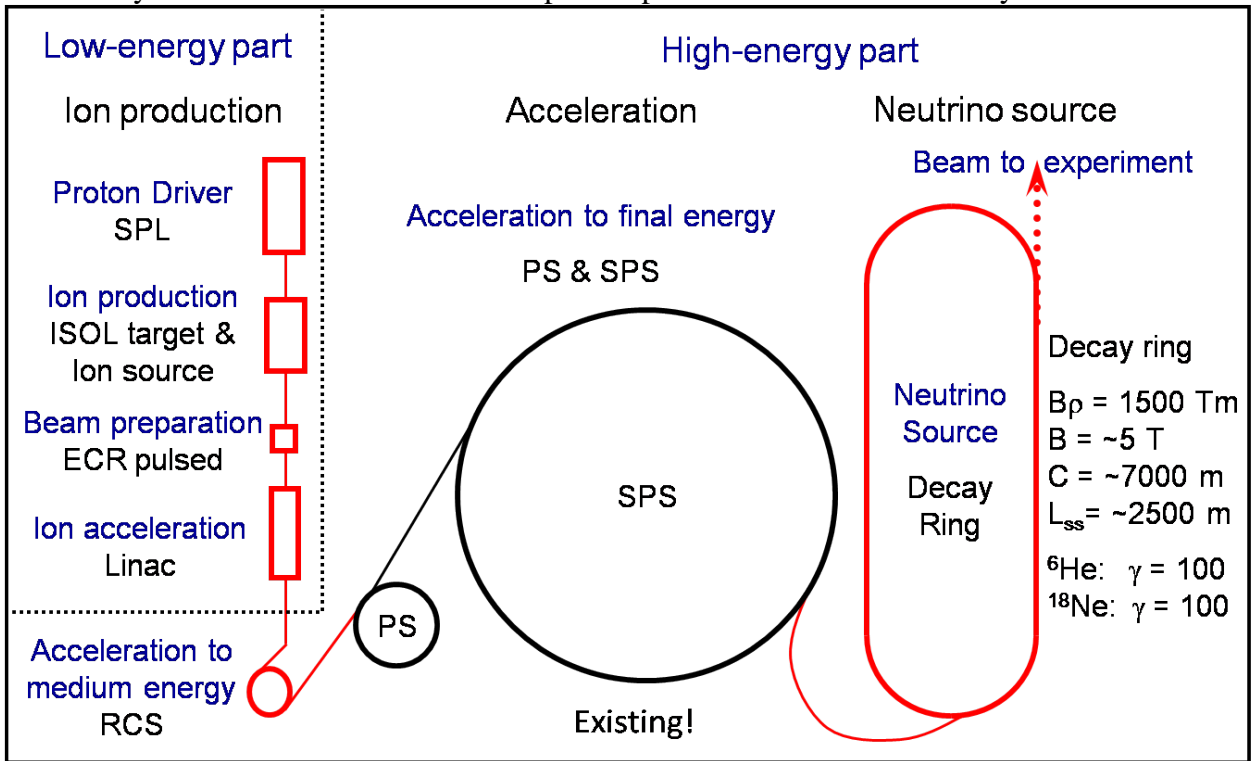
Figure 1: Overview of the CERN-baseline Beta-Beam.

Comments on the ^{6}He and ^{18}Ne production and ionization methods

For an optimal sensitivity of the Beta-Beam facility to the θ_{13} angle and CP violating phase, a total throughput of $1.1 \ 10^{19}$ neutrinos and $2.9 \ 10^{19}$ antineutrinos was generally assumed over a running period of 10 years. In turn, a top-down approach results in the need for production of about $3.3 \ 10^{13}$ ^{6}He radioactive atoms and $2.1 \ 10^{13}$ ^{18}Ne atoms per second, with efficiencies along the accelerator chain as quoted in the next section. While the ^{6}He production rate appeared to be possible from a "standard" 200kW EURISOL target [6], the ^{18}Ne production was found more problematic. The cyclotron laboratory from Louvain-La-Neuve conducted some promising tests for using the reaction ^{16}O(^{3}He,n)^{18}Ne on large size oxide targets. The production rates do not seem out of reach now and the envisaged production methods are briefly summarized in Table 1.

Isotope	Primary beam and target	Reaction	Yields
^{6}He	2GeV p (200kW) on a neutron converter surrounding a BeO target[6]	^{9}Be(n,α)^{6}He	2.10^{13}/s
^{18}Ne	60 cm diameter target MgO 2MW ^{3}He beam (14.8MeV, 130mA)	^{16}O(^{3}He,n)^{18}Ne	10^{13}/s

Table 1: Envisaged production methods for ^{6}He and ^{18}Ne.

A 60 GHz ECRIS is under study for the multi-ionization and bunching of the ^{6}He and ^{18}Ne ions into 10Hz 50μs pulses. A first design was done within the task 9 of EURISOL, and a prototype should be built and tested at LPSC Grenoble within FP7 [7]. Alternative neutrino emitters have been proposed in the frame of FP7, ^{8}B and ^{8}Li that could possibly be produced in copious amounts using the concept of ionization cooling ring [8].

II.   The Beta-Beam database

The flux out of the Beta-beam facility is determined by the number of ions that can be produced, by the number remaining after acceleration and by the total accumulated in the decay ring. A first "bottom-up" analysis of the ion intensities along the accelerator chain and of the neutrino and antineutrino flux out of the decay ring was realized by CERN, starting with the rate at which atoms are transported out of the target [9] [10]. It was lately updated and turned into a "top-down" analysis [11], for which it was assumed that the required 2.9×10^{18} antineutrinos/year and 1.1×10^{18} neutrinos/year [3] could be obtained. We recall here the main arguments which served to the constitution of the database.

A full description of the Beta-Beam can be found in e.g. [2][4]. Figure 1 represents the Beta-Beam facility as described in these articles.

Production

In the Beta-beam baseline it was first assumed that one could produce and transport 2×10^{13} ^{6}He atoms/s and 8×10^{11} ^{18}Ne atoms/s out of the target with a proton driver beam current of 100 μA impinging on the target at 2.2 GeV. These numbers are based on an evaluation of suitable isotopes and their production rates at ISOL facilities and have been presented as part of the Beta-beam contribution to NuFact02. The full write-up of this presentation could not be published as part of the proceedings, but it exists as a CERN internal note [2]. During the course of the study, alternative production methods were envisaged (see *Comments on the ^{6He} and ^{18Ne} production and ionization methods,* in the previous section). It is now assumed that ^{6}He and ^{18}Ne can be produced in sufficient quantities, which are derived from the required neutrinos and antineutrinos throughput of Beta-Beam.

ECR source

Efficient bunching and stripping of the high intensity beam are achieved using a high-frequency ECR source [12]. We assume the efficiency of such a source to be 50% both for ^{6}He in the 2+ charge state and 50% for ^{18}Ne ions in one (e.g., 6+) of several charge states being extracted. We further assume that the ECR operates at 10 Hz with an accumulation time of 97.5 ms, that the source is at a potential of 50 kV relative to the linac, and that the ions are ejected in 50 μs long bunches with a physical transverse emittance of about 50 π.mm.mrad.

Linac and rapid cycling synchrotron

The linac accelerates the ions to 100 MeV/nucleon, after which they are multi-turn injected into a

rapid cycling synchrotron (RCS). We assume an injection efficiency of 80%. Both ion species are accelerated to a magnetic rigidity of 14.47 Tm in a time dictated by the 10 Hz repetition rate of the ECR source. Each cycle provides a single bunch.

PS and SPS acceleration to high energy

The PS waits for 20 shots from the RCS then accelerates the 20 bunches to a magnetic rigidity of 86.7 Tm. Then they are transferred to the SPS and accelerated to $\gamma=100$ and ejected off momentum into the decay ring for stacking. The cycle time of the SPS is a multiple of the 1.2 s basic period of the CERN machines. The extra acceleration required for the ^{6}He results in a 6 s cycle compared with only 3.6 s for ^{18}Ne.

Decay ring

The 20 incoming bunches are combined with the 20 circulating ones of the stack by an asymmetric merging process in the decay ring (see section Decay Ring). The number of times this process can be repeated is constrained by the 1 eVs longitudinal emittance of each bunch delivered by the SPS. Simulations for ^{6}He show that such bunches can be stacked up to 15 times. At given relativistic γ, the aperture of the decay ring defines a longitudinal acceptance limit which scales with ion momentum. Consequently, the more advantageous charge-to- mass ratio of ^{18}Ne ions should allow the number of merging steps to fill the decay ring to be increased by something approaching a factor of 3 with respect to the stacking procedure established for ^{6}He involving 15 merges. However, the sensitivity of the process to phase errors between the two rf components employed in the merging puts an upper limit of about 20 on the number of merges that can realistically be achieved. We therefore assume that the extra acceptance available for ^{18}Ne in the upstream PS and SPS is exploited to stabilize the beam and consider 2 eVs per bunch (cf., 1 eVs for ^{6}He) injected into the decay ring, giving 40 eVs in the stack.

The resultant relative momentum spread of the stack is $\pm2.5\times10^{-3}$ at the start of merging for both ion species and, applying the full 20+20 MV of the 40+80 MHz rf systems in the decay ring, the duration of each bunch is 5.2 and 4.5 ns for ^{6}He and ^{18}Ne, respectively.

The annual integrated flux of potentially useful neutrinos and antineutrinos emanating from the decay ring is linearly dependent on the relative length of the straight section that points towards the detector. This is taken to be 36% of the decay ring circumference [2].

Transverse emittance and tune shift

The transverse emittance and tune shift evaluations were reported in [10][11].

Results

The above parameters result in the numbers of ions at each stage of the CERN Beta-beam facility quoted in Table 2. The decay losses are properly accounted for, but the transfer efficiencies between the different machines are assumed to be 100% except for the multi-turn injection into the RCS (80% efficiency). The figures "Decay Ring accumulated" correspond to 10.7 effective merging steps for helium and to 17.4 for neon and are based on idealized stacking but with beta-decay taken into account between the 15 or 20 shots that fill the machine. Detailed simulations indicate that the stacking efficiency is in excess of 80% of the idealized one in both cases [13],[14].

	$^6\text{He}^{2+}$	$^{18}\text{Ne}^{10+}$
RCS injected	8.5×10^{11}	2.6×10^{11}
RCS ejected	8.3×10^{11}	2.6×10^{11}
PS accumulated	1.1×10^{13}	4.5×10^{12}
SPS injected	9.5×10^{12}	4.3×10^{12}
SPS ejected	9.0×10^{12}	4.3×10^{12}
Decay Ring injected	1.8×10^{14}	8.5×10^{13}
Decay Ring accumulated	9.7×10^{13}	7.4×10^{13}

Table 2: Ion intensities in the EURISOL baseline scenario

From the number of ions at RCS injection, the intensities required from the production chain can be estimated. It is assumed that 50% or the ions extracted from the ECR source have the desired charge state and that the linac transmission efficiency is 80% and the RCS injection efficiency is 80%. This results in an average of 2.6×10^{13} ^{6}He ions per second or 8.1×10^{12} ^{18}Ne ions per second to be extracted from the source, pulsed in 10 bunches spaced by 100 ms.

III.   Post-accelerating LINAC

It was originally believed that the design of the EURISOL post-accelerator could be replicated for the injector into the Rapid Cycling Synchrotron of the beta-beam facility. It turned out in the middle of the study that the superconducting LINAC of EURISOL would not be suited to the post-acceleration of the intense pulses of ^{6}He and ^{18}Ne. For this reason, a separate study was done by IAP Frankfurt for delivering specifications of a normal-conducting LINAC that would fulfill the Beta-Beam requirements (Table 3).

Due to the low duty cycle of 0.05% and the high pulse beam current up to 13 mA as required by Beta-Beam, the use of normal conducting NC-RF-structures instead of superconducting cavities even up to the intended final energy of 100 MeV/u seems more favorable. Even at accelerating gradients between 3 and 6 MV/m the thermal load on the cavities is very moderate. For the desired maximum mass to charge ratio of A/q = 3 an operating frequency of 175 MHz at energies up to 10 MeV/u is well adapted, which then would be changed to 352 MHz for further acceleration [15].

β-BEAM LINAC BENCHMARK	
mass to charge ratio A/q	<3
duty cycle	0.05%
beam current	≤13 mA
input energy W_{in}	8 keV/u
output energy W_{out}	100 MeV/u
input emittance $\varepsilon_{in,rms,normalized}$	0.2 π mm mrad

Table 3: Beta-Beam requirements for the post-accelerating LINAC.

RFQ design

First accelerating stage behind the ECR ion source would be a 4-rod-type RFQ [15]. This resonator type has proven its reliability at many instances and is well suited for this field of application here. The 4-rod type provides very comfortable rf-tuning possibilities compared to other resonator structures like IH- or four vane type RFQs. The frequency tuning during operation is accomplished by an inductively operating tuning plunger, which has an only marginal effect on the rf-efficiency of the device. Some preliminary design calculations have been executed [16]; main RFQ parameters

are listed in Table 4. The transition energy between RFQ and DTL has been chosen to be 1 MeV/u, which can be adapted to DTL requirements during further optimization procedures. The RFQ design provides transmission above 90% even with beam currents up to 50 mA.

MAIN RFQ PARAMETERS	
length l	275 cm
frequency f_0	176 MHz
mass to charge ratio A/q	≤ 3
input energy W_{in}	8 keV/u
output energy W_{out}	1 MeV/u
max. electrode voltage at $A/q = 3$ V_{el}	95 kV
input emittance $\varepsilon_{in,rms,normalized}$	0.2 π mm mrad
transmission $T (\leq 50$ mA$)$	>90%
max. pulsed power consumption P_f	350 kW

Table 4: A possible NC-RFQ concept for β-beam application.

The 4-rod structure is basically a chain of strong coupled $\lambda/4$ resonators oscillating in fundamental 0-mode (Figure 2). One resonating ground cell is accomplished by two neighbouring stems mounted on a ground plate forming a short circuit and a capacitive load represented by the electrodes. Frequency and field tuning can easily be done by adjusting additional movable tuning plates. The thermal situation is with 175 W thermal load very relaxed, no extensive cooling system is required.
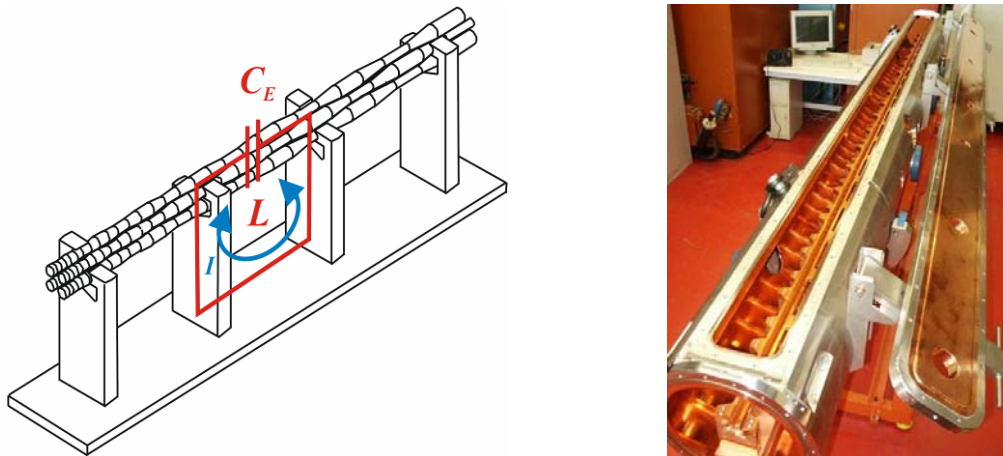

Figure 2: Scheme of the 4-rod-RFQ on the left and - as an example - the SARAF 176 MHz 4-rod RFQ built by NTG Company on the right

DTL design

Possible candidates for NC-DTLs are H-mode cavities (IH-, CH-DTL). In general, H-mode cavities have high shunt impedance. IH-structures are operated in the low energy regime between 0.1 MeV/u and 10 MeV/u with RF-frequencies between 36 and 250 MHz. The IH-DTL structure has no competitor with respect to rf-efficiency. The first DTL part could consist of three IH-structures operated at 176 MHz. The input energy is 1 MeV/u and the output energy 8 MeV/u. The total voltage gain is 22 MV with a length of about 7 m. The total required power per cavity including the beam loading is between 600 and 750 kW. The following DTL section from 8 MeV/u to 100 MeV/u could consist of NC-CH-cavities. CH-cavities are operated in the H_{21}-mode. The CH-

section would be operated at 352 MHz. For this frequency cost efficient klystrons in the MW-range are available. To cover the voltage gain of 276 MV about 46 CH-structures are necessary. The effective voltage per cavity varies between 5 and 7 MV. The total power per cavity is kept below 1 MW including the beam loading. The length of the CH-DTL is about 100 m. Figure 3 shows a prototype of a NC-CH cavity which is being developed for the new proton injector for FAIR [17]. This 70 MeV, 70 mA p-linac will use 11 NC-CH-structures. Figure 4 shows the schematic layout of a possible H-mode linac for β-beam applications. The total length is about 110 m. This corresponds to a real estate gradient of 2.73 MV/m.
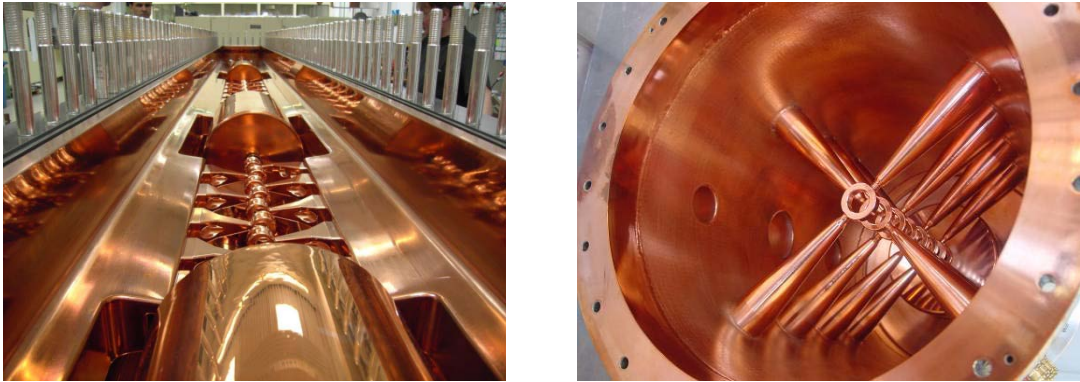

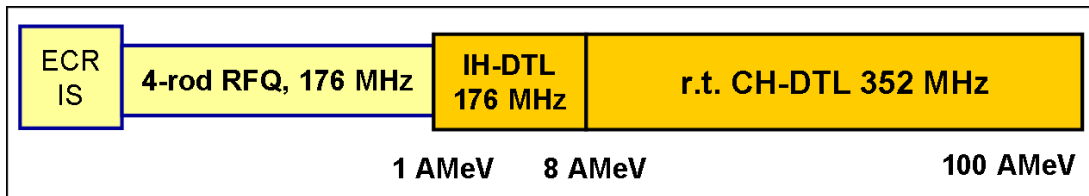*Figure 3: A 217 MHz medicine IH-DTL and the 350 MHz CH-prototype cavity for GSI.*

Figure 4: Schematic layout of an IH/CH-DTL for the production of β-beams.

IV. Accumulation Ring

The possibility to use an accumulation ring using electron cooling between the LINAC and the RCS was studied as a non-baseline option by MSL. Its layout is shown on Figure 5 and its lattice functions on Figure 6. It includes a long section with large β-functions for fast electron cooling, as:

$$1/\text{cooling time} \sim 1/\Theta^3 \sim (\text{ß}/\varepsilon)^{1.5}$$

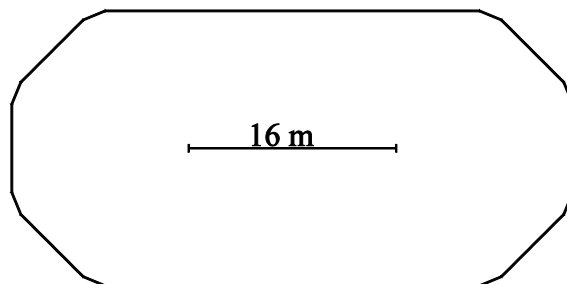with Θ the angle between the electrons and the ions.

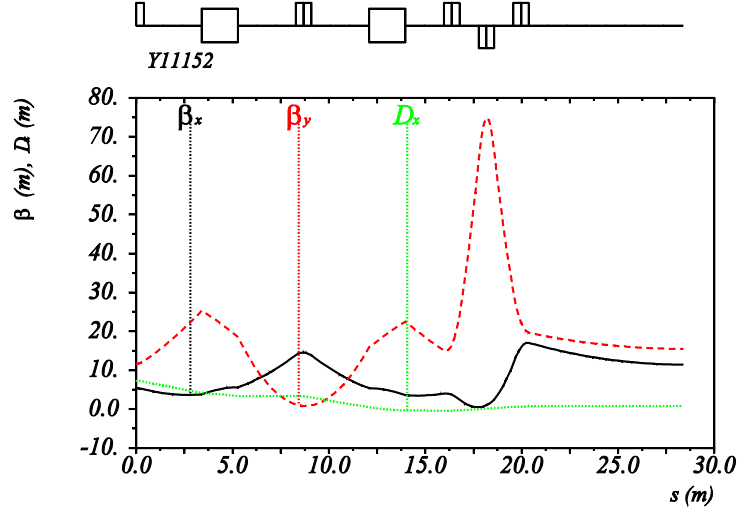*Figure 5 : Schematic layout of an accumulator ring.*

Figure 6 : Lattice functions for a quarter of the cooler ring. The electron cooler would be in the right part of the diagram.

The electron cooling over repetition times of 100ms has been shown to be feasible for $^{18}Ne^{10+}$ as long as ε_x is less than $65\,\pi$ mm mrad, as can be seen in Fig. 3. In the simulations the following parameters were assumed for the electron cooler: 2.5 A electron current, 29 mm electron beam radius and a 0.1 T longitudinal magnetic field. Applying such electron cooling for $^6He^{2+}$ seems more problematic because of the longer time needed for transverse emittance cooling (cooling rate ~ $Q^{1.7}/A$ [18]).
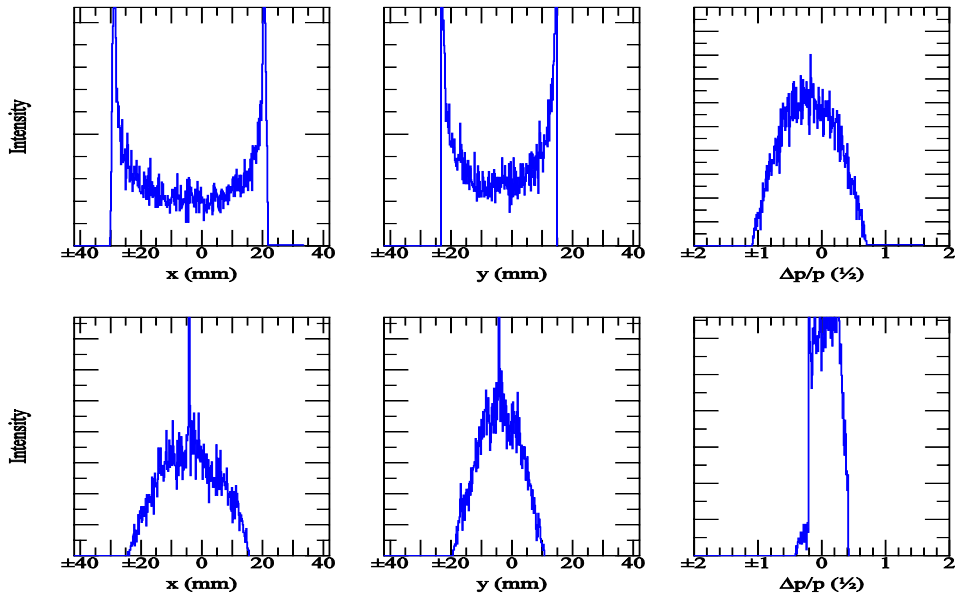

Figure 7 : Simulation of horizontal, vertical, and longitudinal profiles of an $^{18}Ne^{10+}$ beam before (above) and after (below) 0.1 s cooling. Initially all ions have the same emittances, $\varepsilon_x=65\,\pi$ mm mrad and $\varepsilon_y=30\,\pi$ mm mrad. Intrabeam scattering is not included so after cooling the central peak becomes unrealistically high.

Such accumulator ring could make beneficial use of the ramping time of the PS for accumulating $^{18}Ne^{10+}$ ions, which lost in the case of the baseline scenario (see Figure 8). This way it would permit a more flexible mode of operation where bunches could be stored at injection energy in the SPS

9

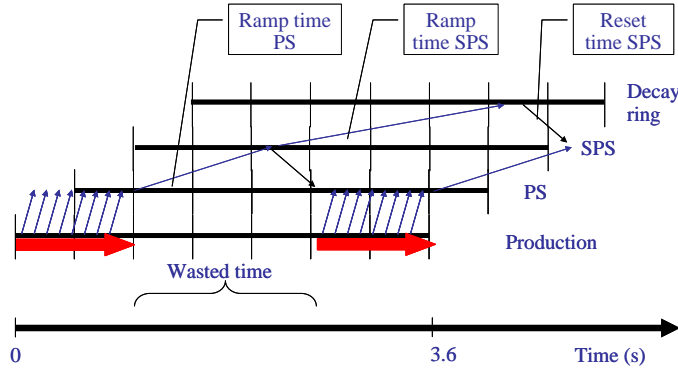rather than in the PS (as shown in Figure 8) for limiting decay losses.

Figure 8 : A complete cycle for the baseline beta-beam complex consists of injection into the PS, storage of bunches at PS injection energy, acceleration in the PS and SPS and finally injection into the decay ring.

Assuming that 10 bunches are stored within the SPS, an optimum of 23 ECR bunches accumulated in the ring has been found for optimizing the throughput of Beta-Beam for neutrinos arising from the decay of ^{18}Ne (Figure 9). In such conditions, the ^{18}Ne in-target yield required for achieving the annual rate of 10^{18} neutrinos would be reduced by a factor of 4 compared to the baseline scenario.
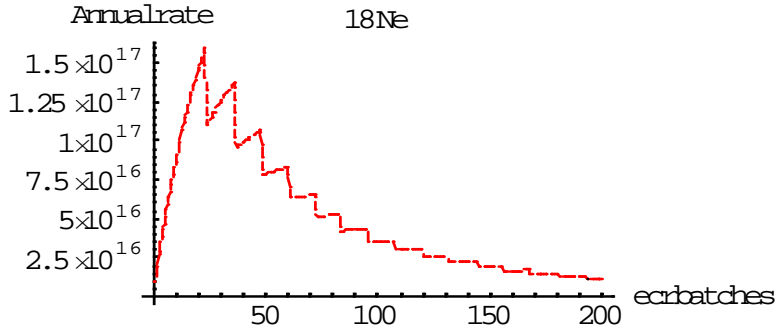

Figure 9 : The annual rate of neutrinos along one straight section of the decay ring as a function of the number of pulses from the linac that are accumulated in the accumulator ring. A total of 10 bunches from the accumulator ring is stored in the SPS before further acceleration and injection into the decay ring. The discontinuities in the curve are due to a requirement that the PS and SPS cycle time must be a multiple of 1.2 seconds.

The accumulation ring is presented with more details and a cost estimate in [16].

V. Design of the Rapid Cycling Synchrotron

The RCS is described in detail in [19] (IPNO, CNRS/IN2P3). Its preliminary design was presented in [20]. We recall here the main elements of its conceptual design report [19], [21]. A dedicated Radio-Protection study was performed at CERN, showing no showstopper for the RCS. It is reported here and in [16] together with dynamic vacuum studies performed by GSI.

RCS general parameters

The RCS accelerates He and Ne ion beams from 100 MeV/u to a maximum magnetic rigidity of

14.47 T.m (that is the rigidity of 3.5 GeV protons) with a repetition rate of 10 Hz. The threefold symmetry lattice proposed is based on FODO cells with missing magnets providing three achromatic arcs and three sufficiently long straight sections for accommodating the injection system, the high energy fast extraction system and the accelerating cavities. According to the first design, the number of dipoles has been increased to obtain a transition energy allowing acceleration of protons up to 3.5GeV. These latters have been split into two parts separated by a drift space for inserting absorbers to intercept the decay products. Finally the physical radius has been adjusted to 40m in order to facilitate the synchronization between the CERN PS and the RCS and therefore the transfer of bunches from one ring to the other. As a consequence, the ring is composed of 60 short dipoles and 48 quadrupoles. A schematic view of the RCS layout is shown in Figure 10 and the main parameters are summarized in Table 5.
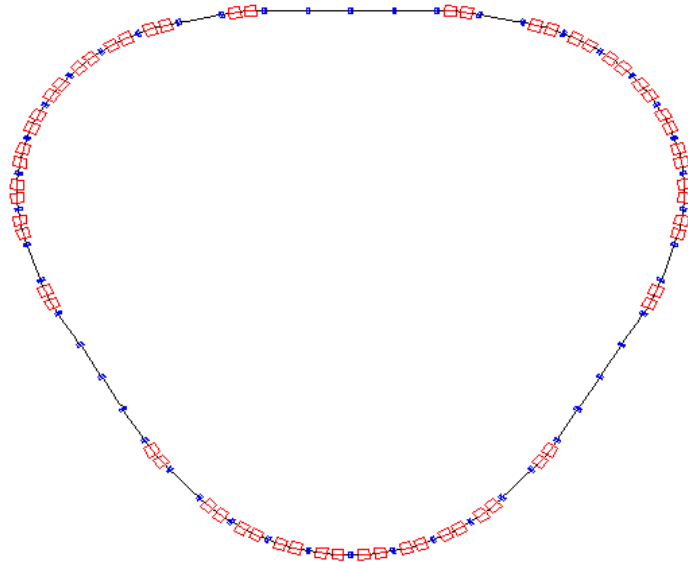

Figure 10: Schematic layout of the RCS

Circumference	251.32 m
Superperiodicity	3
Physical radius	40 m
Injection energy	100 MeV/u
Maximum magnetic rigidity	14.47 T.m
Repetition rate	10 Hz
Number of dipoles	60
Number of quadrupoles	48

Table 5: Main parameters of the ring

Optical design

The RCS is partitioned into 24 FODO cells, 6 in arcs and 2 in a straight section. The betatron phase advance per cell (i.e quadrupole strength) and the length of the 2 sections without dipoles in the arcs have been adjusted so as to cancel the dispersion function in long straight sections and to obtain, with only two quadrupoles families, a working point located in a region of the tune diagram which is free of systematic resonances up to the fourth order. Lattices function of one period calculated

with BETA [22] are shown in Figure 11. Dipoles are only 1.4m long in order to obtain a maximum magnetic field of 1.08T and therefore to avoid a large ramping rate for the 10Hz operation. Quadrupoles have a length of 0.4 m and a maximum gradient of less than 11 T/m. The diluted transverse emittances in the RCS after multi-turn injection are calculated from the emittances required in the PS at the transfer energy with a possible blow-up of 20 %
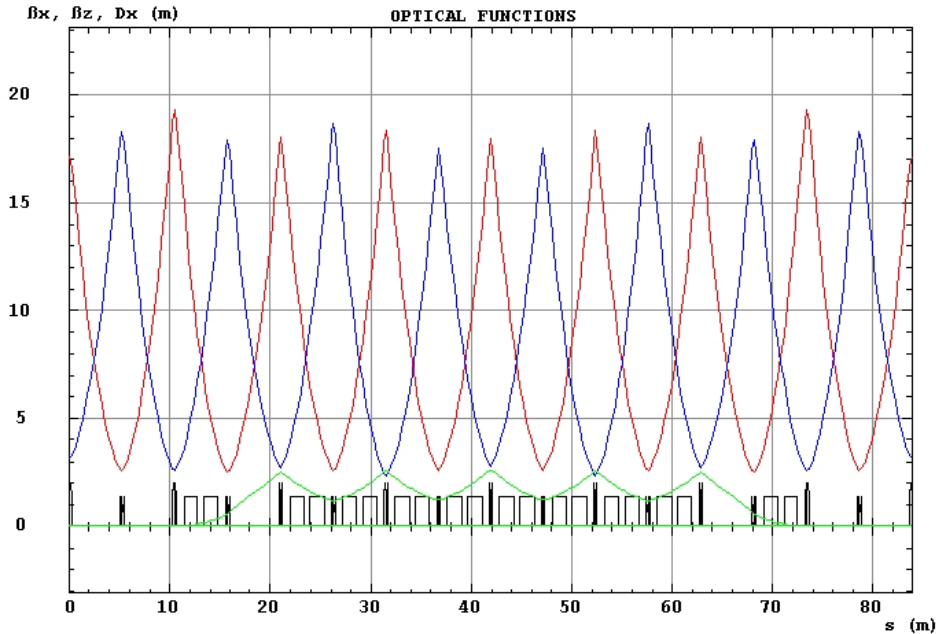

Figure 11: Optical functions for one superperiod

.

Injection

It is assumed that the ion source delivers a beam pulse of 50 μs. The revolution period of ions at 100 MeV/u being 1.96μs, the injection process takes place over several (26) turns in the machine and is therefore referred to as multi-turn injection. Ions are injected into one of the long straight section by means of an electrostatic septum and at least 2 pulsed kickers producing a local closed orbit bump which places the distorted orbit near the septum for the first injected turn and which moves it away from the septum on subsequent turns until it has collapsed and which moves it away from the septum on subsequent turns until it has collapsed. The aim of the injection process is to maximise the number of injected ions within the specified transverse emittance. Optimum filling in the horizontal phase space is achieved when incoming ions are injected with a position and a slope which minimize their Courant and Snyder invariant. In the vertical phase space the dilution is obtained by a betatron function mismatch and a beam position offset. The Figure 12 shows the diluted emittances in transverse phase spaces after multiturn injection, obtained with the Winagile code. We obtain an injection efficiency of 80% after optimization.
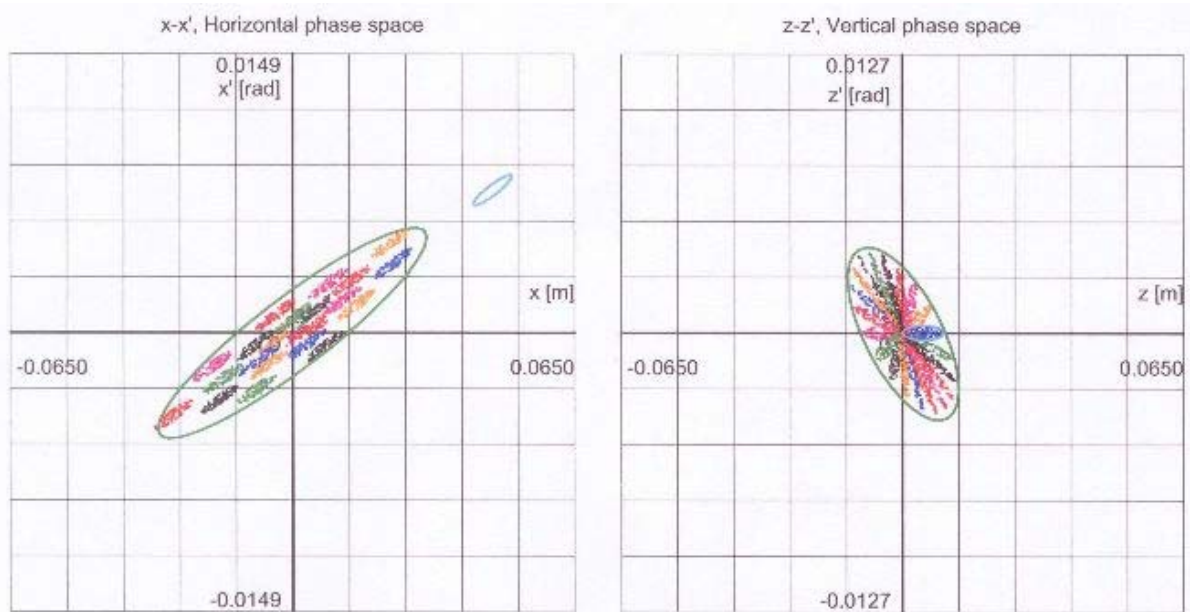
Figure 12: Phase space distributions of the multi-turn injected beam (left : horizontal plane, right : vertical plane)

Acceleration

The Programs for RF voltage and synchronous phase are determined by the following requirements:
- In order to maintain the central trajectory on the reference orbit, the energy gain per turn must be related to the variation of the magnetic field.
- The voltage must provide a sufficient bucket area to enclose all the longitudinal emittance.
- The trapping process must be optimized to minimize the beam losses.
- At extraction the bunch must be matched to the bucket of the next machine.

After injection the circulating beam is continuous and occupies a rectangle in the longitudinal phase space. To capture the injected beam, one stationary bucket is created. During trapping, the magnetic field is clamped at is minimum value for a period of few ms and the synchronous phase is zero. The RF voltage is optimized to obtain a beam rotation of about 90° and a momentum spread as small as possible before the acceleration phase.

When the magnetic field starts to ramp, the synchronous phase is shifted and the beam is accelerated. The program of the rise of the RF voltage and the synchronous phase variation are defined to obtain a sufficiently large bucket area and to minimize losses. Finally, at the end of the cycle, the bunch is manipulated so as to be matched to one of the PS RF buckets. The RF cycle has been simulated and optimized with the code ACCSIM developed at TRIUMF [23]. The Figure 13 shows the variation of the synchronous phase and voltage during cycle for He ions.
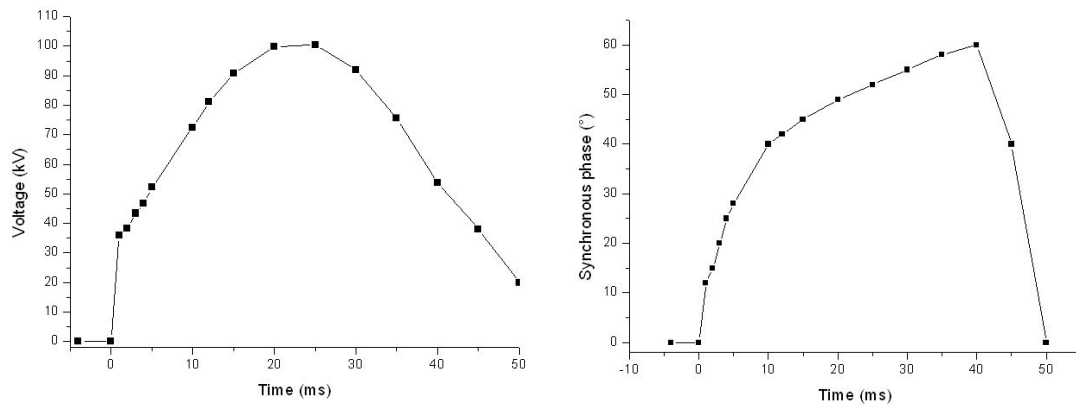
Figure 13: Synchronous phase and voltage evolution during cycle for He ions

Other beam optics aspects

Several beam dynamics studies have been investigated in order to assess the feasibility of the RCS, in addition to the results presented here. Unavoidable magnets misalignments and dipole field errors can affect the RCS closed orbit. Distortions to be expected have been statistically estimated assuming standard error tolerances and a correction system has been defined. In fast ramping machines such as the Beta-Beam RCS, eddy currents induced in metallic vacuum chamber walls by the time varying magnetic field produce various field components acting on the beam. In dipoles vacuum chambers, one important component is a sextupole which modifies the natural chromaticity of the ring. The associated effects have been estimated and it has been shown that they could be compensated for so that they do not pose problems from the point of view of beam dynamics. Finally, after injection , ions beams are extracted in a single turn and directed towards the CERN PS. A fast extraction system consisting of fast kickers and septum magnets has been defined to produce the deflection angle required to eject the beam from the ring. All the beam dynamics studies made on the RCS have shown that there are no showstoppers on this ring. It can be realized with the present technology.

Vacuum System Requirements for the RCS

The parameters used for the simulations of the dynamic pressure are listed in Table 6 and Table 7. The data in Table 6 were taken from "The EURISOL Beta-beam Facility Parameter and Intensity Values" generated at 12. March 2009.

The loss distribution for both ^{6}He^{2+} and ^{18}Ne^{10+} ions are shown in Figure 14. The losses are dominated by radioactive decay. Losses due to charge exchange are negligible, as the cross sections for electron capture are very small. The ^{6}He^{2+} ions which decay within the straight sections hit the vacuum chamber within the first and second dipole doublet. Due to their higher magnetic rigidity the decayed ^{18}Ne^{10+} ions hit the chamber between the first and second dipole doublet and the corresponding quadrupole magnets, while some ions hit the magnets themselves.

14

Parameter	Value for $^6\text{He}^{2+}$	Value for $^{18}\text{He}^{10+}$
Energy (Injection)	100 MeV/u	100 MeV/u
Mag. Rigidity (Injection)	4.45 Tm	2.660 Tm
Energy (Ejection)	787 MeV/u	1650 MeV/u
Mag. Rigidity (Ejection)	14.49 Tm	14.46 Tm
Ramping Rate	24 T/s	21.27 T/s
Cycle Time	0.1 s	0.1 s
Cycle Frequency	10 Hz	10 Hz
Losses at Injection	20 %	20 %
Emittance (horizontal)	72.4 mm mrad	72.32 mm mrad
Emittance (vertical)	38.8 mm mrad	38.68 mm mrad
Injected Ions/Cycle	8.53×10^{11}	1.5×10^{11}

Table 6: Beam parameters used with StrahlSim.

Parameter	Value
Typical Aperture (horizontal)	10 mm
Typical Aperture (vertical)	8 mm
Volume of Beam Pipe	$1.58 \, \text{m}^3$
Static Residual Gas Pressure	1×10^{-9} mbar
Effective Pumping Speed	see text

Table 7: Vacuum parameters used with StrahlSim.

The transmission is almost independent of the pumping speed and the residual gas pressure. This is due to the low cross sections for electron capture. Beam losses at injection are crucial for the transmission. Figure 15 shows the number of particles in the RCS ring and the accumulation of particles in the PS. This calculation assumes a beam loss at injection of 20 %. This assumption leads to 6.58×10^{11} ejected $^6\text{He}^{2+}$ ions and 2.07×10^{11} $^{18}\text{Ne}^{10+}$ ions per cycle. The number of accumulated particles within the PS after 20 injections from the RCS considering ongoing decay is about 8.12×10^{12} for $^6\text{He}^{2+}$ and 3.39×10^{12} for $^{18}\text{Ne}^{10+}$. This is less than the designated numbers of 1.1×10^{13} and 4.51×10^1 for $^6\text{He}^{2+}$ and $^{18}\text{Ne}^{10+}$ respectively.

One possibility to increase the number of particles accumulated within the PS is to reduce the losses at injection. Figure 16 shows the dependence of the number of ejected particles on the losses at injection. In order to eject more than 8×10^{11} $^6\text{He}^{2+}$ ions or 2.5×10^{11} $^{18}\text{Ne}^{10+}$ ions per cycle one has to reduce the losses to about 3 %.
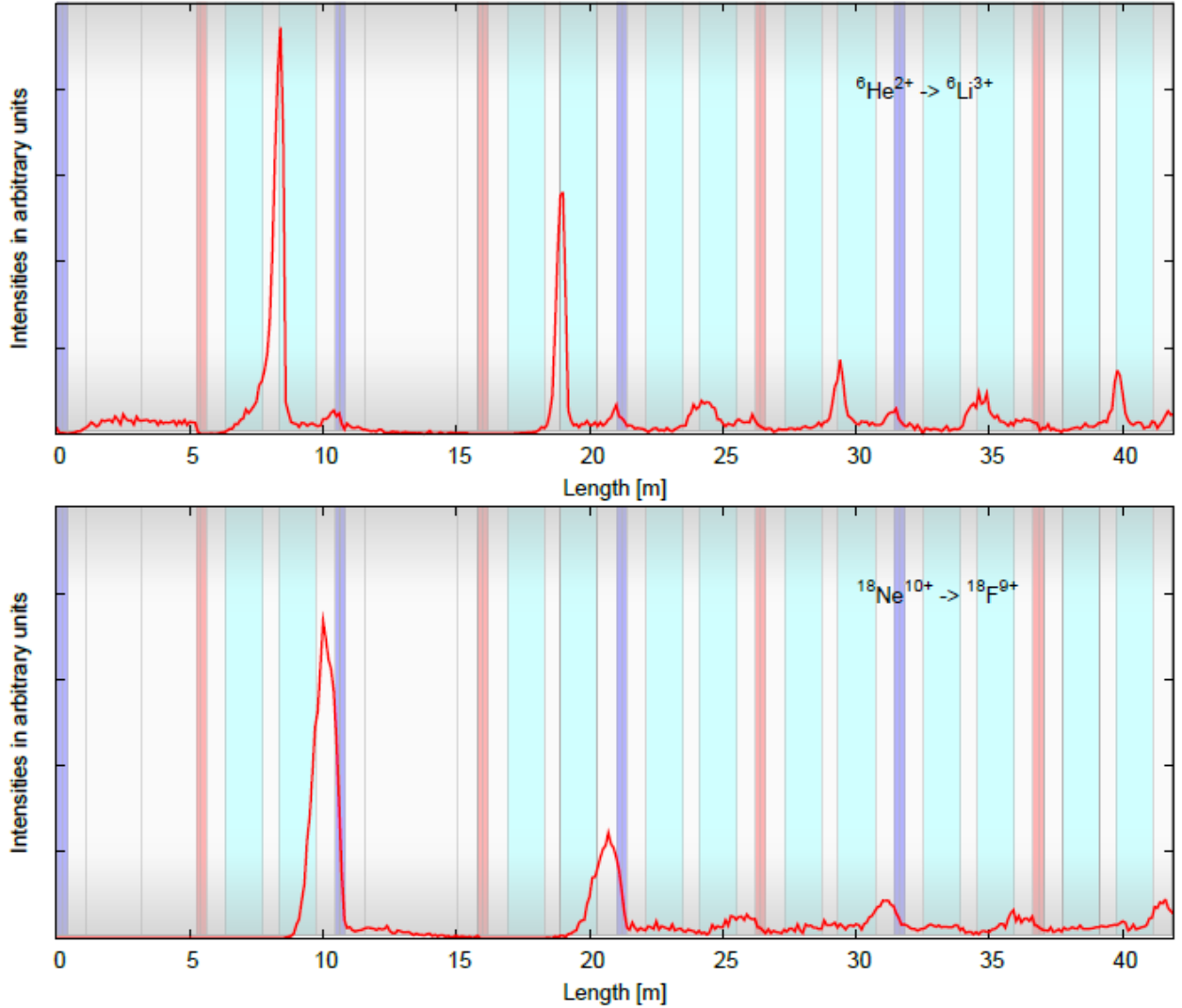
Figure 14: Loss distribution for $^6He^{2+} \rightarrow ^6Li^{3+}$ (top) and $^{18}Ne^{10+} \rightarrow ^{18}F^{9+}$ (bottom) at injection energy. Dipole magnets are shown in light blue, quadrupole magnets in red and blue.

In the following, the required pumping speed of the vacuum system in order to maintain a residual gas pressure below 1×10^{-8} mbar is investigated. Figure 17 shows the pressure within the RCS over 20 cycles for effective pumping speeds varying between 2 and 10 m^3/s. Using $^{18}Ne^{10+}$ as projectile ion the pressure stays below 1×10^{-8} mbar for pumping speeds greater than 2 m^3/s, reaching a maximum for S_{eff}=5 m^3/s of about 6.5×10^{-9} mbar. The situation for $^6He^{2+}$ is different. For pumping speeds less than 10 m^3/s the pressure goes up exceeding the 1×10^{-8} mbar limit. This is due to beam losses at injection. The pumping speed is not sufficient to remove enough of the gas desorbed at injection before the next cycle starts.
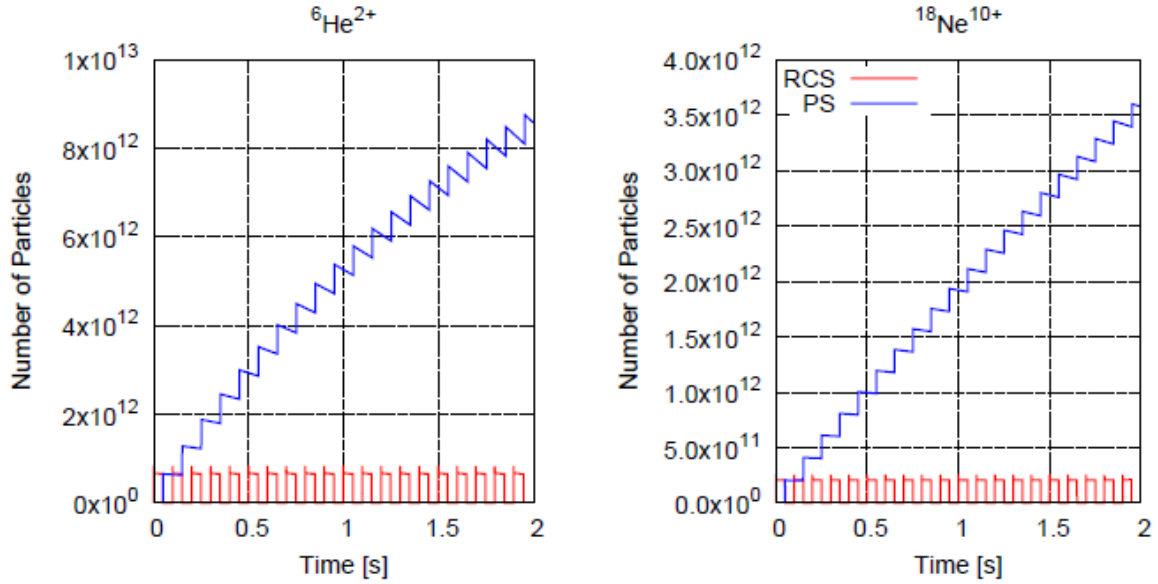
16

Figure 15: Number of particles over twenty cycles for $^6He^{2+}$ (left) and $^{18}Ne^{10+}$ (right). The blue line shows the accumulation of the particles within the PS.
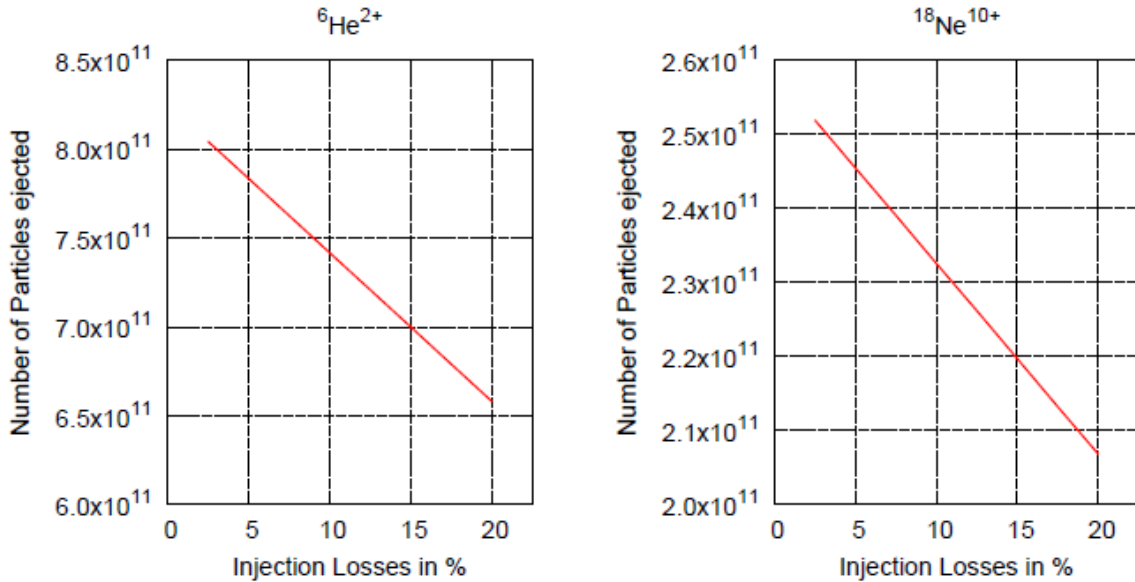

Figure 16: Number of ejected particles against beam losses at injection for an effective pumping speed of $S_{eff}=5$ m^3/s for $^6He^{2+}$ (left) and $^{18}Ne^{10+}$ (right).

As it is desirable to have a conventional pumping system installed in the RCS, the best way to work around this problem would be to reduce the beam losses at injection. If it is possible to reduce the losses to about 10% an effective pumping speed of $5m^3/s$ would be sufficient to stay below the 1×10^{-8} mbar limit. This is visualized in Figure 18. If the injection losses cannot be reduced one has to consider an increase of the pumping speeds for example by applying NEG-coating to a part of the vacuum chamber. This analysis was done for $^6He^{2+}$ only, since the pressure evolution for $^{18}Ne^{10+}$ is not critical. Because most beam losses occur within or close to the dipole magnets, it is best to apply an eventually needed NEG-coating to these. Figure 19 shows the pressure in case of NEG-

17

coated dipole chambers for $^6He^{2+}$. The number of NEG-coated dipole chambers was varied between 8 and 20 per arc. For all calculations the maximum residual gas pressure is 5×10^{-9} mbar, while the effective pumping speed due to the NEG ranges from about 310 to 650 m^3/s for 8 and 20 coated dipoles respectively.
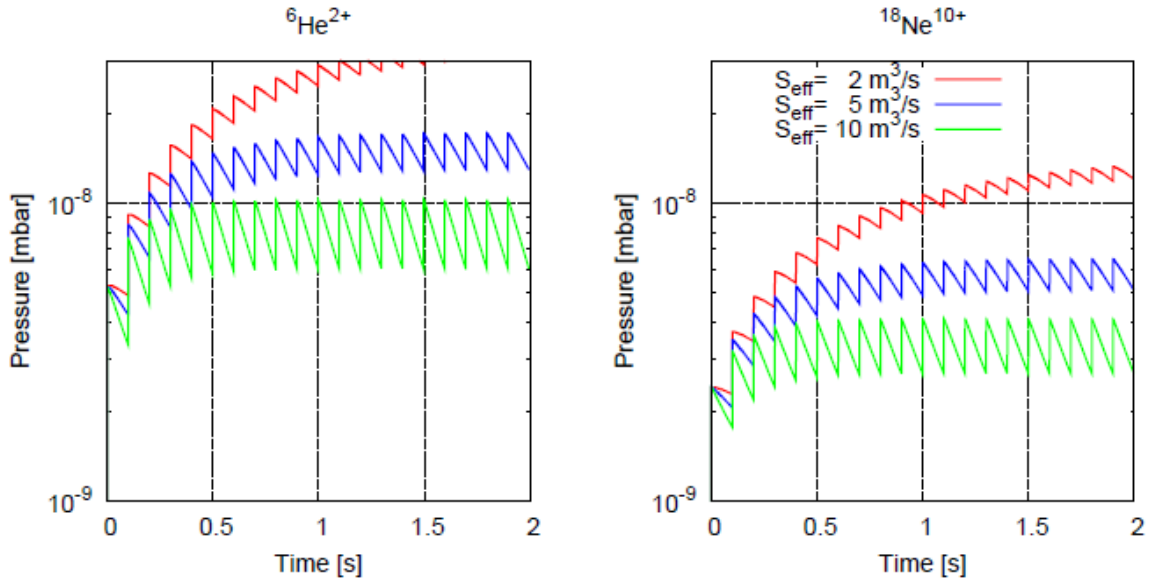

Figure 17: Pressure evolution over 20 cycles for different effective pumping speeds (2 to 10 m^3/s) for $^6He^{2+}$ (left) and $^{18}Ne^{10+}$ (right).
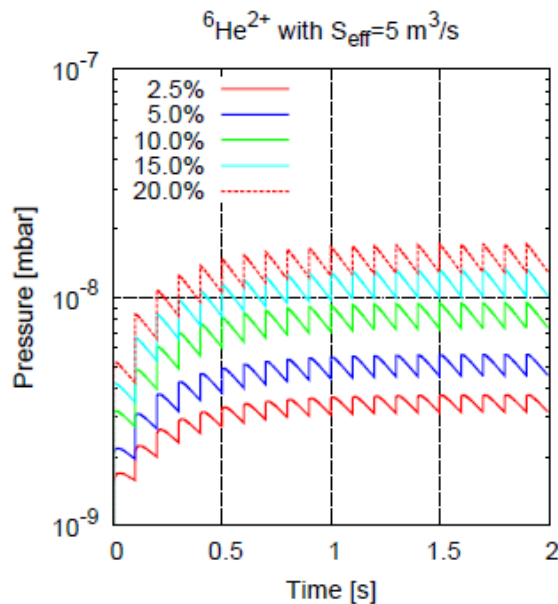
Figure 18: Pressure evolution for different losses at injection ranging from 2.5 to 20 %. The pumping speed for the calculations is S_{eff}=5m^3/s.

Of course one has to consider an ongoing saturation effect, which reduces the pumping speed of the NEG coating over time. If NEG-coating is needed all dipole magnets should be treated with NEG to ensure a stable residual pressure over the whole operation time. It is important to remark, that only beam losses inside the RCS ring are relevant for the calculation of the pressure bump at injection. In

this sense a beam loss of 20% means that all particles are lost inside the machine. Losses outside the machine, e.g. inside a drift line just before injection do not contribute to the pressure rise and must be subtracted. In general it is hard to distinguish these two effects.
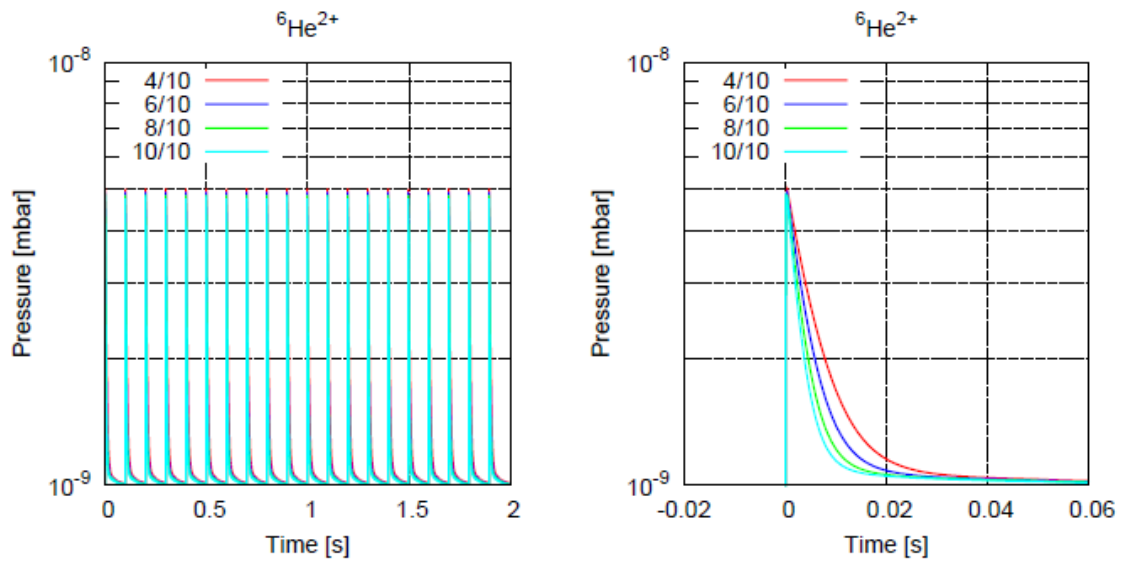

Figure 19: Pressure evolution with NEG-coated dipole chambers. The projectile ion is $^6He^{2+}$ and the pumping speed is S_{eff}=5 m^3/s. The number of NEG-coated dipole doublets per arc was altered in the range from 4 to 10 for the different lines.

The beam losses and their effects on the residual gas pressure have been investigated using the program StrahlSim. Concerning the required effective pumping speed, 5 m^3/s is sufficient to stay below 1×10^{-8} mbar when using $^{18}Ne^{10+}$ as the projectile ion. The maximum pressure for this scenario is 6.51×10^{-9} mbar. In case of $^6He^{2+}$ an effective pumping speed of 5 m^3/s would not be enough if there are 20% beam losses at injection inside the RCS ring. Reducing the beam losses by a factor of two and therefore reducing the pressure bump induced by desorbed gases, would lead to a maximum pressure slightly below the 1×10^{-8} mbar limit.

If the losses at injection cannot be reduced, an effective pumping speed of more than 10 m^3/s would be needed. This is to our best knowledge not achievable by using conventional pumping techniques. If such a pumping speed is required one has to consider applying a NEG-coating to the vacuum chambers of the dipole magnets. It was shown that NEG-coating leads to a maximum residual gas pressure of 5×10^{-9} mbar.

RCS radioprotection studies

Detailed radioprotection studies were realized according to the different loss mechanisms within the RCS. They permitted to define the shielding required by the machine operation, the classification of the area and eventual limits on the release of airborne activity.
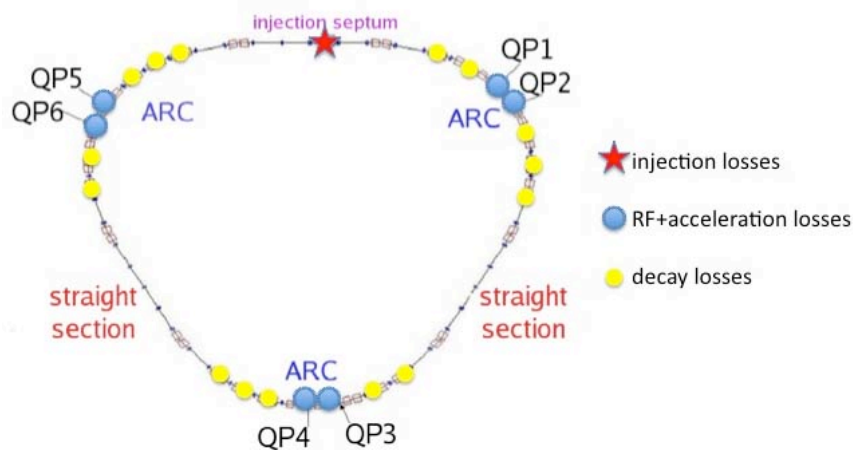
Figure 20 : Layout of the RCS. The different kinds of losses and their locations in the ring are shown.

Beam losses can be divided into injection, decay and RF capture-acceleration losses. At injection 30% of the beam is lost on the septum. Decay losses are uniformly distributed in the dipoles and in the short straight sections in the arcs during all the magnetic cycle. RF capture-acceleration losses are point losses that occur in the families of quadrupoles in the arcs as indicated in Figure 20 (QP). All the percentages of beam lost in the RCS are summarized in Table 1: they are given for 3 energies in the machine energy range. For injection loss percentages are referred to the incoming beam, for decay and RF-acceleration losses to circulating beam.

Energy (MeV/u)	Injection	Decay	RF capture - acceleration
100	30%	0.10 (0.45) %	5.70 (9.40) %
400 (640)	-	0.80 (0.20) %	2.85 (8.50) %
787 (1650)	-	1.80 (0.70) %	4.75 (5.05) %

Table 8 : Beam loss percentages for ^{6}He (^{18}Ne)

The areas around the RCS tunnel will probably be classified as supervised radiation areas during operation, with a dose rate constraint of 3 μSv h^{-1}: the respect of this value would require concrete shielding thicknesses ranging from 3 to 5 m, depending on the position in the tunnel. In these places where different kinds of losses occur, the thickness imposed by the dominating mechanism was considered.

In the released airborne activity study a constant rate of 10000 m^3 h^{-1} was chosen for the ventilation system in the RCS tunnel. In this condition, the effective dose given to the reference population in one year of operation was estimated to be in the order of 0.7μSv for the worst ion, i.e. ^{18}Ne. It is well below the reference value for CERN emission and could be further decreased enlarging the ventilation outlet dimensions. Figure 21 presents the contributions of the main radionuclides to the annual effective dose.
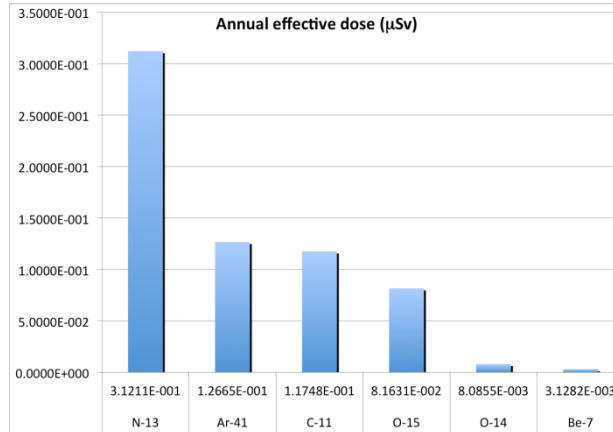
Figure 21 : Annual effective dose to the reference population: contributions from the main radionuclides.

For the inhalation dose to workers that could access the tunnel during shutdown periods a conservative assumption was made: the ventilation system is not operating. The intervention time depends on dose rates and on whether or not the ventilation system is on. For a 1-hour intervention the integrated dose does not exceed the constraints, much less than 1 μSv even without waiting time (see Table 9). Furthermore, if the ventilation system is working a waiting time before access of nearly 20 minutes is enough to completely change the air in the tunnel.

t_{irr}	t_{wait}	t_{int}	Inhalation Dose (μSv)
24 hours	0	1 hour	1.41E-01
24 hours	1 hour	1 hour	6.48E-02
1 week	0	1 hour	2.56E-01
1 week	1 hour	1 hour	1.80E-01
3 months	1 hour	1 hour	9.30E-01

Table 9 : Inhalation dose to workers for various irradiation times t_{irr} and waiting times t_{wait}. t_{int} is the intervention time.

Dose rates from material activation were calculated for a 3-month continuous operation and 3 different waiting times of 1 hour, 1 day and 1 week (Figure 22). The results show that, according to CERN area classification, the RCS tunnel is likely to be classified as a limited stay area, accessible 1 week after the shutdown. The doses do not decrease much after 1 week because the residual radionuclides that mostly contribute to the total dose have half-lives longer than 1 week. The high activation of the machine elements that remains after 1 week may require a remote handling system for the maintenance.
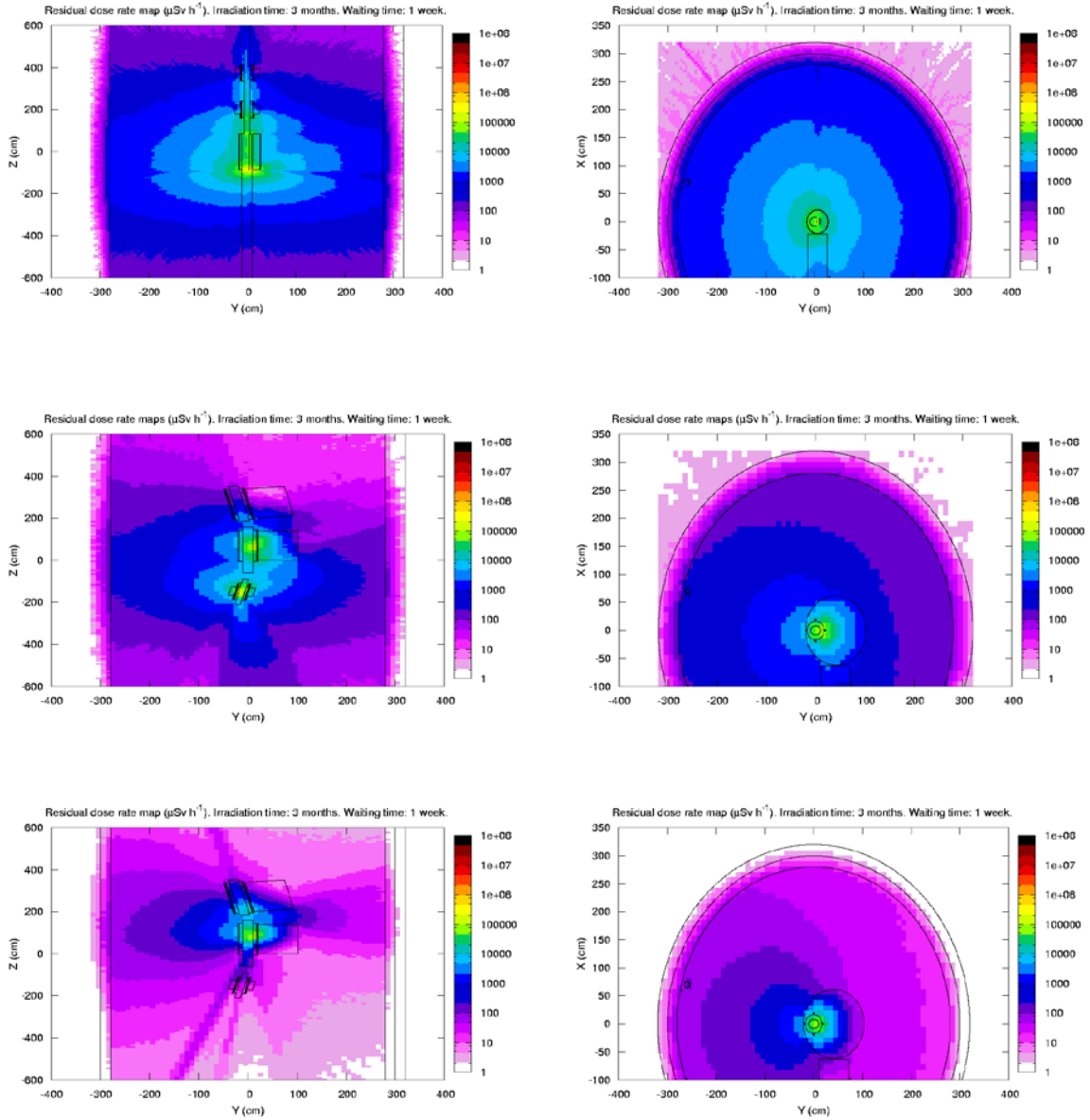
Figure 22 : Residual dose rates for a 3-month irradiation and 1-week waiting times for septum, quadrupoles and dipoles in the arcs for ^{6}He ions. Left: top view. Right: front view.

VI. Ion acceleration scenarios in PS and SPS

Ion acceleration in the PS and SPS is a routine operation since many years. Different ion types from light ions such as sulfur up to heavy ions such as lead have been accelerated. We summarize here the results of the study realized by CERN within FP6 for the acceleration of the Beta-Beam nuclides ^{6}He and ^{18}Ne [24]. Dynamics vacuum studies were in addition performed by GSI. They are reported in [16]. An acceleration in the PS2 is being followed at CERN as a non-baseline option. Finally dedicated studies for protecting the PS magnets from too high power deposition, and Radio-Protection studies were initiated at GSI with the help of CERN [16].

PS - RF considerations

Since the beta-decay lifetime at injection in the PS is much longer than the cycle time of the RCS, it pays to operate the PS at the rf harmonic consistent with the 10 MHz upper frequency limit of the accelerating cavities and to transfer the maximum number of batches from the RCS. Thus, the PS harmonic of choice becomes h=21 and 20 bunches are accumulated one by one leaving one rf bucket empty to accommodate the extraction kicker risetime.

Figure 23 shows how beta-decay diminishes the number of helium ions accumulated on the PS injection plateau. Figure 24 shows the corresponding relative intensity along the bunch train. As little as 40% of the first helium bunch remains when the last one arrives.
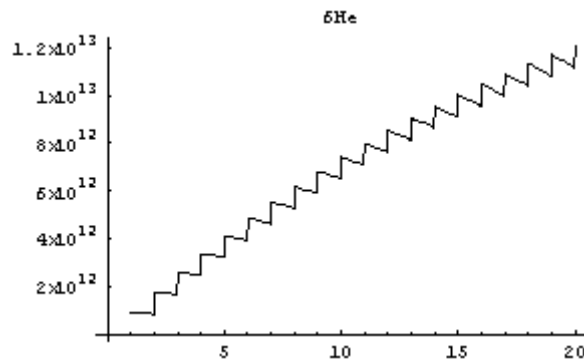

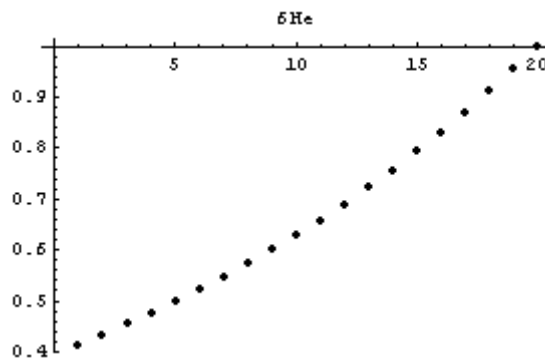*Figure 23: Number of helium ions accumulated in the PS versus RCS batches.*

Figure 24: Relative helium intensity along the bunch train in the PS.

The situation is better in the neon case due to its longer half-life and more advantageous charge-to-mass ratio, but the PS extraction kicker gap must still be established at a different position within the bunch train from batch to batch in order to even out the bunches that are ultimately stored in the decay ring.

The longitudinal emittance that the PS must deliver is 0.80 eVs in the case of helium ions and 1.8 eVs for neon. This implies matching voltages of ~30 kV and ~10 kV, respectively, in order to provide the requisite bunch length of 20 ns at ejection. No bunch shortening gymnastics are required due to the addition of a 40 MHz rf system in the receiving SPS (see next section).

Vacuum System Requirements for the PS

The parameters used for the simulations of the dynamic pressure are listed in Table 10 and Table 11. The data in Table 10 were taken from "The EURISOL Beta-beam Facility Parameter and Intensity Values" generated at 12. March 2009.

Parameter	Value for $^{6}\text{He}^{2+}$	Value for $^{18}\text{He}^{10+}$
Energy (Injection)	787 MeV/u	1650 MeV/u
Mag. Rigidity (Injection)	14.49 Tm	14.46 Tm
Energy (Ejection)	7780 MeV/u	13.5 GeV/u
Mag. Rigidity (Ejection)	86.93 Tm	86.47 Tm
Ramping Rate	1.271 T/s	1.263 T/s
Cycle Time	3.6 s	3.6 s
Cycle Frequency	0.278 Hz	0.278 Hz
Losses at Injection	0 %	0 %
Emittance (horizontal)	26.58 mm mrad	15.92 mm mrad
Emittance (vertical)	14.19 mm mrad	8.52 mm mrad
Injected Ions/Cycle	8.29×10^{11}	2.59×10^{11}

Table 10: Beam parameters used with StrahlSim.

Parameter	Value
Typical Aperture (horizontal)	14.6 mm
Typical Aperture (vertical)	8.6 mm
Volume of Beam Pipe	6.2 m^3
Static Residual Gas Pressure	1×10^{-9} mbar
Effective Pumping Speed	11.5 m^3/s

Table 11: Vacuum parameters used with StrahlSim.

The loss distributions for both $^{6}\text{He}^{2+}$+and $^{18}\text{Ne}^{10+}$ ions are shown in Figure 25 for one section of the PS. The losses are dominated by radioactive decay. Losses due to charge exchange are negligible, as the cross sections for electron capture are very small. For both $^{6}\text{He}^{2+}$ and $^{18}\text{Ne}^{10+}$ the losses are spread over the whole ring.

The transmission was checked by using an ideal cycle assuming the maximum number of particles coming from the RCS. The numbers were taken from"The EURISOL Beta-beam Facility Parameter and Intensity Values". A graphical representation is given in Figure 26.

For $^{6}\text{He}^{2+}$ there are 20 injections from the RCS with 8.29×10^{11} ions per injection, which accumulates to 1.06×10^{13} particles before the acceleration starts. This leads to 9.37×10^{12} ejected ions. This number is close to the desired number of 9.53×10^{12}. For $^{18}\text{Ne}^{10+}$ there are 20 injections with 2.59×10^{11} particles each. The number of accumulated particles is 4.51×10^{12}. Given these numbers there were 4.29×10^{12} particles ejected. This is again very close to the desired number of 4.31×10^{12}.
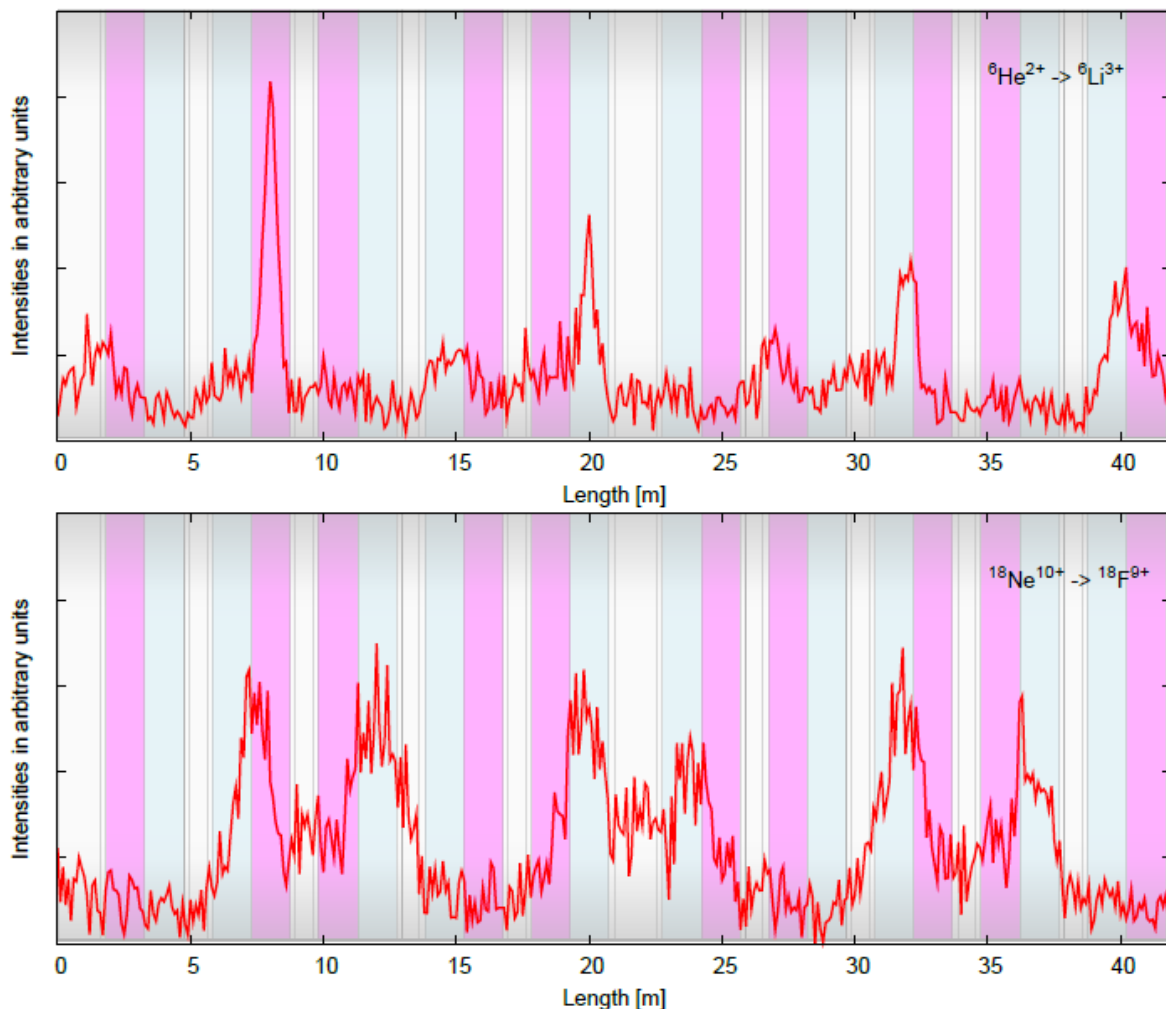
Figure 25: Loss distribution for $^6He^{2+}\rightarrow{}^6Li^{3+}$ (top) and $^{18}Ne^{10+}\rightarrow{}^{18}F^{9+}$ (bottom) at injection energy. The combined function magnets are shown in light blue/magenta.

The effective pumping speed is essential for the simulation with StrahlSim to get a reliable pressure evolution. The effective pumping speed used in the simulations was estimated as follows. There are 147 vacuum pumps along the PS ring, which were assumed to be equally distributed. Together with the given total pumping speed of 38 m^3/s, StrahlSim calculates an effective pumping speed of about 11.5 m^3/s.

The pressure evolution over one and five cycles for $^6He^{2+}$ and $^{18}Ne^{10+}$ is shown in Figure 27. The pressure stays well below 1×10^{-8} mbar for both $^6He^{2+}$ and $^{18}Ne^{10+}$, when a pumping speed of 11.5 m^3/s is assumed. The maximum pressure is 5.8×10^{-9} mbar and 3.2×10^{-9} mbar for $^6He^{2+}$ and $^{18}Ne^{10+}$ respectively. The minimum effective pumping speed required in order to stay below 1×10^{-8} mbar was estimated to be about 9 m^3/s (dashed lines in Figure 27). If the pumping speed is less and $^6He^{2+}$ is used as the projectile ion, the pressure limit will be exceeded. Operating the PS with $^{18}Ne^{10+}$ the minimum pumping speed is about 7 m^3/s.
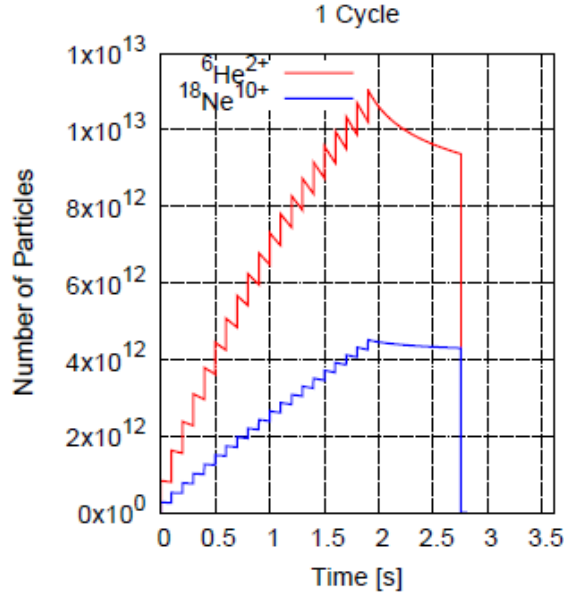
Figure 26: Number of particles over one cycle for $^6He^{2+}$ and $^{18}Ne^{10+}$.
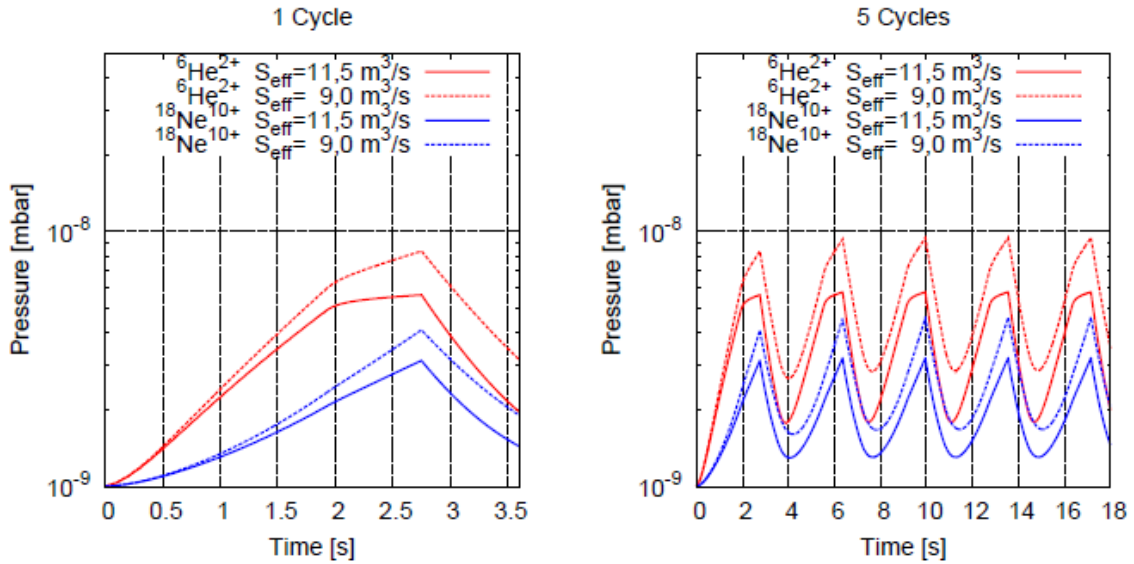

Figure 27: Pressure over one and five cycles for different effective pumping speeds (11.5 and 9.0m³/s) for $^6He^{2+}$ and $^{18}Ne^{10+}$.

The beam losses and their effects on the residual gas pressure have been investigated using the program StrahlSim. At an accelerator operation with $^6He^{2+}$ and $^{18}Ne^{10+}$ as projectile ions an effective pumping speed of 11.5 m³/s in the PS ring is sufficient. This pumping speed is delivered by the existing vacuum system of the PS. The minimum effective pumping speeds needed for a stable operation were estimated to be 9 m³/s and 7 m³/s for $^6He^{2+}$ and $^{18}Ne^{10+}$ respectively.

PS Radioprotection studies

A preliminary study has focused on two radiation protection aspects related to the operation of PS as part of a Beta-Beam facility, namely the induced radioactivity in the magnets and the air activation. A complete study would also include an analysis of the existing shielding (in particular

26

with respect to those points, like the PS bridge, where the shielding is relatively thin), the prediction of induced radioactivity in hot components like septum magnets and the activation of the cooling water of the magnets. At this stage it is not possible to perform such a detailed study because of the lack of information on the operation conditions and on the exact particle loss distribution. Nevertheless, during this study it was possible to assess the impact that the Beta-Beam operation would have on the radiation level expected during maintenance and on the release of radioactivity to the environment.
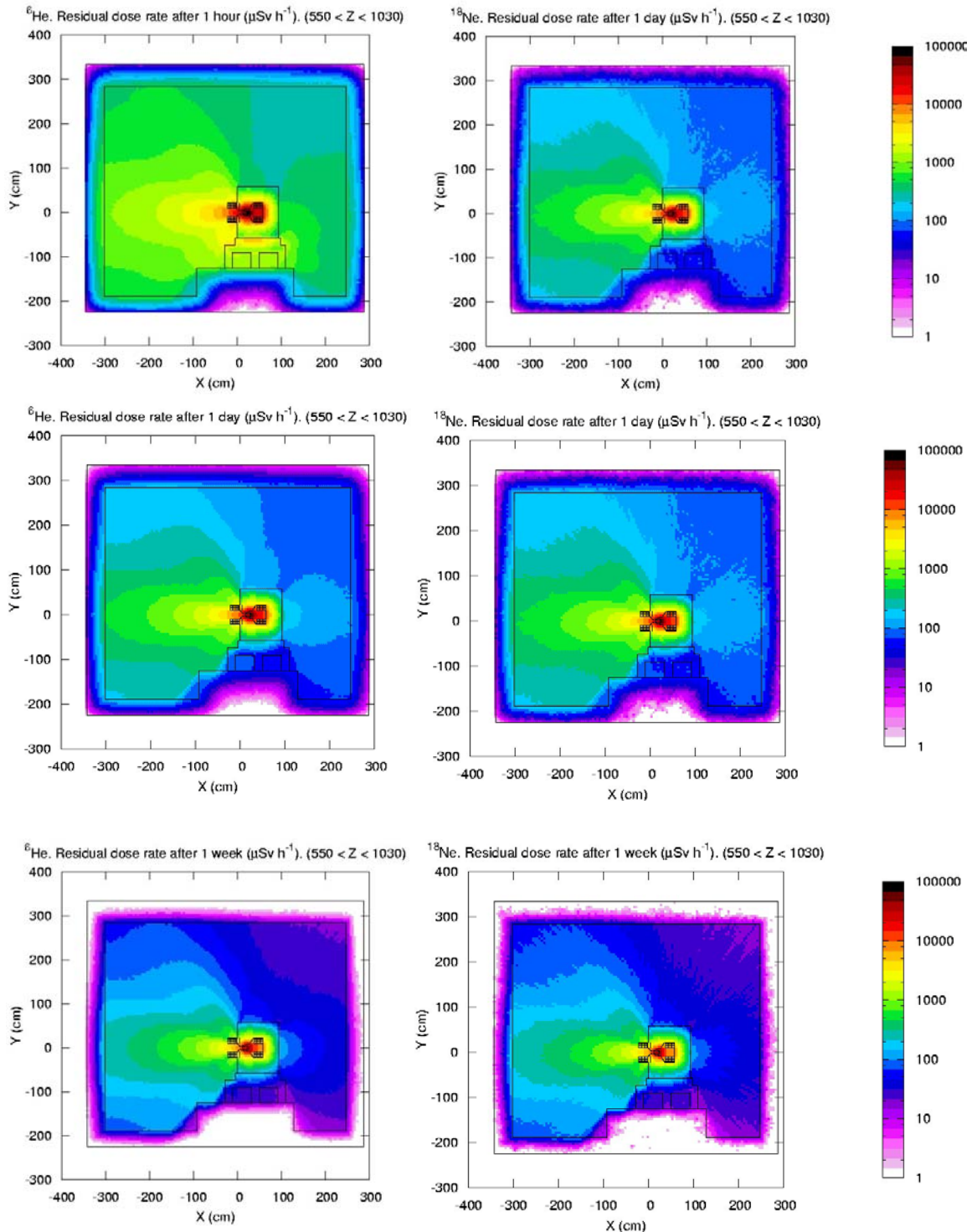

Figure 28 :From top to bottom: ambient dose equivalent rate after 3 month irradiation followed by

1 hour, 1 day and 1 week waiting time. Left: ^{6}He case. Right: ^{18}Ne case.

At the beginning of the annual shutdown period in 2008, radiation survey measurements of ambient dose equivalent rate were performed to gain information about the present radiation levels in the CERN PS [25]. The survey measurements are done at 40 cm distance from the object of concern, usually the vacuum chamber. The average dose rate along the PS ring is about 250 µSv h^{-1}, with 40% of the measured points below 100 µSv h^{-1} and only 5% above 1 mSv h^{-1}.

FLUKA [26][27] simulations with 3-month continuous irradiation of ^{6}Li and ^{18}F and 1-week waiting (Figure 28) show that the dose rate at 40 cm distance from a PS magnet would range between 60 µSv h^{-1} and 2 mSv^{-1} which is relatively high compared to the present level of induced radioactivity. This indicates that the tunnel would remain accessible with limited stay during maintenance – as long as the maintenance operations are well planned and optimized in order to reduce doses to workers. These values also suggest that there might be magnets whose levels of induced radioactivity require remote handling. This eventuality can only be confirmed or ruled out by a detailed study with precise and realistic scenarios of beam losses and with the implementation of the exact material composition (including traces).

The effective dose given to the reference population in a 1-year operation of the PS, due to the air release in the environment, is 0.37 µSv for the He-operation and 0.35 µSv for the Ne-operation. Table 12 shows the contribution of the main radionuclides to the effective dose. As the total effective dose given to the population by all CERN installations must not exceed 10 µSv, the contribution from the PS only is within this value.

Contributions to the effective dose from the main radionuclides (µSv per year)		
	^{6}He	^{18}Ne
^{13}N	0.171	0.156
^{15}O	0.078	0.073
^{11}C	0.078	0.074
^{14}O	0.011	0.010
^{41}Ar	0.020	0.020

Table 12 : Contributions to the effective dose from the main radionuclides (µSv per year).

SPS - RF simulations

Rather than consider another new machine, the space charge bottleneck at SPS injection has been addressed by adding a "modest" 40 MHz rf system to the existing infrastructure. This would allow much longer bunches to be transferred from the PS, the matching voltage for 20 ns bunches being ~120 kV and ~5 kV for helium and neon, respectively. Then, near transition when the bunches are short enough, the standard 200 MHz system of the SPS would take over for the bulk of the acceleration. Conceptually this is fine, but the baton must be passed between buckets of very different aspect ratio so mismatching the bunches is unavoidable.

1 MV at 40 MHz is at the limit of what might be considered as "modest" and constrains the maximum ramp rate to around 0.1 T/s in the early part of the cycle. Even so, the ramp rate must be slowed down still further for the rebucketing because even a small ramp rate reduces the 200 MHz bucket length and buying this back with voltage is costly in terms of mismatch. Assuming a ramp rate of 0.02 T/s and that the emittance the SPS is supposed to deliver is already established before

transition, Figure 29 shows how proximity to transition (γ_{tr}=23) reduces the 200 MHz voltage that is required to accommodate the bunch length accelerated in the proposed new 40 MHz bucket. Performing rf gymnastics close to transition is bound to be a delicate matter, but it incurs no penalty in mismatch because the aspect ratios of the two buckets scale identically with γ.
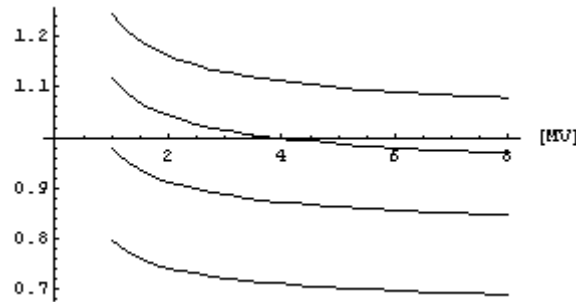
Figure 29:Ratio of 40 MHz bunch length to 200 MHz bucket length versus 200 MHz voltage for helium ions at γ=19, 20, 21, 22 (from top to bottom) and a ramp rate of 0.02 T/s in the SPS.

Figure 30 and Figure *31* show ESME simulations of rebucketing at γ=21.5 from 1 MV at 40 MHz to 1.75 MV at 200 MHz for helium ions. The bunch is mismatched at 200 MHz, but one quarter of a synchrotron period later (Figure *32*) it can be rematched by a step in voltage to 7.9 MV (Figure *33*). Thereafter, the ramp rate can be increased and acceleration can proceed normally.

*Figure 30: 1.0 eVs bunch of helium ions in a 1 MV, 40 MHz
bucket at γ=21.5 and a ramp rate of 0.02 T/s in the SPS.*

Figure 31: The bunch of Fig. 9 after the 40 MHz bucket is superseded by a 1.75 MV, 200 MHz one.

Figure 32: The bunch of Fig. 10 after rotation during a quarter of a synchrotron period.
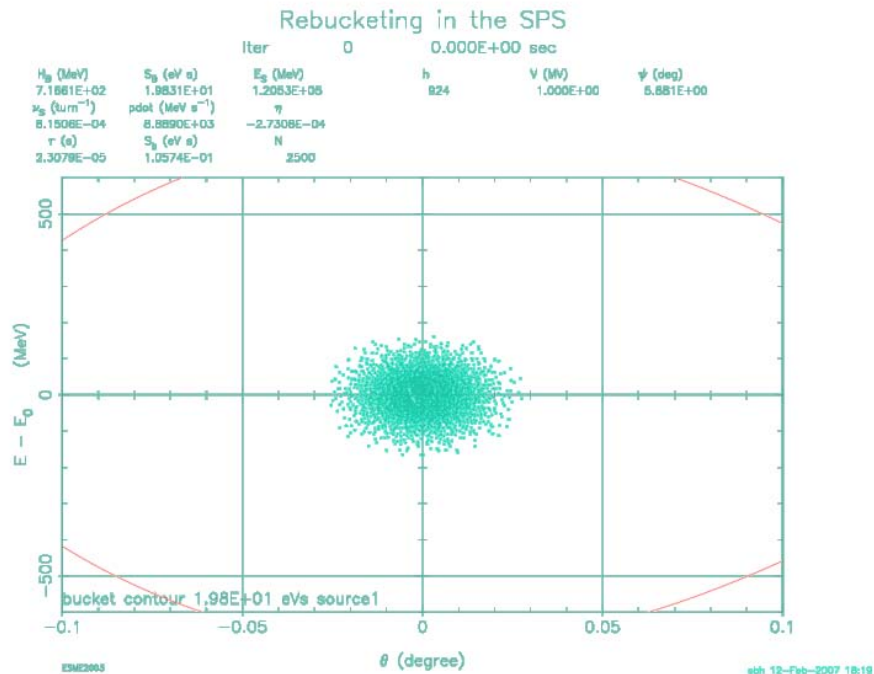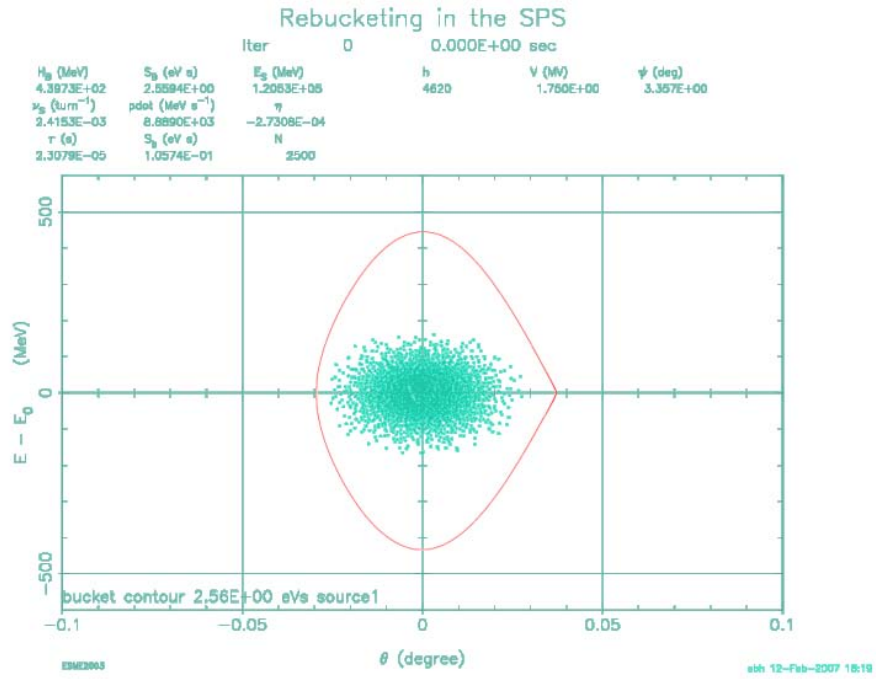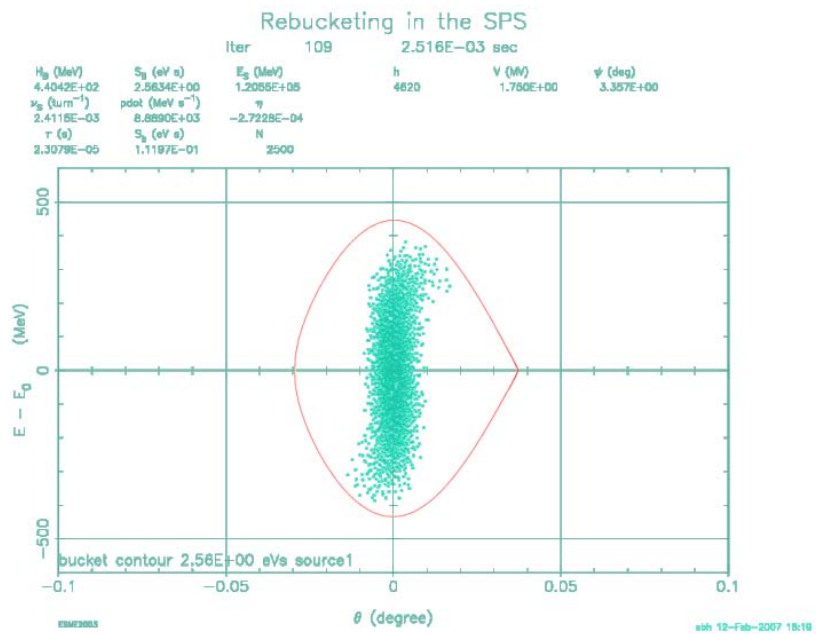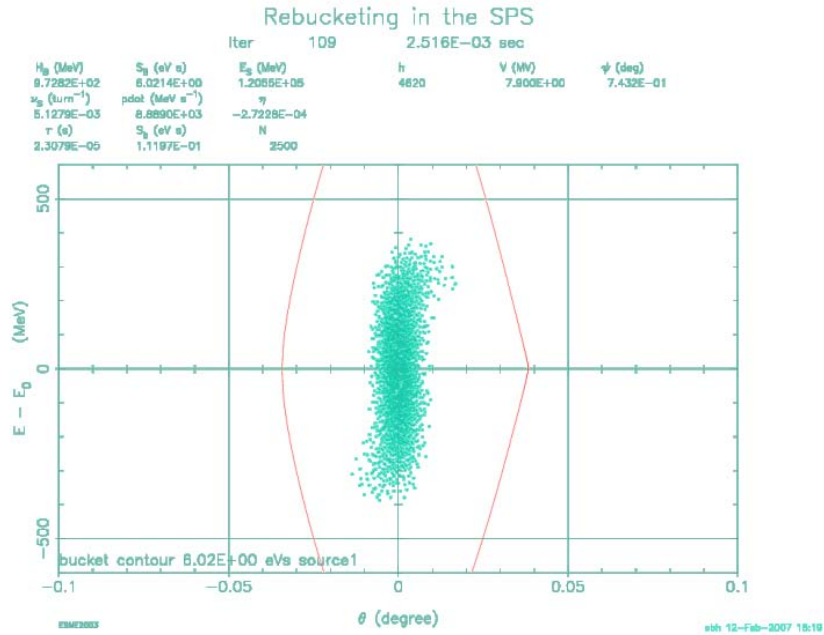
*Figure 33: The bunch of Fig. 11 after a step in 200 MHz
voltage to 7.9 MV. A small fraction of the bunch population
remains at large amplitude.*

Despite a larger emittance, the situation is easier in the neon case due to its advantageous charge-to-mass ratio. Although rebucketing must still be performed at the same miniscule ramp rate of 0.02 T/s, proximity to transition can be decreased to $\gamma=20$ and still have 1 MV at 40 MHz passing the baton to 1.75 MV at 200 MHz. 7.8 MV at 200 MHz is needed to rematch.

1 MV is very much the minimum 40 MHz voltage required. It also costs cycle time because of the need to slow the ramp rate down to permit rebucketing. However, since the 40MHz system sees almost all the frequency swing during acceleration, more voltage would be expensive. Alternatively, one could consider rebucketing at zero ramp rate as this reduces slightly the problem of matching.

The longitudinal emittance that the SPS must deliver is 1.0 eVs in the case of helium ions and 2.2 eVs for neon. These values are derived from the known performance for protons and, allowing an emittance budget of some 25% for blow-up during each acceleration stage, they also fix those in all the upstream machines. The novel injection scheme proposed for the decay ring requires the beam to be delivered off-momentum into the non-linear region of the receiving bucket. Consequently, the bunch is deliberately mismatched before extraction from the SPS by a step down in 200 MHz voltage (see Figure 34). This bunch tilting is a first-order attempt to increase the capture efficiency at the end of a quarter of a synchrotron turn in the decay ring. The fine detail of capture will depend on the large-amplitude distribution created in the SPS.
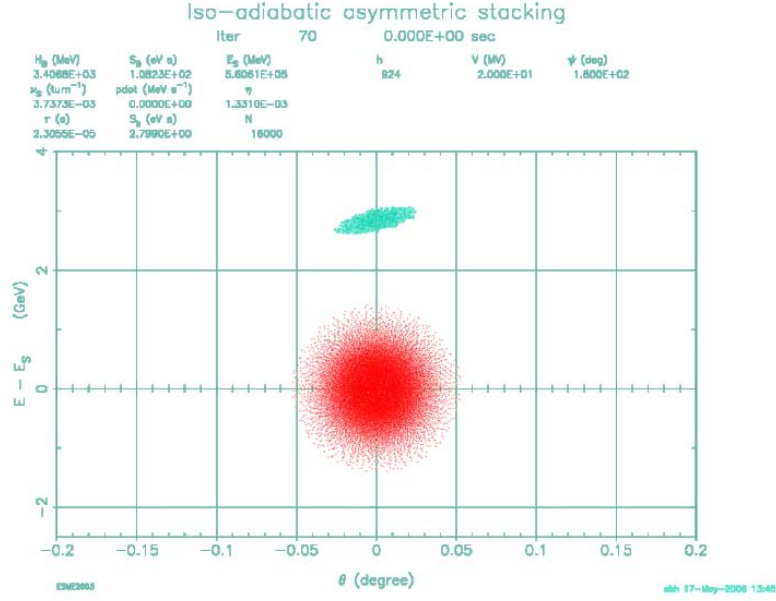
Figure 34: An SPS bunch of helium ions (green) is delivered tilted (following a step down in rf voltage from 2 to 0.5 MV) and 5‰ off-momentum with respect to the stack (red) in the decay ring.

Vacuum System Requirements for the SPS

The parameters used for the simulations of the dynamic pressure are listed in Table 13 and Table 14. The data in Table 13 were taken from"The EURISOL Beta-beam Facility Parameter and Intensity Values" generated at 12. March 2009.

Parameter	Value for $^6\text{He}^{2+}$	Value for $^{18}\text{He}^{10+}$
Energy (Injection)	$7780\,\text{MeV/u}$	$13.5\,\text{GeV/u}$
Mag. Rigidity (Injection)	$86.93\,\text{Tm}$	$86.47\,\text{Tm}$
Energy (Ejection)	$92.5\,\text{GeV/u}$	$92.2\,\text{GeV/u}$
Mag. Rigidity (Ejection)	$937.69\,\text{Tm}$	$559.16\,\text{Tm}$
Ramping Rate	$0.46\,\text{T/s}$ (see text)	$0.46\,\text{T/s}$ (see text)
Cycle Time	$6.0\,\text{s}$	$3.6\,\text{s}$ (see text)
Cycle Frequency	$0.17\,\text{Hz}$	$0.28\,\text{Hz}$ (see text)
Losses at Injection	$0\,\%$	$0\,\%$
Emittance (horizontal)	$6.39\,\text{mm mrad}$	$3.16\,\text{mm mrad}$
Emittance (vertical)	$3.409\,\text{mm mrad}$	$1.72\,\text{mm mrad}$
Injected Ions/Cycle	9.53×10^{12}	4.31×10^{12}

Table 13: Beam parameters used with StrahlSim.

Parameter	Value
Volume of Beam Pipe	$49.8\,\text{m}^3$
Static Residual Gas Pressure	$1 \times 10^{-9}\,\text{mbar}$
Effective Pumping Speed	$2.8\,\text{m}^3/\text{s}$ (see text)

Table 14: Vacuum parameters used with StrahlSim.

The loss distribution for both $^6\text{He}^{2+}$ and $^{18}\text{Ne}^{10+}$ ions are shown in Figure 35 for one section of the

SPS. The losses are dominated by radioactive decay. Losses due to charge exchange are negligible, as the cross sections for electron capture are very small. For both $^6He^{2+}$ and $^{18}Ne^{10+}$ the losses are peaked behind the quadrupole magnets.
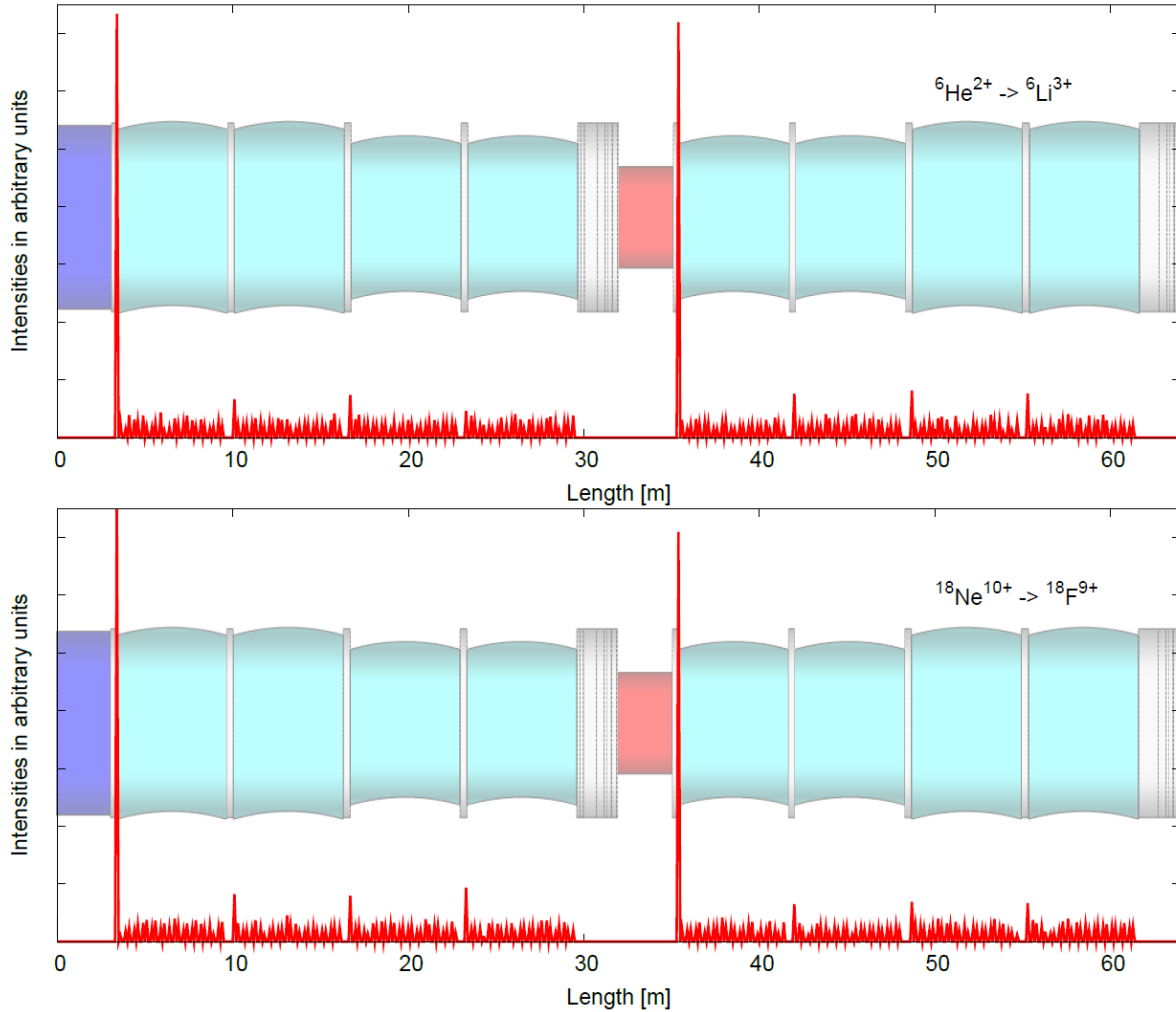

Figure 35: Loss distribution $^6He^{2+} \rightarrow ^6Li^{3+}$ (top) and $^{18}Ne^{10+} \rightarrow ^{18}F^{9+}$ (bottom) at injection energy. Dipole magnets are shown in light blue, quadrupole magnets in red and blue.

The transmission was checked by using the proposed cycle assuming the maximum number of particles coming from the PS. The numbers were taken from "The EURISOL Beta-beam Facility Parameter and Intensity Values". For $^6He^{2+}$ there are 9.53×10^{12} ions injected coming from the PS. This leads to 8.99×10^{12} ejected ions. For $^{18}Ne^{10+}$ there are 4.31×10^{12} injected and 4.25×10^{12} ejected particles. These numbers are arguably identical with the desired numbers of 9.0×10^{12} and 4.26×10^{12} for $^6He^{2+}$ and $^{18}Ne^{10+}$ respectively.

The effective pumping speed used in the simulations was estimated as follows. Every SPS magnet has an ion pump with a pumping speed of 20 l/s. Considering the MBA, MBB, QF and QD magnets only, StrahlSim calculates a conductance corrected effective pumping speed of $S_{eff}=2.6$ m^3/s. Placing pumps at the positions were are no dipoles in the ring, leads to $S_{eff}=2.8$ m^3/s. This is close to the value of $S_{eff}=2.28$ m^3/s. given in the "Parameter and Intensity Values" document. All simulations carried out for the SPS assuming $S_{eff}=2.8$ m^3/s (differing values are given explicitly).

During the simulations it turned out, that ionization of residual gas particles by the revolving beam, called target ionization, is the dominant effect that causes a pressure rise in the SPS during Beta

Beam operation. The cross sections for target ionization are given by a scaled Bethe formula [28]. The ionized gas particles are accelerated away from the beam by its space charge potential. When these particles hit the vacuum chamber a low energy desorption process takes place. The desorption rate η for this process is considered to be in the range between 1 and 10 desorbed particles per ionized gas particle hitting the vacuum chamber [29], while the "Parameter and Intensity Values" document states a value of 10.

Figure 36 shows the pressure evolution for the proposed cycles using $^6He^{2+}$ and $^{18}Ne^{10+}$ as projectile ions. The pressure evolution strongly depends on the assumed desorption rate. For $^6He^{2+}$ the residual gas pressure is not stable when a desorption rate greater than 5 is assumed, while for $^{18}Ne^{10+}$ even in case of $\eta=1$ the pumping speed is not sufficient to stabilize the pressure. For comparison Figure 36.shows the pressure evolution for $^{18}Ne^{10+}$ with an effective pumping of 7.5 m^3/s and $\eta=1$.

Figure 36: Pressure evolution over several cycles for $^6He^{2+}$ (left) and $^{18}Ne^{10+}$ (right) for different desorption rates using the proposed cycle. For $^{18}Ne^{10+}$ there is one simulation with an increased effective pumping speed of 7.5 m^3/s.

One possibility to reduce the pressure build up is to reduce the acceleration time within the SPS. The acceleration time can be shortened from 2.54 s to 1.58 s for $^6He^{2+}$ and from 1.42 s to 0.90 s for $^{18}Ne^{10+}$, when using the maximal available ramping rate of the SPS of 0.74 T/s. Furthermore the cycle time of the $^{18}Ne^{10+}$ cycle was extended to 6 s in order to give the vacuum more time to relax.
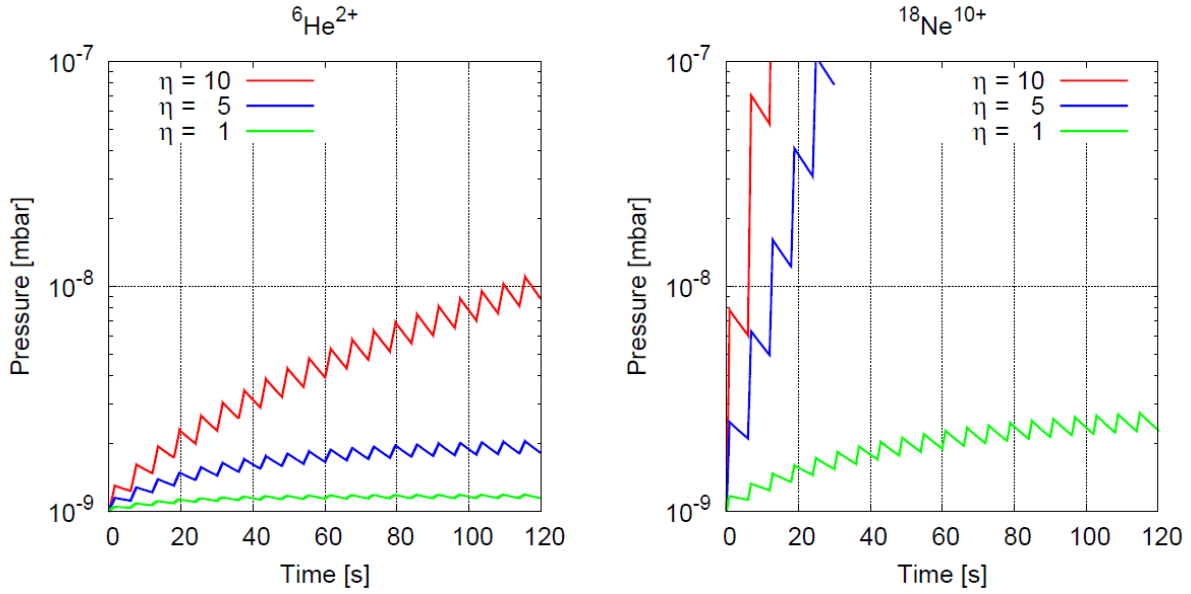
Figure 37 shows that this measurement would slow down the pressure rise for $^6He^{2+}$ operation with η=10 and stabilize the $^{18}Ne^{10+}$ operation with η=1. In this scenario accelerating $^{18}Ne^{10+}$ ions with η>1 is still not feasible. In the following paragraph the effect of an increased effective pumping speed will be discussed.

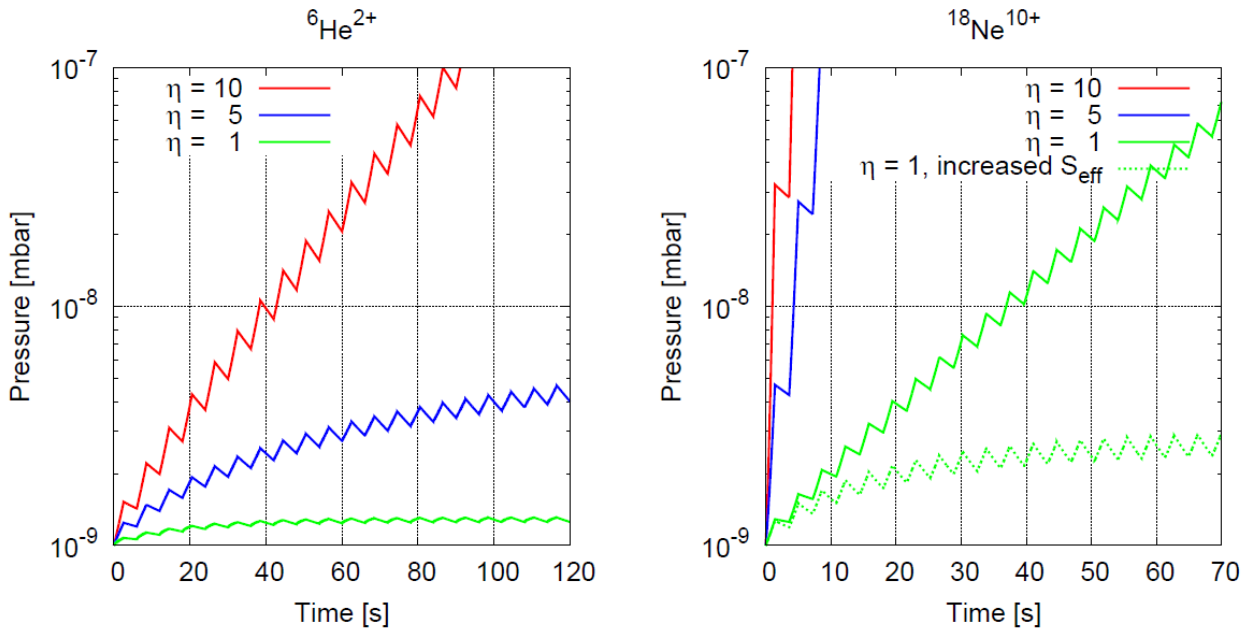*Figure 37: Pressure evolution over several cycles for $^6He^{2+}$ (left) and $^{18}Ne^{10+}$ (right) for different desorption rates using the maximal available ramping rate and extending the $^{18}Ne^{10+}$ cycle to 6 s.*

As shown before the operation with $^6He^{2+}$ is stable for η=5. In Figure 38 the pressure evolution for $^6He^{2+}$ operation with the increased ramping rate and η=10 is shown for several effective pumping speeds. At a pumping speed of 4 m^3/s the pressure is stabilized below 1×10^{-8} mbar. For $^{18}Ne^{10+}$ various combinations of η and S_{eff} have been calculated assuming the maximal ramping rate and an extended cycle time of 6 s. Figure 13 shows a selection of the obtained results. For each η=1, 3 and 5 the required pumping speeds were estimated to be 2.8 m^3/s, 7.5 m^3/s and 12.0 m^3/s respectively.

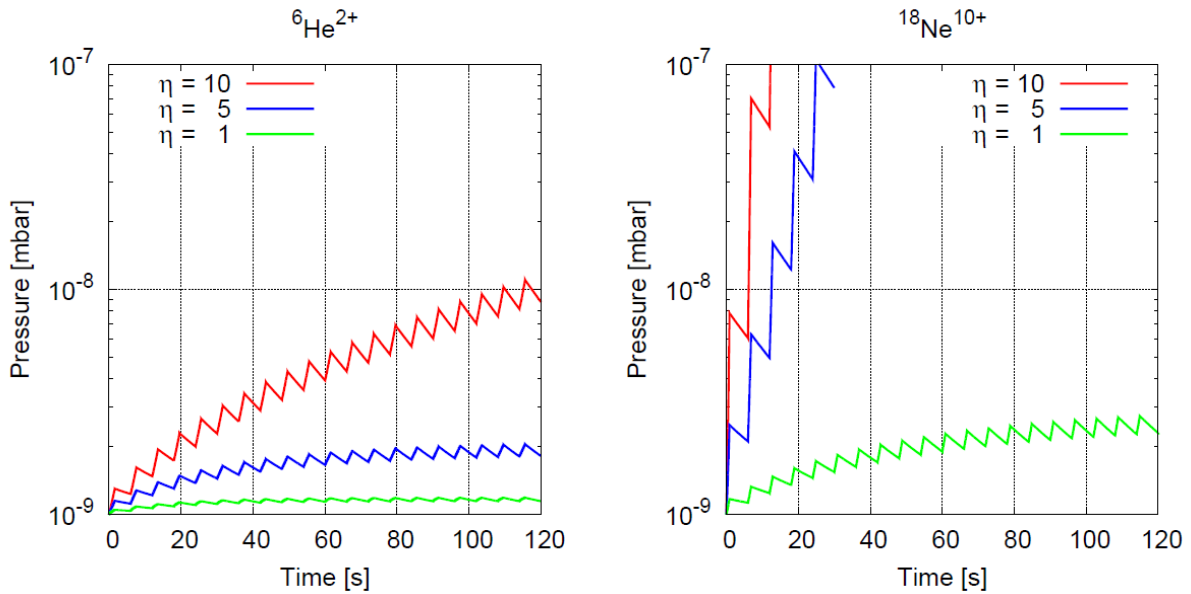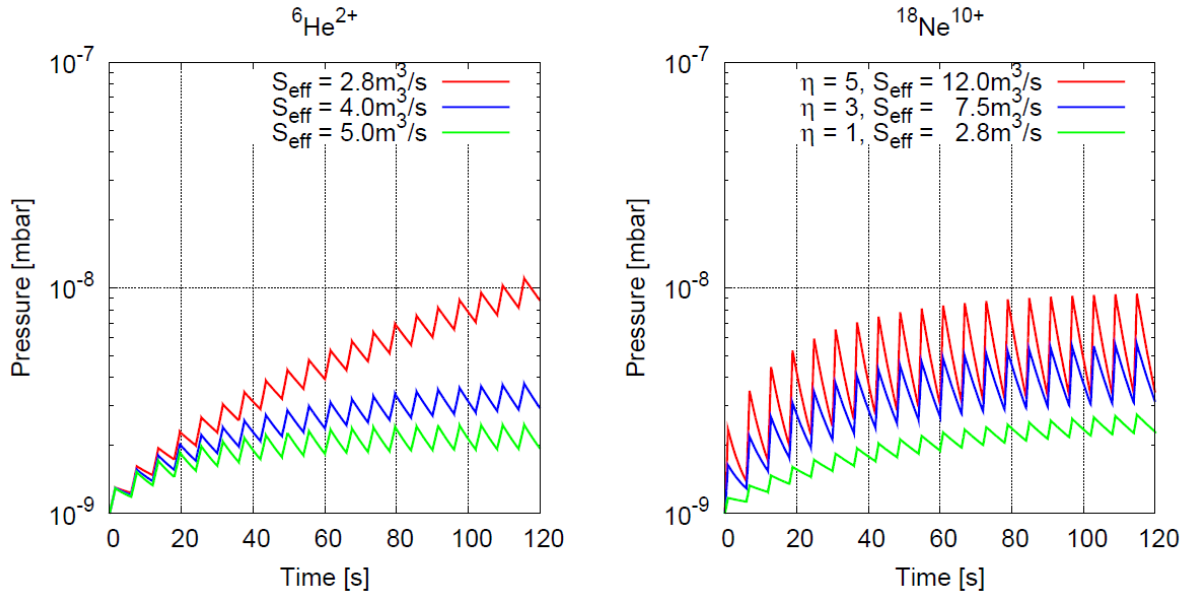*Figure 38: Pressure evolution over several cycles for $^6He^{2+}$ (left) and $^{18}Ne^{10+}$ (right) for different effective pumping speeds. For both projectiles the maximal available ramping rate of the SPS was assumed and for $^{18}Ne^{10+}$ the cycle time was extended to 6 s. The desorption rate used for $^6He^{2+}$ was $\eta=10$. The rates for $^{18}Ne^{10+}$ are given in the legend.*

The interactions of the beam with residual gas particles and their effect on the pressure evolution inside the SPS ring have been investigated using the program StrahlSim. The simulations show, that during SPS operation with $^6He^{2+}$ or $^{18}Ne^{10+}$ as the projectile ions, there is a massive pressure build up due to ionization of residual gas particles induced by the circulating beam.

It could be shown, that an operation with $^6He^{2+}$ ions is possible, if the desorption rate for ionized gas particles hitting the vacuum chamber is less or equal to five. In this case the residual gas pressure stays below 1×10^{-8} mbar. Should the desorption rate be greater than five, the pressure can be stabilized by reducing the acceleration time from 2.54 s to 1.58 s by using the maximal available ramping rate of 0.74 T/s and increasing the total effective pumping speed to approximately 4 m^3/s.

An operation using $^{18}Ne^{10+}$ ions with the proposed cycle is not possible without adjusting the cycle or the pumping speed. In case of a desorption rate $\eta=1$ either the effective pumping speed has to be increased to about 7.5 m^3/s or the acceleration time has to be minimized by using the maximal available ramping rate of the SPS, while the cycle has to be extended to 6 s in order to give the vacuum enough time to relax. The increased ramping rate reduces the acceleration time from 1.42 s to 0.90 s. If the desorption rate is greater than one, the higher ramping rate and the extended cycle of 6 s have to be combined with a higher effective pumping speed. For desorption rates $\eta=1$, 3 and 5 effective pumping speeds of 2.8 m^3/s, 7.5 m^3/s and 12.0 m^3/s have to be applied.

Identification of limitations in PS and SPS

The budget of decay losses within PS and SPS was estimated and compared to CNGS operation by CERN in [30]. From that study, it turned out that the power losses occurring for the Beta-Beam operation are in the same order of magnitude than CNGS for nominal intensities of ^{6}He and ^{18}Ne and are therefore not a showstopper for the project.

VII.   Design of Decay ring

The design of the decay ring of the beta-beam facility was performed by CEA Saclay [31],[32] using a stacking mechanism as was originally proposed by CERN [13],[14]. CERN has conducted a preliminary design of the collimation section starting from the optics proposed by CEA, and a study of the dipoles of the arcs for protecting them from high energy deposition using FLUKA and ACCSIM softwares. The RF was studied by CERN and an original solution was proposed (see section *RF system*, also presented in [31]).

Optics

The decay ring is a 6911.5 m-long racetrack-shaped-ring with two 2468-m-long straight sections, of which one is directed toward the detector situated in the Fréjus tunnel [33]. The useful section is around 36 % of the circumference. Table 15 presents the lattice parameters of the decay ring.

The parameters of the beam are given in Table 16. A first consequence to store high intensity beams is that the tune spread due to the space charge effects may not be negligible. The tune shift was calculated for $^6He^{2+}$ and $^{18}Ne^{10+}$ and is given in Table 16. With nominal parameters, the space charge effects can be neglected in $^6He^{2+}$ case contrary to $^{18}Ne^{10+}$ case. A solution to decrease the space charge effect would be to increase the rms emittance of the stored beam by injecting a mismatched beam. To have a manageable tune shift for $^{18}Ne^{10+}$ of -0.063 in the horizontal plane and -0.055 in the vertical one, the rms emittance must then be enlarged up to 0.22 π mm.mrad in both planes. In the following, we assume this rms emittance for $^{18}Ne^{10+}$ to neglect space charge effects.

Total length	M	6911.5
Radius	M	1100
Straight section length	M	2468
Arc length	M	988
Q_x	-	22.226
Q_z	-	12.161
Q'_x	-	-1.717
Q'_z	-	-2.351
A	10^{-3}	1.512
H	10^{-3}	1.412
ARC DIPOLES		
Angle	Rad	$\pi/86$
$1/\rho$	m^{-1}	6.43×10^{-3}
QUADRIPOLES		
Total number	-	176
K_{max}	m^{-2}	$+4.848 \times 10^{-2}$
G_{max}	T/m	+45.326
SEXTUPOLES		
Family number	-	6
Total number	-	44
$S_{max}L$	m^{-2}	0.151
$H_{max}L$	T/m	141.174

Table 15: Lattice parameters of the Beta-Beam decay ring.

	Units	6He2+	18Ne10+
γ	-	100	100
$B\rho$	T.m	938	563
Bdipole	T	6	3.6
τ at rest	S	0.8	1.67
Ninjected (ions/batch)	-	9.05×10^{12}	4.26×10^{12}
Nstored (ions/batch)	-	9.71×10^{13}	7.40×10^{13}
Bunch number	-	20	20
rms ε_x	π mm.mrad	0.11	0.11
rms ε_y	π mm.mrad	0.06	0.06
$\Delta\nu_x$	-	-0.015	-0.127
$\Delta\nu_y$	-	-0.024	-0.201

Table 16: Nominal parameters for the decay ring.

The arcs are 2π insertions of which the optics is given on Figure 39. Four functional parts were distinguished in the arcs [32]: a regular FODO lattice in the arc, a matching section between the long straight section and the FODO lattice, which is used to extract the decay products coming from the long straight section too, a low β – high dispersion insertion for the injection and a matching section between the regular FODO lattice and the insertion. Moreover, large betatron functions are needed in the FODO lattices of the long straight sections to maximize the neutrino flux going to the detector.
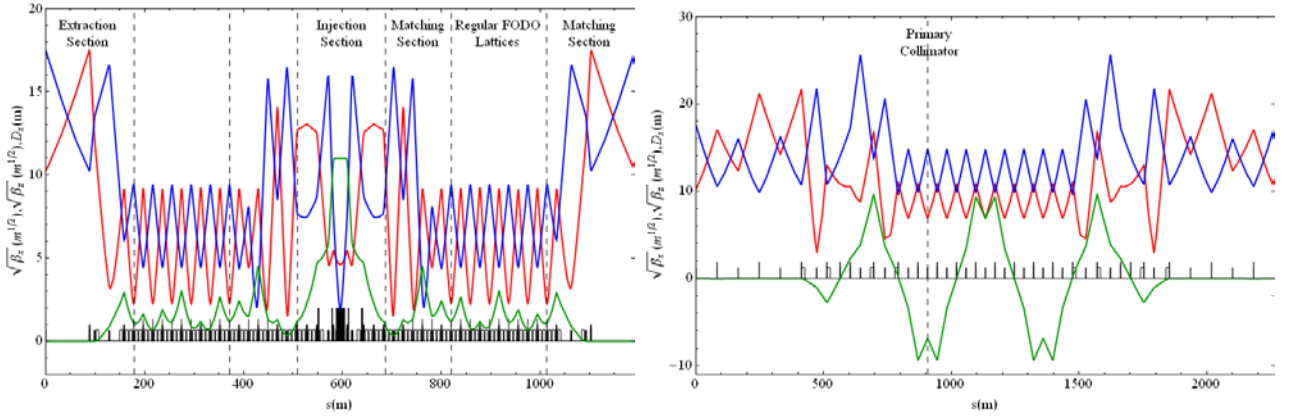

Figure 39: Optical functions in the arcs (left) and in the energy collimation section (right). In red, horizontal betatron functions, in blue vertical betatron function and in green horizontal dispersion.

Injection

The number of injected ions from the SPS is limited by the space charge effects in the PS and the source [9]- [11]. In order to increase the number of stored ions in the decay ring and reach the required neutrino flux, the injection has to enable an accumulation of the ions in the decay ring in presence of the circulating beam. An insertion in the arcs for an off-momentum injection was then designed following the principle presented in Figure 40. The injection insertion is presented in detail in [31] and [34], we recall here only its basic principles. The natural dispersion present in the arcs and the need to keep the long straight sections safe make the arcs the natural location to put the injection insertion. Moreover, the arc and thus the insertion for the injection are symmetric and present a waist at the centre of the insertion. During injection the kickers are on, and the injection septum deflects the incoming beam without perturbing the stored beam. The closed orbit of both

beams are forming a bump, with the injected beam running above the septum blade and the circulating one still running below. The fast kickers are then switched off before the fresh beam has made a turn, and both beams circulate under the blade. The injection is realized in a high dispersion - low β_x area. For both ^{6}He and ^{18}Ne, an off-momentum injection at $\delta = 5{\times}10^{-3}$ was assumed. The optics of the injection section was realized with the code BETA [22] and is presented on Figure 41. The beam sizes in the injection insertion are represented on Figure 42. A specific RF program with two variable cavity families, of which one is at double frequency, is then used to merge both beams. It is summarized in the next section.
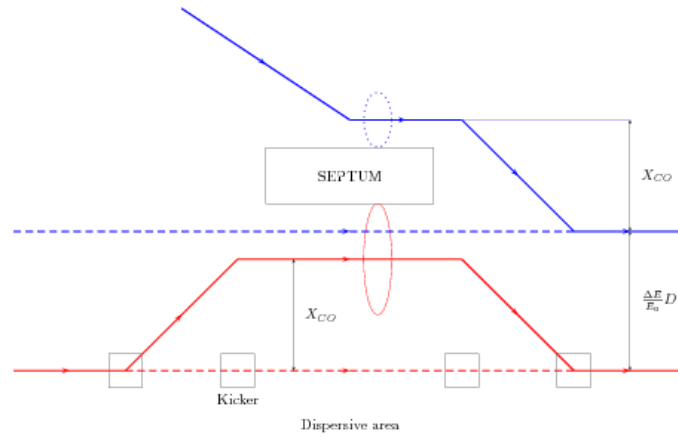
Figure 40: Injection principle. In blue, injected beam and in red, stored beam. In dashed, central axes of both beams one turn after injection (kickers off).
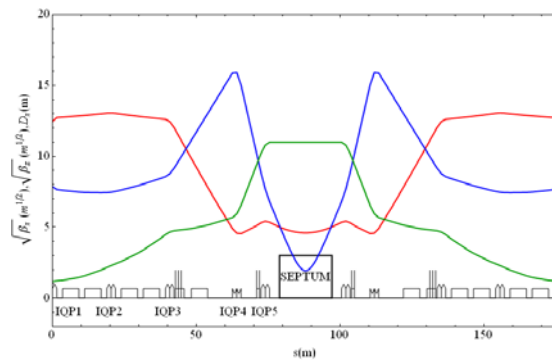
Figure 41: Optical functions in the injection section. In red/blue, horizontal/vertical betatron function and in green horizontal dispersion.
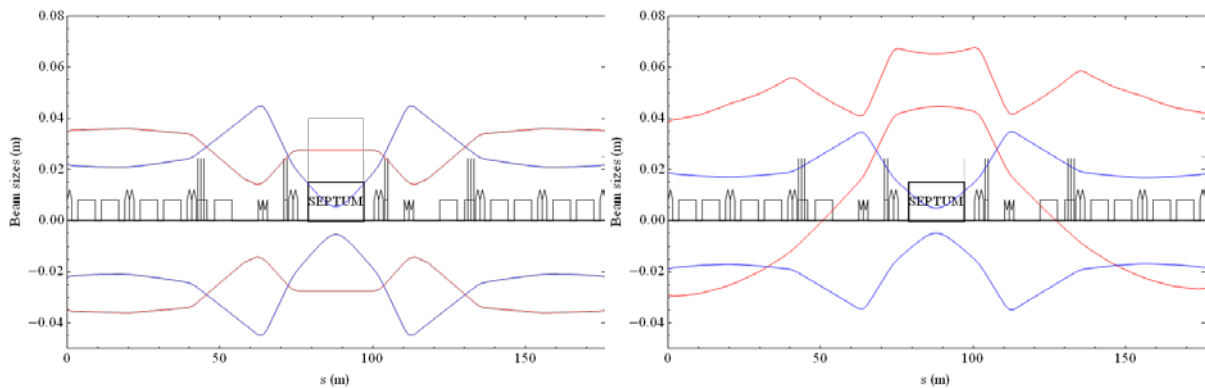
Figure 42: On left, sizes of the stored beam at 6 sigma in the injection insertion. On right, sizes of the injected beam at 5 sigma in the injection insertion. In red, beam sizes in the horizontal plan and

Asymmetric bunch merging

After injection, the stored and fresh bunches are horizontally separated and circulating both under the septum blade. The merging is realized using 2 RF cavities at 40 and 80 MHz. It consists of four phases terminated with the insertion of the new fresh bunch in the center of the circulating one, as described on Figure 43 for ^{6}He. The corresponding RF program is detailed in [13][14] and [31].
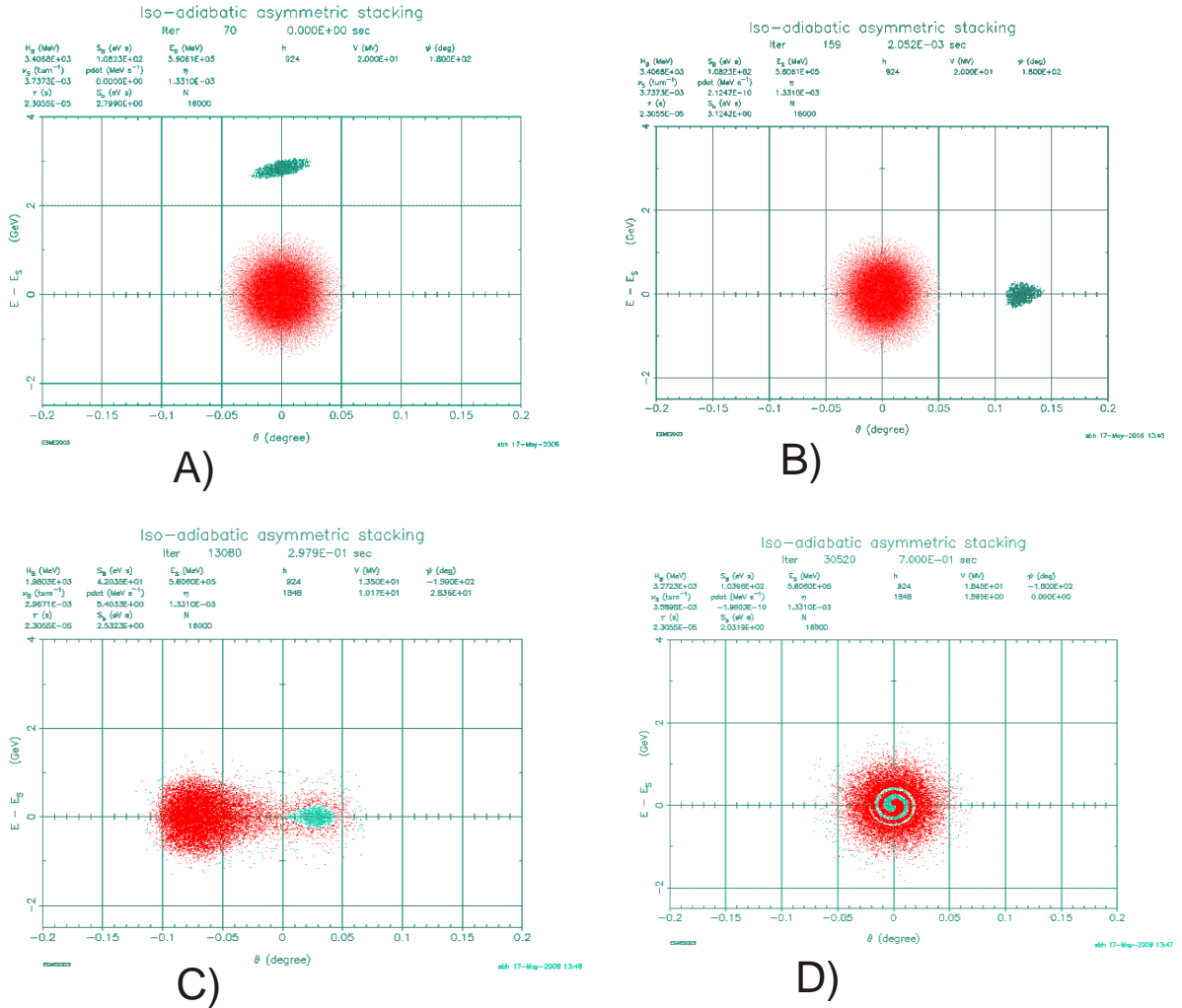
*Figure 43 : The four phases of the bunch merging for ^{6}He as simulated by ESME. A) off-momentum injection. B) rotation in the longitudinal phase space (synchrotron motion). C) asymmetric bunch merging. D) symmetric merging leading to the insertion of the fresh bunch into the center of the stored one.*

RF system

This section presents a method to cope with the heavy transient beam loading in the decay ring. The beam in the decay ring with few but very high intensity bunches leads to heavy transient beam loading, which is a potential issue for the RF system. The problem is that, with a large beam current in quadrature to the gap voltage, the cavity will be effectively detuned. In order for the final amplifier to remain matched, this reactive beam current must be compensated with another reactive

element – the tuner. While this may be still feasible for a constant beam current, such a tuner would become impracticable for a partially filled machine, since it would have to act very fast.

In the following, we will use the existing PS 40 MHz RF system as a reference: it is designed for bunching of the LHC beam, has a moderate $\frac{R}{Q} = 33\,\Omega$ and a relatively high Q of 18000. More details can be found in Chapter 8 of Reference [35]. The system is designed for a nominal gap voltage of 0.3 MV and can cope with 1.2 A of RF beam current. However, a beam current of around 100 A would induce an unacceptably high voltage of 30 MV in a single gap. An even lower $\frac{R}{Q}$ could mitigate this, but at the expense of proportionally higher installed RF power. We will show in the following how one could conceive to use a similar RF system in spite of this extremely high beam current. For a total required gap voltage of 20 MV, about 50 of these cavities would be required.

For illustration, we consider the case of a stationary bucket in a partially filled circular machine. This is simplifying the situation of the decay ring with its double harmonic RF system somewhat, but the findings can be generalized. Stationary bucket implies no acceleration, i.e. there is no net power transfer necessary between the RF system and the beam. Power from the final amplifier will just have to compensate for ohmic losses in the cavity. Partially filled machine implies a special class of transient beam loading – i.e. there is either beam or no beam at all (cf. Figure 45).

For a synchrotron above transition and with the bunched beam in the stable phase, the beam represents an inductive current, which will tune the cavity "up". For steady state (constant beam current and gap voltage), the beam could be replaced in the equivalent circuit (Figure 44) by an inductivity $\frac{V_{gap}}{\omega |I_B|}$.
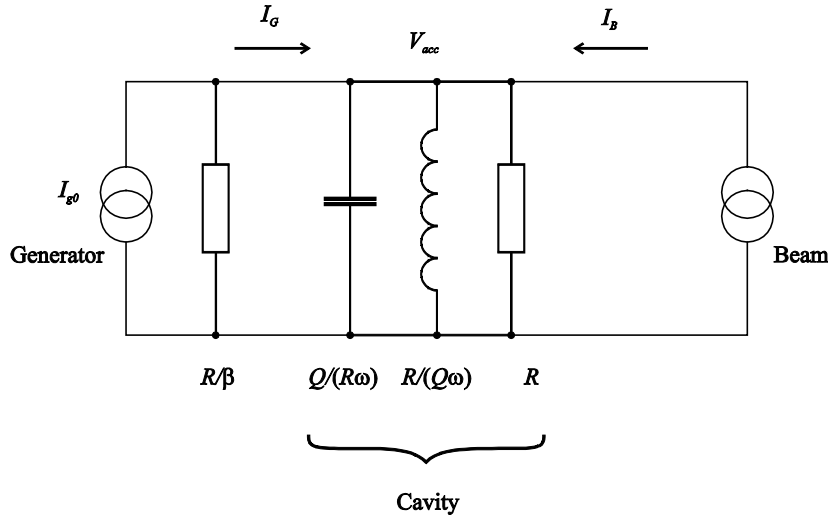
Figure 44: Equivalent circuit of a cavity including beam loading.

To compensate for this inductive beam current, the cavity should be tuned "down" to a frequency $\omega_0 < \omega$, given by $\frac{\omega_0}{\omega} = \frac{1}{2}\left(\sqrt{4 + g^2} - g\right) \approx 1 - \frac{g}{2}$, where $g = \frac{R}{Q}\frac{|I_B|}{V_{gap}}$, ω is the operation frequency and ω_0 resonance frequency of the cavity. Assuming that the cavity was tuned to the frequency ω initially, this could for example be achieved by adding a parallel capacitor of approximately $\frac{2\,g\,Q}{\omega\,R}$ (Figure 44).

As an example, we calculate the necessary detuning for the existing PS 40 MHz cavity $\left(\frac{R_S}{Q} = 33\,\Omega\right)$, for a nominal gap voltage of 300 kV and an RF current of 100 A; in this case, $g = 0.011$

and $\frac{\omega_0}{\omega} = 0.9945$, i.e. the empty cavity should be tuned to 39.78 MHz for operation at 40 MHz. In the stationary case (constant beam current), this could be implemented for example by adding a (tuner) capacitor of 2.6 pF in parallel to the existing $\frac{Q}{\omega R} = 120$ pF.

As mentioned above, a practicable tuner with this relatively large tuning range (0.5 %) would not be fast enough in the case of transient beam loading implied by a partially filled machine. The amplifier would consequently have to remain mismatched either in the presence of beam or in the absence of beam.

In the following, we will describe a concept of how the problem of heavy transient beam loading could be overcome; the approach is based on the assumption that one may choose any gap voltage while the beam current is zero. For example, the frequency can be chosen such that the final amplifier remains matched also in the absence of the beam, while keeping the gap voltage and thus the stored energy constant.

Let us assume that a circular machine with revolution period T is partly filled: there is full beam current I_B for $0 < t < T_B$, followed by zero beam current in the interval $T_B < t < T$ (see Figure 45). In order for the RF fields in the cavity to be correct in amplitude and phase again at the next passage of the beam, the frequency offset must however satisfy the condition that $\Delta\omega(T - T_B)$ is an integer multiple of 2π.

Figure 45: Transient beam current in a partially filled machine.

If we can allow to drive the amplifier in this latter interval at ω_0 rather than ω, it will remain permanently matched. With the RF on harmonic h equal to $\omega = h \frac{2\pi}{T}$, this additional phase condition now reads: $-h \, g \left(\frac{T - T_B}{T} \right) \approx \frac{h}{T} \left(\sqrt{4 + g^2} - g - 2 \right)(T - T_B) = 2N$, where N is an arbitrary integer. For the non-trivial case $N \neq 0$ and small g, this condition can only be met if both h and $T - T_B$ are large enough; for the value of g from the above example and $T_B \ll T$, one would require a harmonic of at least 181 for the phase slip to be -2π ($N = -1$). For larger harmonics, this condition still results in discrete possible values of g for which it can be satisfied exactly; Figure 46 shows these discrete possible values for g plotted over the parameter $\frac{T_B}{T}$ for a harmonic of 924 (corresponding to the 23.1 µs of the decay ring). With given beam current and cavity parameters, each of those discrete values corresponds to a gap voltage for which the matching condition is satisfied. For the limiting case $T_B \to 0$, the increment in g would become $\Delta g = \frac{2}{h}$, corresponding with the above parameters to acceptable gap voltage increments of below 15 kV for a bandwidth of 1 % of the RF system. Since the decay ring will have several tens of these RF systems (with a gap voltage per cavity of 400 kV, e.g., the number of systems would be 50), any total gap voltage could be programmed using different voltages in different cavities. This would result in a more complicated low level RF system, in which different phase programs would have to be programmed for different cavities, each as function of beam current, the overall voltage and the parameter $\frac{T_B}{T}$, but this is not a conceptual difficulty.
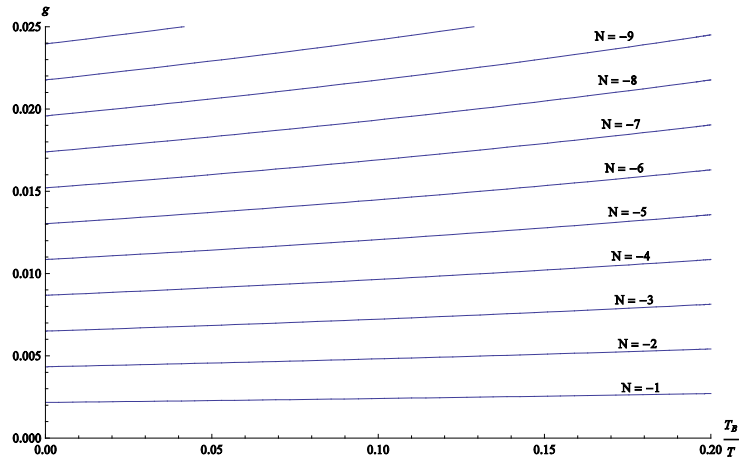
Figure 46: Discrete values of g as function of T_B/T for harmonic 924.

For illustration, we look again at a single cavity with the above parameters. For $T - T_B = 21\,\mu s$ ($\frac{T_B}{T} = 0.0866$), e.g., one could chose $N = -5$, resulting in $g = 0.01158$, very close in fact to the optimum $g = 0.011$. Without changing any other parameters, the matching would again be perfect for a gap voltage of 278.5 kV (instead of the nominal 300 kV). Figure 47 shows the simulation of this case. The generator current is 0.85 A, constant in amplitude and always in phase with the gap voltage, i.e. the generator has to deliver around 65 kW in CW (The unloaded shunt impedance is 600 kΩ). Note small ratio of generator current to beam current of below 1%!

The situation in the beta beam decay ring is slightly more complicated since it is using a double harmonic RF system, the basic idea of the above is however still applicable, since there is no significant net energy transfer for acceleration. For stability reasons, the RF systems would certainly have to be dimensioned for higher power than the number given in the above example. Also the voltages on the 80 MHz system ($h = 1848$) could be produced using the same principle. A more thorough analysis is required to determine the needs and possible implementations of the low-level RF system.

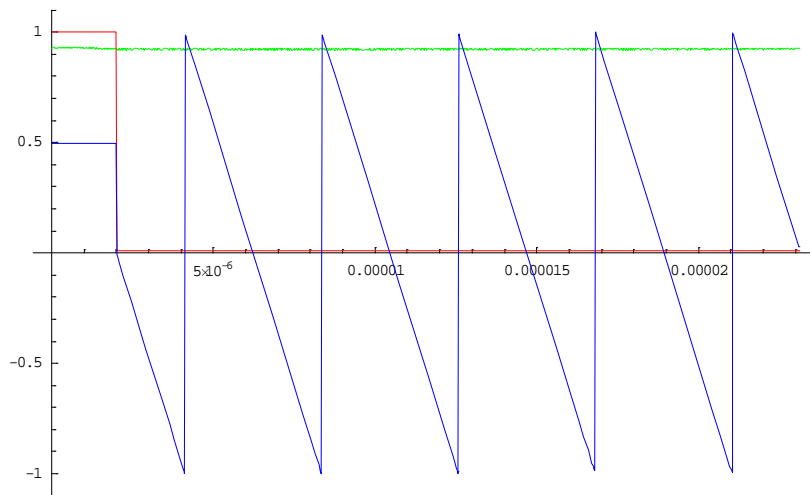*Figure 47: Mathematica simulation of one revolution period with heavy transient beam loading, assuming a period of 23 μs and a beam current of 100 A over 2 μs. Total current (beam + generator) in units of 100 A (red); phase of this current in units of π (blue); the resulting gap voltage in units of 300 kV (green).*

Momentum collimation

Two loss sources were identified by simulating the injection and stacking processes as described in the former sections . The first one comes from the fresh ions which are not captured at the injection. The second one is due to the blow-up in the space (l,δ) injection after injection. On Figure 48, the survival of a beam injected at $t = 0$ is represented as a function of the number of injection cycles. After around 15-20 injections, most ions are not accepted anymore. When the steady state is reached, the loss amount between two injections is compensated by the injection itself. About 50 % (Helium) and 20 % (Neon) of the losses which occurred between two cycles are due to the β decay. The mean power to collimate in the ring can then be evaluated to 74 kW for $^6He^{2+}$ and 248 kW for $^{18}Ne^{10+}$. Therefore, a two-step collimation system is needed and was designed to collimate in energy at $\delta = 2.5\times10^{-3}$ (Figure 49). It is located in the long straight section which is not directed toward the detector.
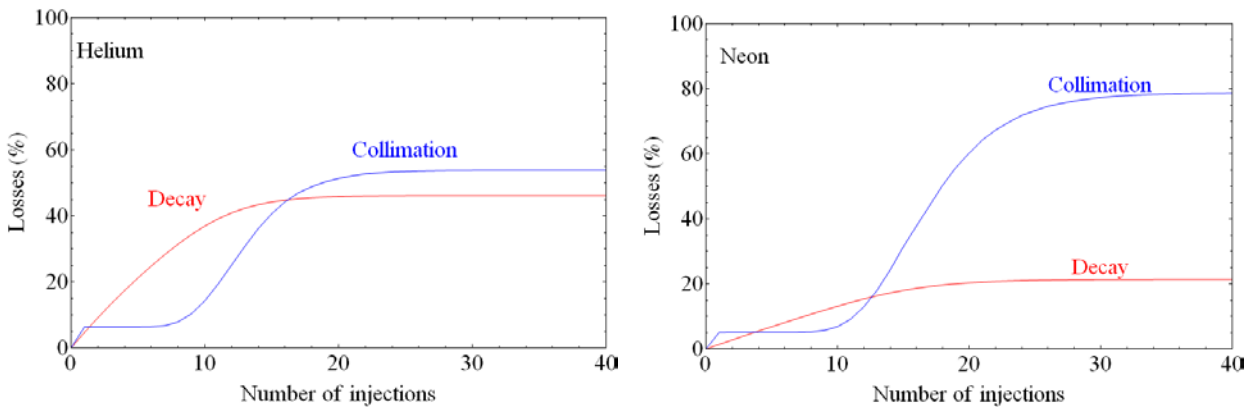

Figure 48: Loss amount as a function of time for Helium (left) and Neon (right).

A 6D simulation of the collimation section has been done with FLUKA with losses generated by ACCSIM. At the end of the symmetric bunch merging, the collimation rate can be controlled by increasing the second harmonic, which shortens the time spread and widens the energy spread. The energy spread is limited cutting negative energy shifts E_s-E_0 beyond 2.5‰, as shown on Figure 49. After a few synchrotron periods, the bunch phase space is homogeneously cut. Such an asymmetric collimation permits the off-momentum, positive energy shift injection while limiting the longitudinal phase-space blow-up of the bunches.
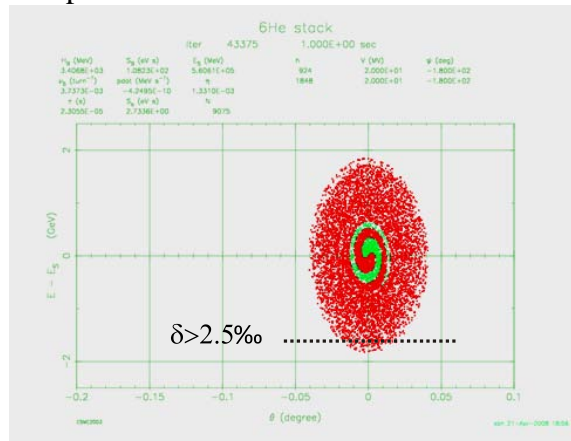

Figure 49: ^6He bunch phase space stretching after the ramping up of the second harmonic, as calculated by ESME.

The primary collimator is placed to fulfill the condition: $\dfrac{D'}{D} = -\dfrac{\alpha}{\beta}$ [32][36]. The secondary collimators are placed on the beam envelope of a beam with maximum negative dispersion of 2.5‰, alternatively on one side and the other from the collimation section (Figure 50). The energy distribution of the collimated halo, as estimated in 2D by ESME, could be satisfactorily reproduced using ACCSIM for calculating the actual evolution of the full 6D phase space of the bunches during the ramping up of the second harmonic (Figure 51). The loss map as generated by ACCSIM was then used as an input to FLUKA for simulating secondary particle showers and energy deposition within the collimation section.
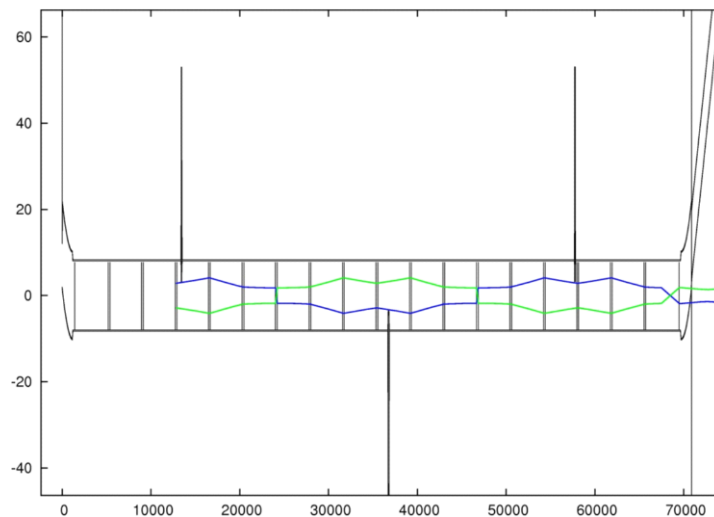
Figure 50 : Placement of the primary and secondary collimators along the collimation section. The x and z axis are in meters, and the blue and green lines are the limits of the beam envelope for a beam emittance of 2.6pi.mm.mrad and maximum δ=2.5‰.
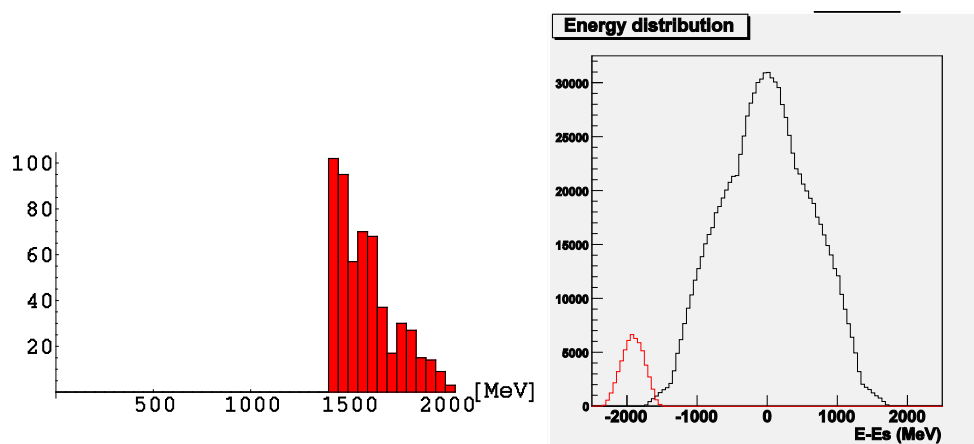
Figure 51 : Left: energy spread of the collimated ^{6}He halo as estimated by ESME. Right: energy spread of the merged bunch before the ramping up (in black) energy spread of the collimated ^{6}He halo as after the ramping up (in red), as calculated by ACCSIM.

The size and materials of the collimators were optimized with respect to deposited power and activation. Graphite collimators of thickness 30 cm were found suitable for the primary and

secondary collimators. The deposited power for those should below 10kW, which is commonly accepted as the limit beyond which deformation issues appear [37]. The use of graphite absorbers after the collimators and before the second bump of the collimation section decreases considerably the power losses in the magnet coils [31]. Table 17 and Table 18 present the doses absorbed in the coils per year for the different magnets of the collimation section when graphite absorbers are used and placed according to Figure 52. The lifetime of warm magnets is commonly assumed to correspond to a dose of 10 MGy, beyond which the magnet components such as the resins of the coils start to deteriorate [37]. For some of the quadrupoles following the primary collimator and for a running period of 10 years, the doses are still above this limit. This preliminary design of the collimation section (dipole and quadrupole magnets details, collimators and absorbers) is therefore being further refined using FLUKA to obtain compatible magnet lifetimes with the 10 years operation of Beta-Beam.

Dose absorbed in the coils (MGy/Year)				
Beam	1st Qdrupole	2nd Qdrupole	3rd Qdrupole	4th Qdrupole
$^{6}He^{2+}$	2.3	1.9	0.4	0.4
$^{18}Ne^{10+}$	3.0	2.9	1.3	1.08

Table 17 : Dose absorbed in the coils of the quadrupoles located after the Primary Collimator

Dose absorbed in the coils (MGy/Year)			
Beam	1st Dipole	2nd Dipole	3rd Dipole
$^{6}He^{2+}$	0.9	0.7	0.6
$^{18}Ne^{10+}$	1.0	0.8	0.7

Table 18 : Dose absorbed in the coils of the dipoles located in the 2nd bump
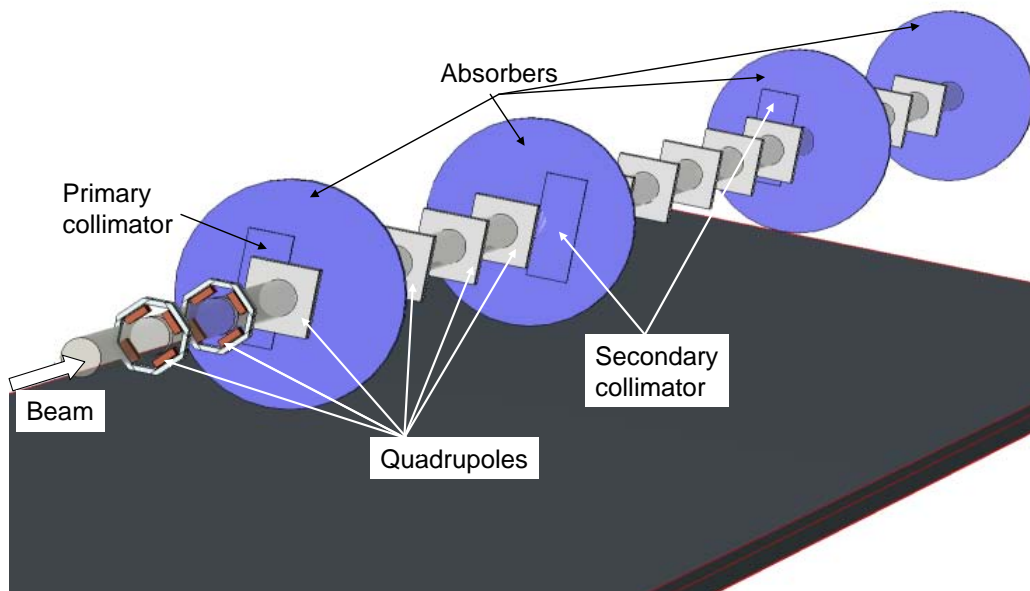

Figure 52 : Placement of graphite absorbers in the collimation section. (SimpleGeo view [38])

Losses by β decay

The decay of the stored ions implies a continuous power loss with a mean value of 10.8 W/m for $^6He^{2+}$ and 11.8 W/m for $^{18}Ne^{10+}$[32]. The relative rigidity difference between the decay products and the reference one is around -33% for $^6He^{2+}$ and +11% for $^{18}Ne^{10+}$. In turn, the decay products are lost after the dipoles. Two principal issues can be underlined. After the long straight sections, the deposition is equal to several tens of kilowatts: a dedicated extraction section at the arc entry is needed. Moreover, the deposition in the superconducting magnet coils must be low enough to avoid quenching. A solution to this problem is to insert absorbing elements between the magnets. For this layout, a model of a large aperture dipole for the decay ring is needed and it was shown that an 80 mm magnet aperture could be envisaged for the case absorbers between the magnets were needed [39]. From energy deposition studies of this layout it was concluded that open mid plane dipoles, which are dipoles without coils around the horizontal plane, could be a better choice. In this case, absorbers are not necessary which would make the arcs more compact. The required field could then be 5T instead of 6T and the minimal dipole aperture required would be reduced (±50 mm against ±80 mm). In addition the structure changes would then be simpler if other ions have to be used.

To evaluate the power deposition of the decay products in the vacuum chamber, a simple 1D model was implemented in BETA [22]. It does not take into account any interaction with the walls. It was applied to the case where absorbers are inserted between the arc dipoles. To improve this study, a 3D simulation was run, including particle tracking in matter (FLUKA). Particle maps were generated by ACCSIM. The 1D simulation in BETA and the FLUKA simulation both showed that the average value deposited in the dipoles is then less than 10 W/m. However, peaks in power deposition exceed the recommended limit for LHC like magnets (4.3 mW/cm³) for both dipoles and quadrupoles. The power deposition along an arc cell as calculated with FLUKA using the $^6Li^{3+}$ ions loss map from ACCSIM is presented in Figure 53. As an example, the loss profile of the peak heat along D2 is presented in Figure 54. The maximum deposited peak power was found to be in the order of 30 mW/cm³.
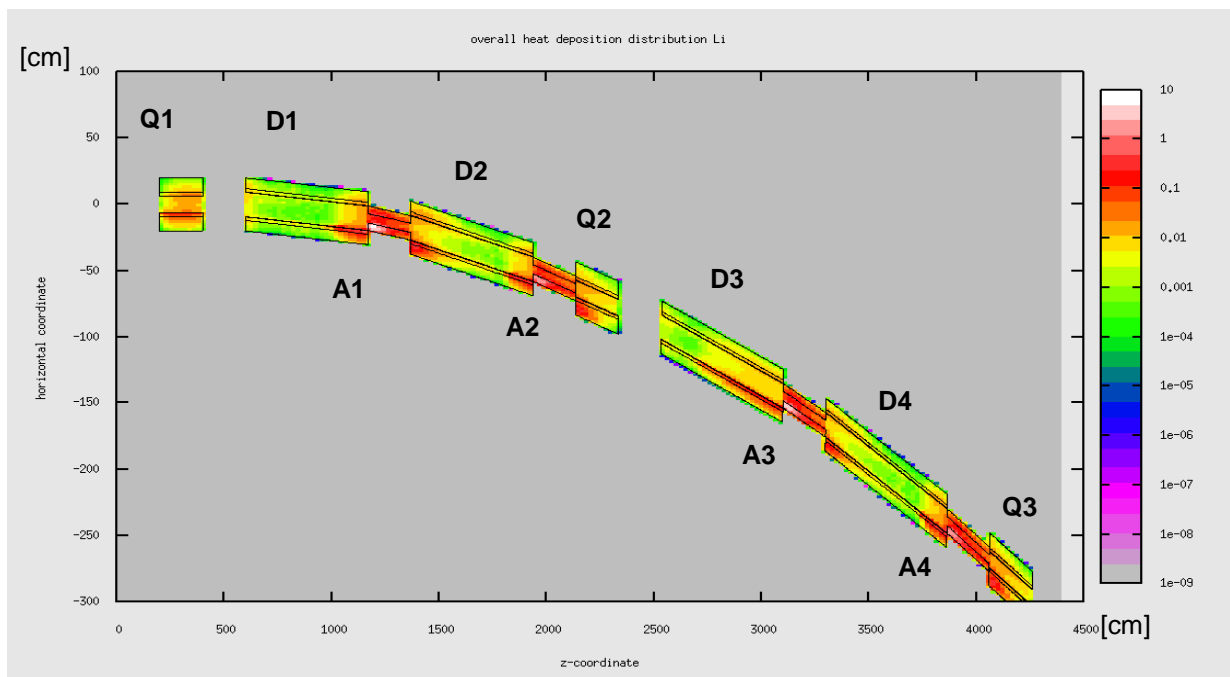
Figure 53 : Overview picture of the energy deposition in an arc cell (including one extra quadrupole for checking) projected on the horizontal plane for the Li $^{3+}$ ions (averaged). Q stands for Quadrupole and D stands for Dipole. The absorbers (A) are placed after the dipole magnets.
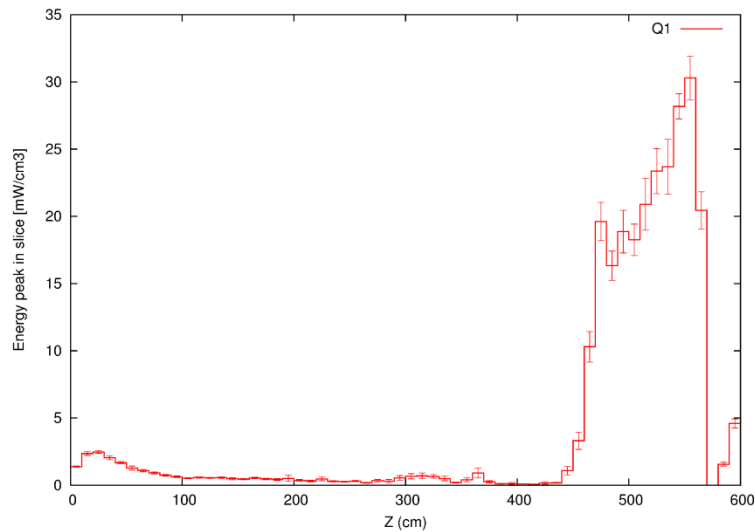

Figure 54 : Peak energy deposition in each longitudinal bin along the superconducting cable on the dipole D2 in the lattice cell. Recommended limit value for quenching is 4.3 mW/cm³. The bars represent statistical errors.

Figure 55 shows that the peak energy deposition is situated on the bending plane of the magnets. The first calculations permitted to estimate the opening angle that could reduce sufficiently the peak power deposition in the magnet coils. A study of cosθ-design solutions for open mid plane dipole design [40] shows that this technology is a possible approach. Complementary studies including energy deposition should follow, to tune the magnet and shielding design in the decay ring.
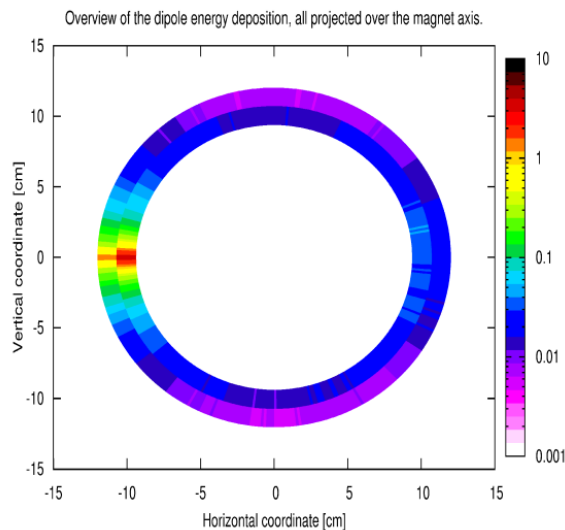
Figure 55 : Overview of the energy distribution in the superconducting cable on the dipole 3 in the lattice cell. The superconducting cable is modeled, for simplicity, as a cylinder. Transverse projection, averaged over the length of the magnet.

Different options of open mid-plane dipoles were studied. From first estimations, based on energy deposition calculations on large aperture magnets for the solution with absorbers, magnets having

5° half-opening angle of the coils in the mid-plane (see Figure 57) were assumed to reduce the deposited peak power by a factor 10. At 1.9K, open midplane magnets of aperture radius up to 90mm reaching the required field of 6T are feasible. At 4.2K, the radius has to be reduced, coil layers have to be added and the yoke thickness enlarged (see Figure 56 and Table 19).
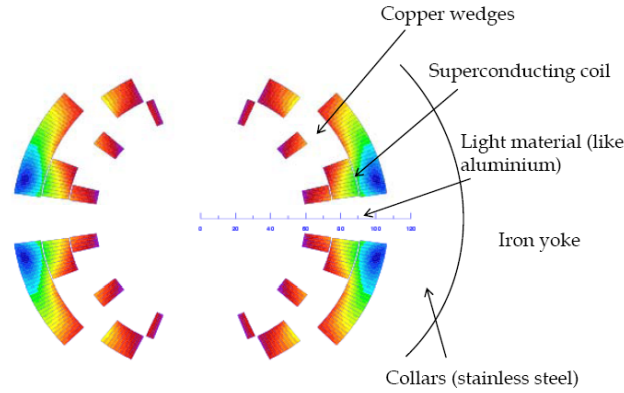
Figure 57 : Transverse cross-section of the coil of an open mid-plane dipole magnets for the beta-beam decay ring.
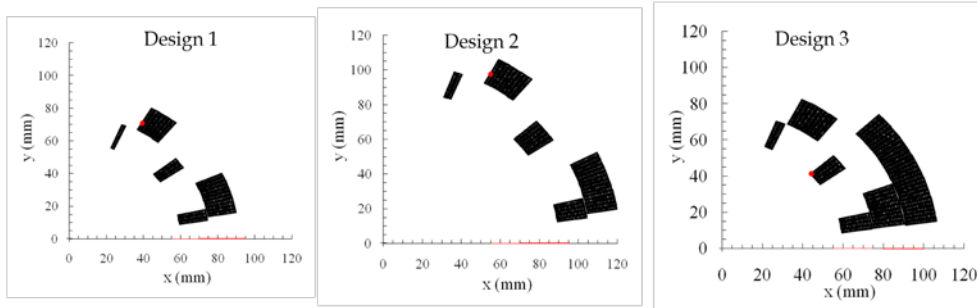
Figure 58: Possible open mid-plane magnet designs for the decay ring.

Design	1	2	3
Aperture radius (mm)	60	90	60
B_{ss} at 1.9 K (T)	6.5	6.8	8.7
Operational field at 1.9 K (T)	5.2	5.5	7.0
B_{ss} at 4.2 K (T)	4.9	5.3	6.7
Operational field at 4.2 K (T)	4.0	4.2	5.4
Gap in midplane (mm)	8.9	12.5	8.7
Yoke (mm)	180	270	240

Table 19 : Parameters and performances of the possible open mid-plane magnets presented in Figure 58.

Parametric studies of the open midplane quadrupoles [41] permit to choose an optimum solution (field, length, aperture). Needed opening angles were estimated from energy deposition calculations [42] to be less than 6 ° (see Figure 59).

Figure 59 : Parametric dependence of quadrupole gradient on aperture for different midplane opening angles.

Dynamic aperture

The study of the dynamic aperture is presented in detail in [31]. We recall here the main results.

The natural normalised chromaticity in the decay ring is respectively Q'_x= -1.72 and Q'_z= -2.35 in the horizontal and vertical planes. In order to accept the injected beam at δ=5‰, the natural 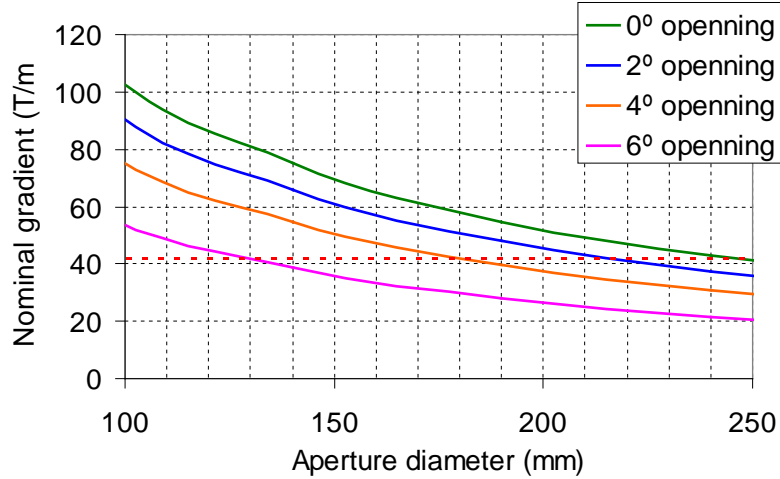chromaticity must be corrected by sextupole families in the dispersive areas. Normally, only two sextupole families situated in the regular FODO lattices are necessary. We obtain then the blue curve on Figure 60. The dynamic aperture is large enough. Nevertheless, the coupling resonances are not corrected and the transfer between the two planes is not negligible. Therefore, other sextupole families were added in order to correct the sextupole resonances. After correction, we obtain the red curve on Figure 60. The dynamic aperture is much larger and the beam keeps an elliptic shape during its transport in the structure by assuming all magnetic elements perfect. The variation of the dynamic aperture with the momentum is plotted on Figure 61 assuming that the chromaticity is corrected with six sextupole families. In the energy range of the stored beam (±2.5‰), the dynamic aperture stays large enough to accept the whole beam.
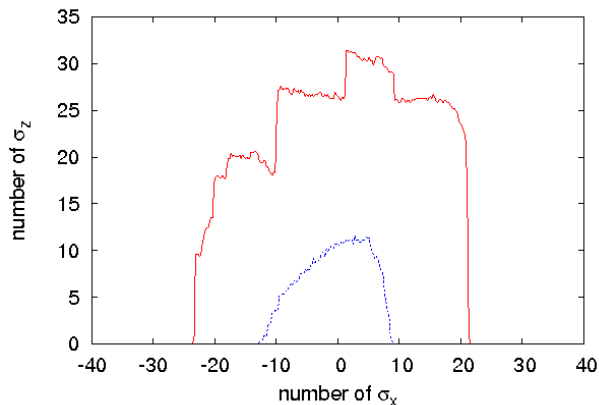

Figure 60: Dynamic aperture for 10,000 turns at the middle of the injection insertion. In red, with 6 sextupole families and in blue with 2 sextupole families.
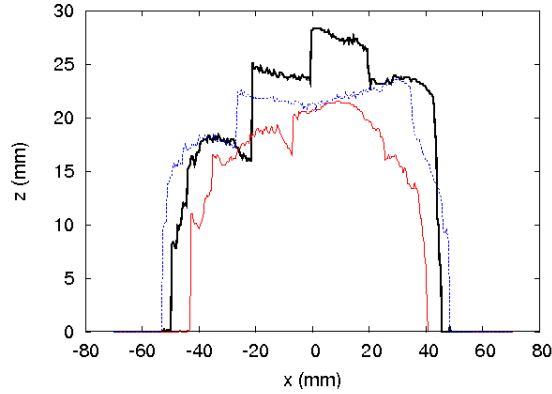
Figure 61: Dynamic aperture around the chromatic orbit for 10,000 turns at the middle of the injection insertion. In black, at δ=0, in red at δ=2.5 ‰ and in blue at δ=-2.5 ‰.

The impact of defects in the magnetic elements was in addition studied. The large aperture of the dipoles implies unavoidable multipole components. Until now, only systematic multipole components were considered. The assumed systematic multipole components in the dipoles are $b_3 = -1.68 \times 10^{-4}$, $b_5 = 33.02 \times 10^{-4}$, $b_7 = -50.12 \times 10^{-4}$ and $b_9 = 29.58 \times 10^{-4}$ at the reference radius 60 mm [39]. A direct consequence is a reduction of the dynamic aperture. In order to identify the main multipole effects, Figure 62 gives the dynamic aperture calculated for each alone multipole component for the same reference structure. The strongest contribution comes from the fifth and the seventh order multipole components. In order to decrease their effects, different working points were considered and an automatic enlargement program of the dynamic aperture was added in BETA, which enabled to obtain a dynamic aperture of more than 6 σ [43].
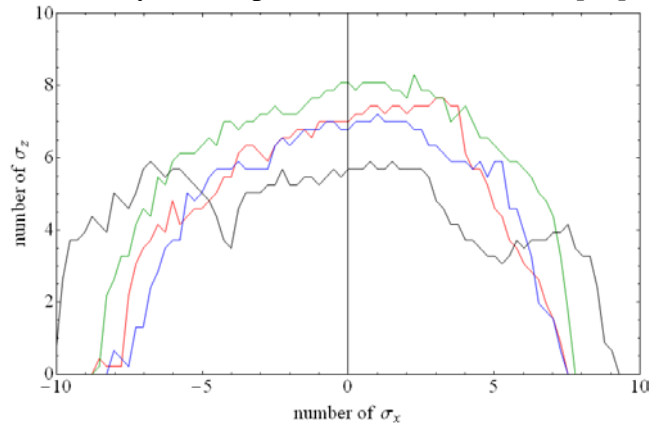
Figure 62: Dynamic aperture for 1,000 turns without optimization and after applying the fifth order (red), the seventh order (blue), the ninth order (green) or every (black) multipole component.

Decay ring radioprotection studies

Losses are present all over the DR and can be subdivided into:
- Injection and merging losses
- Decay losses
- Collimation losses

The decay losses and collimation losses were described in previous sections. Preliminary radioprotection studies were performed for these two types of losses, while the study of injection and merging losses remains to be done. The main results of these studies are summarized here.

51

All calculations are performed with the Monte Carlo code FLUKA [26][27]: realistic geometries are implemented to calculate the residual dose rates during the machine maintenance due to the activation of the materials and the activation induced in the air in the tunnel. For both types of losses the loss maps were provided from ACCSIM.

DECAY LOSSES

Recoils from decay are lost after the dispersive elements of the ring. The activation of magnet materials was therefore estimated both in the arcs and in the collimation section where respectively superconducting and warm magnets are used. In the collimation section the geometry of typical warm magnets [44] using typical materials was implemented. In the arcs, both open mid-plane and standard magnets with absorbers were implemented with geometries consistent with those used for the study described in section "*Losses by β decay*". The losses at the entrance of the arcs or bumps are assumed to be sent to appropriate beam dumps [31]. An example of residual dose rate map is shown on Figure 63 for the first bump of the collimation section. For the arcs as well as for the collimation section, the residual dose rate after 3 month of irradiation and 1 week waiting time is a few mSv (5-10 mSv·h^{-1}), which corresponds to a "high radiation area" according to CERN rules (>2mSv·h^{-1} and <100mSv·h^{-1}).
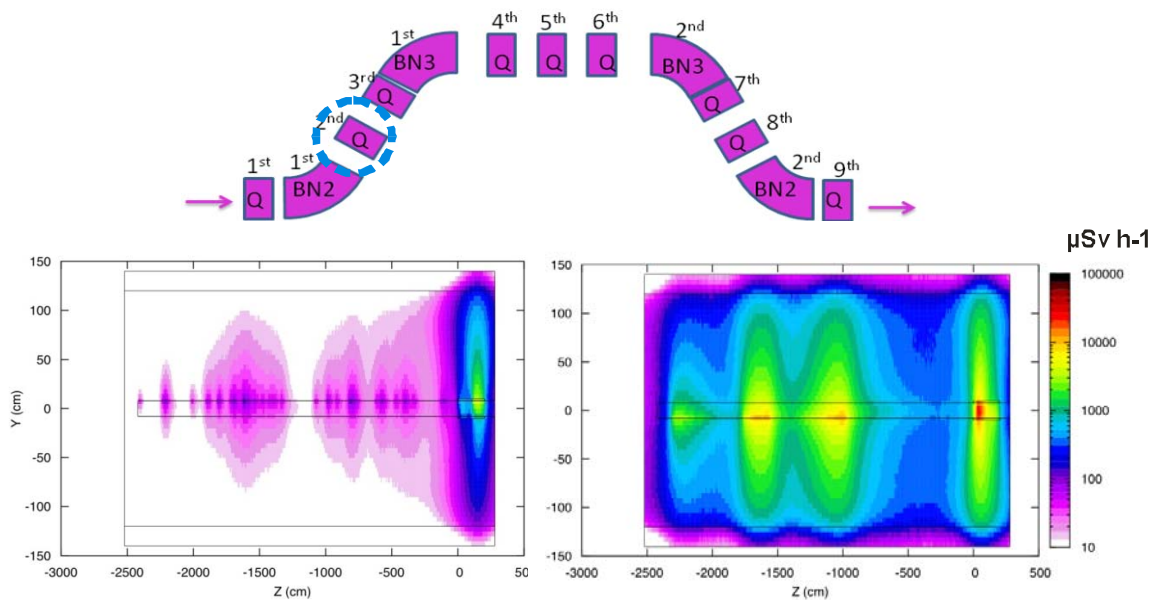
Figure 63: Residual dose in the 2nd quadrupole of the first bump of the collimation section after 3 month of irradiation and 1 week waiting time. The upper picture represents the magnets arrangement within the first bump. Left bottom: residual dose map for ^{6}He, right bottom: residual dose map for ^{18}Ne.

COLLIMATION SECTION

The procedure discussed in section "*Momentum collimation*" was used for generating the collimation loss map. After 3 months of irradiation and 1 week of waiting time, the area around the primary collimator exhibits a peak value above 100mSv·h^{-1} (prohibited area, see Figure 64) whilst the entrance of the second bump shows a maximum dose rate of 50mSv·h^{-1} compatible with a high radiation area. Remote handling would therefore be highly recommended for the maintenance of the primary collimator.

Figure 64: Residual dose rate in the straight section of the collimation section, after 1 week waiting time and 3-month ^{18}Ne irradiation.

AIR ACTIVATION

Using the same approach and parameters as for the RCS, a very preliminary calculation has shown that the annual effective dose given to the reference population exceeds the 10μSv limit value for both the ion cases. This latter could certainly be efficiently reduced by optimizing the tunnel-ventilation parameters on which they are k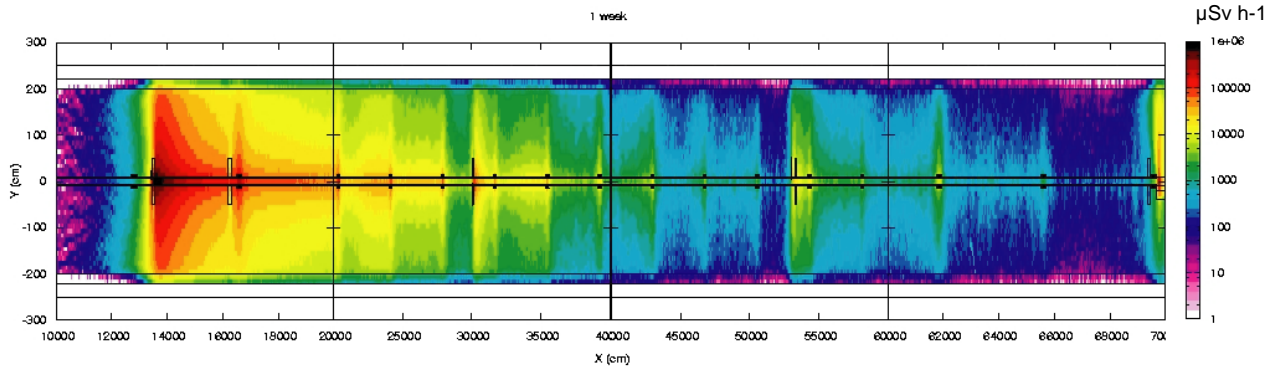nown to be highly depending. Ad-hoc solutions can be found to reduce the emissions, like e.g. high efficiency filters, different ventilation rates in different segments of the tunnel, etc.

Vacuum System Requirements for the Decay Ring

The parameters used for the simulations of the dynamic pressure are listed in Tables 20 and 21. The data in Table 20 were taken from "The EURISOL Beta-beam Facility Parameter and Intensity Values" generated at 12. March 2009.

Parameter	Value for ^{6}He^{2+}	Value for ^{18}Ne^{10+}
Energy (Injection)	92.5 GeV/u	92.2 GeV/u
Mag. Rigidity (Injection)	1875,37 Tm	5591,51 Tm
Energy (Ejection)	—	—
Mag. Rigidity (Ejection)	—	—
Ramping Rate	—	—
Cycle Time	6.0 s	3.6 s
Cycle Frequency	0.17 Hz	0.28 Hz
Losses at Injection	0 %	0 %
Emittance (horizontal)	0.6 mm mrad	0.6 mm mrad
Emittance (vertical)	0.32 mm mrad	0.32 mm mrad
Accumulated Ions	9.66×10^{13}	7.42×10^{13}

Table 20 : Beam parameters used with StrahlSim.

Parameter	Value
Volume of Beam Pipe	64.6 m^3
Static Residual Gas Pressure	10^{-11} mbar (see text)
Effective Pumping Speed	1000 m^3/s

Table 21 : Vacuum parameters used with StrahlSim.

The loss distribution for both ^{6}He^{2+} and ^{18}Ne^{10+} ions are shown in Figure 65 for a part of one of the

53

arcs. The figures distinguish between lost particles hitting the vacuum chamber and particles hitting the ion catcher. The ion catcher were positioned at a distance of 4 cm from the beam axis. The extraction of the decayed particles at the end of the straight lines is modeled using an ion catcher, because StrahlSim is only capable of simulating an extraction at the end of a cycle. The desorption from this ion catcher, which is very small at the ion energies in the Decay Ring, can be considered to be ejection losses, which will occur anyway. The simulation furthermore assumes that all lost ions hitting an ion catcher are stopped inside the catcher. Fragmentation effects are not considered.

The losses shown are dominated by radioactive decay. Losses due to charge exchange are negligible, as the cross sections for electron capture are very small. For both $^6He^{2+}$ and $^{18}Ne^{10+}$ the losses are peaked at the positions of the ion catchers. Unfortunately it was only possible to perform tracking simulations with a relatively low number of ions due to the size of the decay ring. This leads to the peaked structure of the longitudinal distribution of ions hitting the vacuum chamber. In reality this should be a continuous distribution. This does not affect the simulations of the pressure evolution, which will be discussed later.
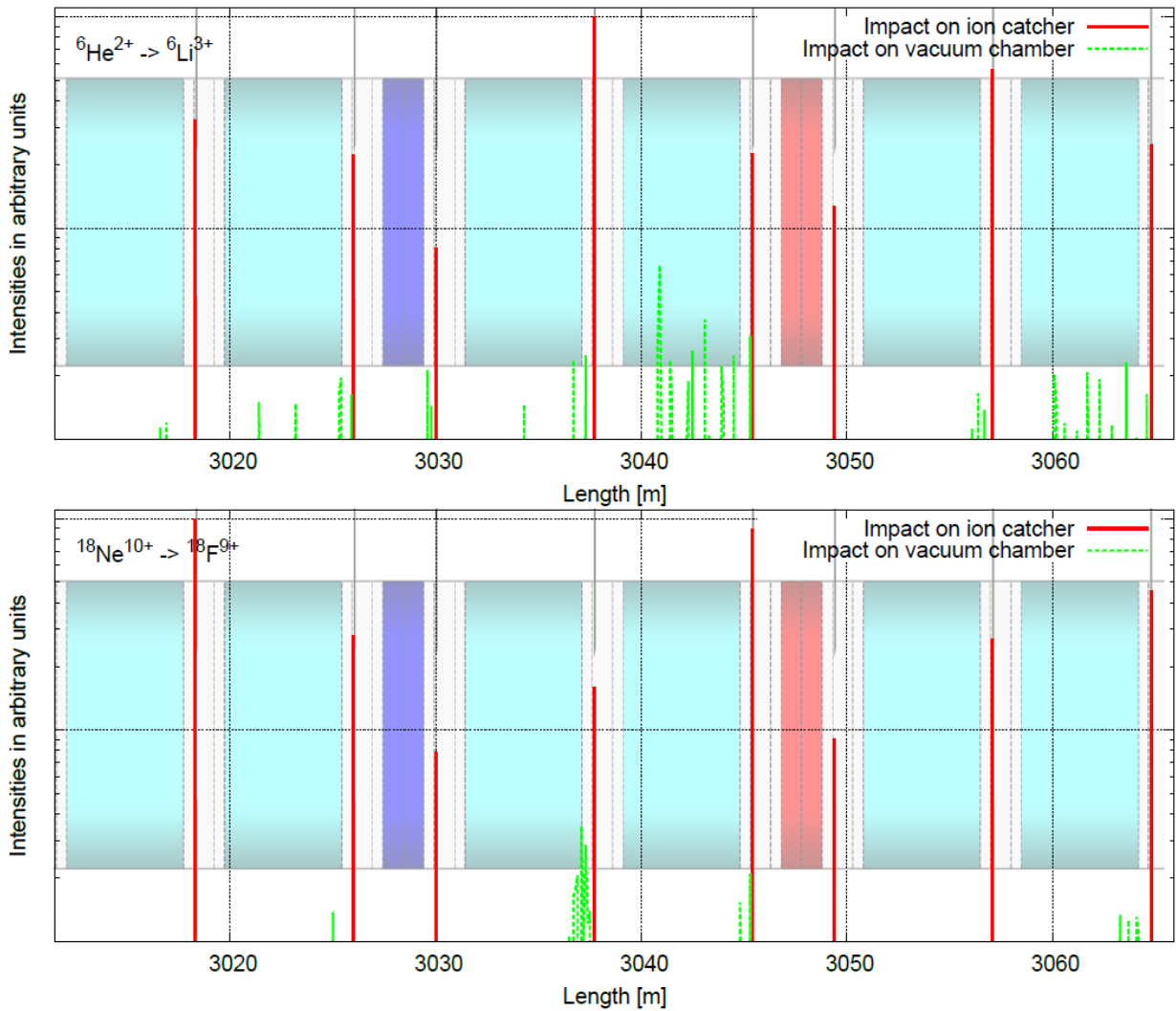
Figure 65: Loss distribution for $^6He^{2+} \rightarrow$ $^6Li^{3+}$ (top) and $^{18}Ne^{10+} \rightarrow$ $^{18}F^{9+}$ (bottom) at injection energy. Dipole magnets are shown in light blue, quadrupole magnets in red and blue and ion catchers as gray lines. The peaked distribution of ions hitting the vacuum chamber is due to the low number of tracked particles (see text). Note that the intensities are scaled logarithmically.

The number of particles accumulated in the Decay Ring are 9.66×10^{13} for $^{6}He^{2+}$ and 7.42×10^{13} for $^{18}Ne^{10+}$. In the $^{6}He^{2+}$ cycle there is a reinjection every 6 s and every 3.6 s for an operation with $^{18}Ne^{10+}$, which brings the number of particles back to the desired numbers.

The simulations done with StrahlSim start with the maximal number of particles and inject the number of lost particles due to radioactive decay after 6 s and 3.6 s respectively. For $^{6}He^{2+}$ there are 4.82×10^{12} and for $^{18}Ne^{10+}$ 1.10×10^{12} particles reinjected.

The main mechanism for a pressure build up in the Decay Ring is the ionization of residual gas particles by the circulating beam, called target ionization. The cross sections for target ionization are given by a scaled Bethe formula [28]. This effect was already observed in the simulations for the SPS. The ionized particles are accelerated towards the vacuum chamber due to the space charge potential of the revolving beam. When these particles hit the vacuum chamber a low energy desorption process takes place. The desorption rate η for this process is considered to be in the range between 1 and 10 desorbed particles per ionized gas particle hitting the vacuum chamber [29], while desorption rates less than 1 have been observed [45]. Additionally the re-emission coefficient has to be considered. This coefficient describes the probability that an incidenting particle is reflected from the surface of the vacuum chamber. The value of this coefficient was measured for $^{15}N_2$ to be less than 0.1 [45] at energies of 2 keV. The simulations for $^{6}He^{2+}$ were taken out with an re-emission coefficient of 1, which is a worst case approximation. Due to the strong dependence of the pressure evolution on the target ionization in case of $^{18}Ne^{10+}$ as projectile ion, re-emission coefficients of 0 and 1 have been used.

Obviously the starting pressure is a crucial parameter for the simulations. At higher starting pressures there are more particles that can be ionized by the beam. For the simulations three different pressures have been used, namely 10^{-10}, 10^{-11} and 10^{-12} mbar. As the Decay Ring is a cold machine 10^{-10} mbar is already very high. A starting pressure below 10^{-11} mbar is more realistic. Nevertheless the value of 10^{-10} mbar was used to show an upper limit for $^{6}He^{2+}$.

The ionization of residual gas particles creates free electrons. Effects caused by these electrons like electron multipacting are not considered in the StrahlSim code. It has to be ensured, that such effects do not affect the Decay Ring operation.

The conventional effective pumping speed of the Decay Ring was estimated by using the value of the SPS of 2.8 m^3/s. Compared to the pumping speed delivered by the cold surfaces of the cryogenic arcs of the machine this value is very small and contributes very little to the total effective pumping speed. The pumping speed of the cold surfaces depends on their temperature.

The temperature of the arcs was assumed to be 10 K, while simulations for 15 K and 20 K have been taken out as well. For sufficiently cold vacuum chambers, with a temperature below 16 K (see text below), the pumping speed of the cold surfaces was calculated by StrahlSim to be about 1000 m^3/s. As the whole arcs are cold the vacuum conductance is very high, and the total and the effective pumping speed is the same. It should be pointed out, that the model used by StrahlSim assumes that the pressure in the machine is everywhere the same. This means, that the pressure in the arcs and the straight lines are averaged. But in the Decay Ring the arcs and the lines are going to have very different pressures due to the completely different pumping techniques used to maintain the vacuum. In reality the pressure in the arcs will be lower and the pressure in the straight sections will be higher than the average pressure used by StrahlSim. As StrahlSim cannot calculate a dynamic longitudinal pressure profile at the moment, this effect is not reflected in the results presented in this report.
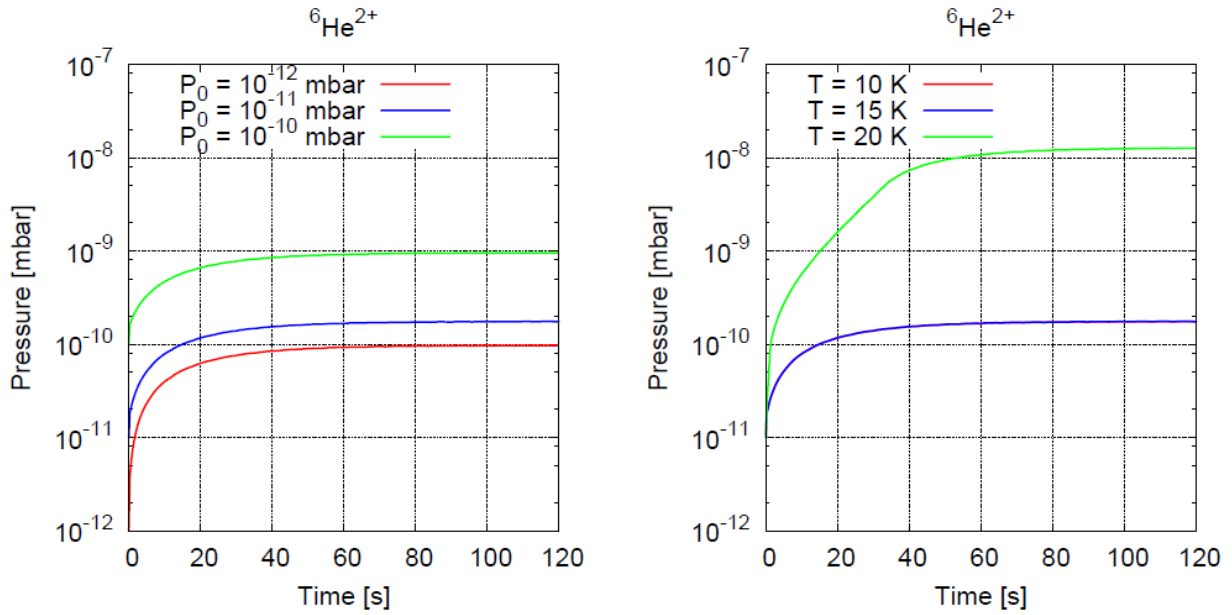
Figure 66: The figures show the pressure evolution over several cycles for $^6He^{2+}$. In the left figure the temperature of the arcs was set to 10 K, while the starting pressure P_0 was varied in the range from 10^{-12} to 10^{-10} mbar. In the right figure the starting pressure for all simulations was 10^{-11} mbar and the temperature was varied from 10 K to 20 K. Please note that the lines for T = 10 K and T = 15 K are almost on top of each other.

All simulations show a very steep pressure rise at the beginning of the simulation. This is, because the simulations start with the maximal number of particles which is supposed to be stored in the Decay Ring. The accumulation phase is neglected. This can be justified, as it is only relevant whether the pressure inside the Decay Ring stabilizes at a value that is low enough for a stable operation.

For $^6He^{2+}$ here was a desorption rate for perpendicular incidents of $\eta = 10$ and a re-emission coefficient of 1 assumed. Simulations were taken out for different starting pressures in the rage from 10^{-12} to 10^{-10} mbar and for different temperatures of the cold surfaces between 10 and 20 K. Figure 66 shows the results. For all reasonable starting pressures and a temperature of 10 K the pressure evolution stabilizes at sufficiently low values. For temperatures above 15 K the pumping speed is not sufficient any more to maintain a residual gas pressure below 10^{-8} mbar. Above this temperature the residual gas particles do not freeze out any more on the cold surfaces. For temperatures less than approximately 16 K the pumping speed is almost constant what can be seen in the right plot in figure 66. The starting pressure of 10^{-10} mbar gives the upper limit of an acceptable starting pressure, which should be easily achieved by a cold machine.

The operation of the decay ring with $^6He^{2+}$ as the projectile ion is feasible according to the simulation results obtained using StrahlSim.
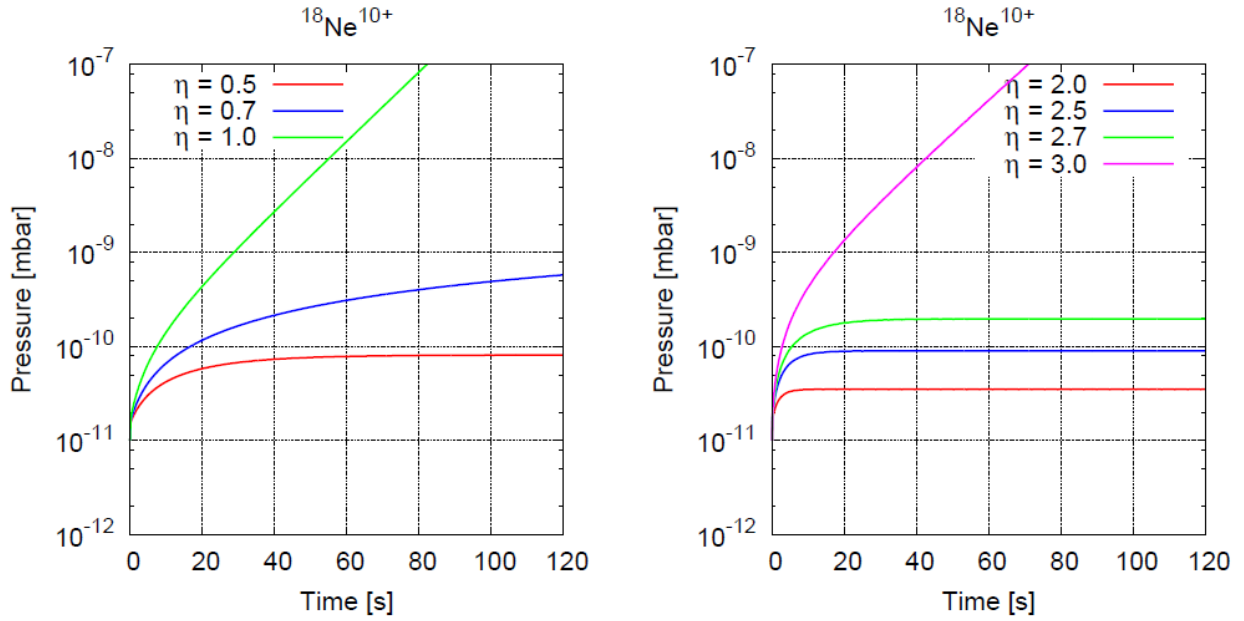
Figure 67: This figure shows the pressure evolution for $^{18}Ne^{10+}$ in the Decay Ring for a re-emmission coefficient of 1 (left) and 0 (right). The desorption rates were varied from 0.5 to 1 and 2.0 to 3.0 respectively. All simulations were done with a starting pressure of $P_0 = 10^{-11}$ mbar and a temperature of the cold surfaces of $T = 10$ K.

For $^{18}Ne^{10+}$ the situation is different. Like in the SPS the operation with $^{18}Ne^{10+}$ is subject to an enormous amount of residual gas ionization. Figure 67 shows the pressure evolution for a starting pressure of 10^{-11} mbar and a temperature of the cold surfaces of 10 K. The simulations have been taken out for a re-emission coefficient of 0 (left plot in Fig. 67) and 1 (right plot in Fig. 67).

For a re-emission coefficient of 1 the pressure exceeds acceptable values already for desorption rates $\eta < 1$. For a re-emission coefficient of 0 η can be larger than 2 and the vacuum is still stable. The real coefficient should be closer to 0 according to [45]. Due to special surface treatments of the vacuum chambers very low desorption rates η can be achieved. The Beta Beam Operation with $^{18}Ne^{10+}$ ions in the Decay Ring could be feasible when the low energy desorption rates can be reduced accordingly.

Assuming a desorption rate $\eta = 2.7$, Figure 68 shows the dependence of the pressure evolution on the starting pressure. Under this condition the residual pressure in the Decay Ring stabilizes at sufficiently low pressure values, as long as the surface temperature of the cold arcs stays below 16 K. The temperature dependence is identical to the dependence observed for $^{6}He^{2+}$.
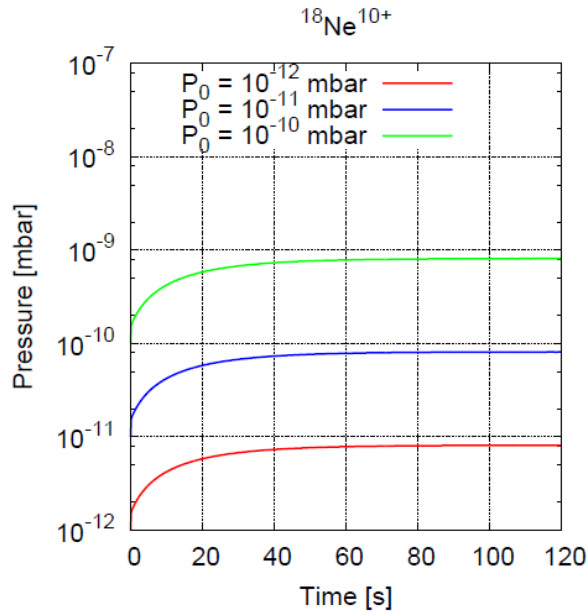
Figure 68: The figure shows the pressure evolution for $^{18}Ne^{10+}$ assuming a desorption rate of η = 2.7 and a re-emission coefficient of 0. The temperature was set to T = 10 K.

The interactions of the beam with residual gas particles and their effect on the pressure evolution inside the Decay Ring have been investigated using the program StrahlSim. The simulations show, that during Decay Ring operation with $^6He^{2+}$ the pressure does not exceed critical values as long as the temperature of the cold surfaces in the arcs is less than approximately 16 K. The dependence on the starting pressure is rather weak. For all considered values of 10^{-12}, 10^{-11} and 10^{-10} mbar the equilibrium pressure stays below 10^{-8} mbar.

For $^{18}Ne^{10+}$ there is a massive pressure build up due to ionization of residual gas particles induced by the circulating beam. This effect was already observed in the simulations done for the SPS. Only for small values of the desorption rate of about η < 3 combined with a re-emission coefficient close to~0, the residual gas pressure in the Decay Ring stabilizes at sufficient pressure values below 10^{-8} mbar, as long as the surface temperature of the cold arcs stays below 16 K. Low desorption rates, even below 1, have been observed and can be achieved by special surface treatments [45]. For Beta Beam operation such low values have to be assured.

VIII.   Conclusion

A summary has been made of a conceptual design report on a CERN/EURISOL baseline scenario for the Beta-beam facility. The study focused on the accelerator chain, which incorporates some of the existing CERN infrastructure. Particular attention was paid to the RCS and Decay Ring machines that are not part of the latter. An original stacking mechanism has been proposed in the Decay Ring involving off-momentum injection and novel rf gymnastics to accumulate ions in longitudinal phase space with minimal emittance dilution. The resultant high stack intensities present their own problems and detailed studies have been made of momentum collimation in the Decay Ring and of beam loss, dynamic vacuum and radiation protection issues throughout the accelerator chain. In addition, since the stack comprises only a small number of bunches, transient beam loading is a major issue for the rf systems of the Decay Ring. A conceptual approach to counteract this has been proposed, but further study is required. Even with stacking there remains pressure on ion production rates and methods to improve these have been investigated within other

tasks of the EURISOL design study.

From the outset, this study has been based as far as possible on known technology. Nevertheless, the challenge of unprecedented neutrino production rates has produced, for example, a new stacking process and an open-midplane superconducting magnet design. The combination of the novel with the tried-and-tested - underscored by the use of existing CERN machines - has allowed that challenge to be met without compromising the chances of converting the conceptual design into a technical one.

IX.   References

[1] P. Zucchelli, "A novel concept for a neutrino factory: the beta-beam", Phys. Let. B, 532 (2002) 166-172.

[2] B. Autin, M. Benedikt, M. Grieser, S. Hancock, H. Haseroth, A. Jansson, U. Köster, M. Lindroos, S. Russenschuck and F. Wenander, "The acceleration and storage of radioactive ions for a neutrino factory", CERN/PS 2002-078 (OP), Nufact Note 121, J. Phys. G 29 (2003) 1785-1796 and long internal CERN version, PS/OP/Note 2002-181.

[3] M.Mezzetto, "Physics reach of the beta-beam", J. Phys. G: Nucl. Part. Phys. 29 (2003) 1771–1776

[4] J. Bouchez, M. Lindroos and M. Mezzetto, 5th International Workshop on Neutrino Factories and Superbeams; NuFact 03. AIP Conference Proceedings, Volume 721, pp. 37-47 (2004).

[5] Letter of Intent: FP6 Design Study for a beta-beam facility , September, 2003

[6] N Thollieres et al., EURISOL-TN03-25-2006-0004

[7] http://www.euronu.org/

[8] C. Rubbia et al., Beam cooling with ionization losses, NIM A 568 (2006) 475–487

[9] Parameter and Intensity Values, Version 1, April 2005, EURISOL DS task note 12-25-2006-0003

[10] Parameter and Intensity Values, Version 2, July 2005, EURISOL DS task note 12-25-2006-0004 (revised 13th October 2005, see equation 2 and table 2)

[11] Parameter and Intensity Values, Version 3, July 2007 (doc-version), EURISOL DS Task note 12-25-2009-0014 (RCS energy 3.5GeV proton equivalent)

[12] High frequency ECR source (60 GHz) in pre-glow mode for bunching of beta-beam isotopes, T. Thuillier, NuFact08 proceedings, PoS(Nufact08)089

[13] M. Benedikt, S. Hancock, A novel scheme for injection and stacking of radioactive ions at high energy, Nucl. Instr. Meth. A 550 (2005) 1–5

[14] S. Hancock et al., Stacking Simulations in the Beta-Beam Decay Ring, in proceedings of EPAC'06.

[15] A. Bechtold, H. Podlech, "Proposal of a Normal Conducting CW-RFQ for the EURISOL Post-Accelerator and a Dedicated β-Beam Linac Concept", EPAC2006.

[16] CERN Baseline Beta Beam, CERN yellow report in preparation

[17] G. Clemente et. al, Status of the 70 mA, 70 MeV CH Proton-DTL for FAIR, EPAC'06.

[18] H. Danared et al., EPAC 2000, Vienna, p. 301.

[19] A. Lachaize and A. Tkatchenko, EURISOL DS Task Note 12-25-2009-0018

[20] A. Tkatchenko, presentation at the first task meeting, EURISOL DS Task Note 12-25-2009-0016

[21] A. Lachaize and A. Tkatchenko, EURISOL DS Task Note 12-25-2006-0006

[22] J.Payet, Code BETA, jpayet@cea.fr.

[23] F.Jones, ACCSIM Code, Jones@triumf.com

[24] M. Benedikt and S. Hancock, EURISOL DS Task Note 12-25-2009-0017

[25] I. Floret, M. Widorski, Radiation survey results PS Complex 2008, CERN-SC-2008-096-RP-SN, EDMS 978763.

[26] "The FLUKA code: Description and benchmarking" G. Battistoni, S. Muraro, P.R. Sala, F. Cerutti, A. Ferrari, S. Roesler, A. Fasso, J. Ranft, Proceedings of the Hadronic Shower Simulation Workshop 2006, Fermilab 6--8 September 2006, M. Albrow, R. Raja eds., AIP Conference Proceeding 896, 31-49, (2007)

[27] "FLUKA: a multi-particle transport code" A. Fasso, A. Ferrari, J. Ranft, and P.R. Sala, CERN-2005-10 (2005), INFN/TC_05/11, SLAC-R-773

[28] Gillespie, G.H., Impact ionization scaling cross sections for fast highly stripped ions colliding with H_2 and He., Phys. Lett. A(93), 1983

[29] Omet, C., Kollimatorsystem zur Stabilisierung des dynamischen Restgasdrucks im Schwerionensynchrotron SIS18. Dissertation, Helmholtzzentrum für Schwerionenforschung GmbH, 2009.

[30] A. Fabich, M. Benedikt, EURISOL DS Task Note 12-25-2006-0005

[31] A. Chancé, E. Bouquerel, S. Hancock, E. Jensen and J. Payet, EURISOL DS Task Note 12-25-2009-0019

[32] A. Chancé, Etude et conception de l'anneau de désintégration d'une usine à neutrinos utilisant les décroissances beta des noyaux Hélium 6 et Néon 18 produits par un faisceau intense de protons frappant diverses cibles, PhD thesis, Université Paris Sud, 2007.

[33] M. Benedikt et al., Baseline Design for a Beta-Beam Neutrino Facility, in proceedings of EPAC'04.

[34] A. Chancé and J. Payet, "Studies of the injection system in the decay ring of a beta-beam neutrino source", in Proc. Particle Accelerator Conf., Knoxville (2005).

[35] M. Benedikt, P. Collier, V. Mertens, J. Poole, K. Schindl (editors), "LHC Design Report, Vol. 3, the LHC Injector Chain", CERN-2004-003-V-3, Geneva, 2004.

[36] J. B. Jeanneret, Phys. Rev. ST Accel. Beams 1, 081001 (1998)

[37] A. Bertarelli, R. Assmann, 'Permanent deformation of the LHC collimator jaws induced by shock beam impact: an analytical and numerical interpretation', Proceedings of EPAC 2006, Edinburgh, Scotland.

[38] SimpleGeo, Theis C., Buchegger K.H., Brugger M., Forkel-Wirth D., Roesler S., Vincke H., "Interactive three dimensional visualization and creation of geometries for Monte Carlo calculations", Nuclear Instruments and Methods in Physics Research A 562, pp. 827-829 (2006).

[39] C.Vollinger, E. Wildner, "A large aperture superconducting Dipole for Beta Beams to minimize heat deposition in the coil", Proceedings of PAC07.

[40] J. Bruer, M.Sc. Thesis, Linköping University, 2008.

[41] F. Borgnolutti, private communication.

[42] E. Wildner, F. Jones, "Simulation of Decays and Secondary Ion Losses in a Betabeam Decay Ring", PAC07, Proceedings of PAC07.

[43] A. Chancé et al., Studies of dipole field quality for the beta-beam decay ring, in proceedings of PAC'07.

[44] Sesame, the white book, chapter 6, July 2002.

[45] A.G. Mathewson, "Ion induced desorption coefficients for titanium alloy, pure aluminium and stainless steel", CERN-ISR-VA/76-5, 1976